California Institute of Technology
Division of Geological and Planetary Sciences
Seismological Laboratory
Pasadena, California 91125

FINAL AND SEMI-ANNUAL TECHNICAL REPORT

15 March 1976 - 30 September 1976

ARPA Order No.:	3291
Program Code:	TF 10
Name of Contractor:	California Institute of Technology
Effective Date of Contract:	15 March 1972
Contract Expiration Date:	30 September 1976
Amount of Contract:	$576,622
Contract Number:	F44620-72-C-0078, Mod. No. P00010
Principal Investigators and Phone Number:	David G. Harkrider (213) 795-8806 Donald V. Helmberger (213) 795-8806
Program Manager and Phone Number:	William J. Best (202) 694-5456
Short Title of Work:	Body and Surface Wave Modeling of Observed Seismic Events

Sponsored by
Advanced Research Projects Agency
ARPA Order No. 3291

Unclassified

SECURITY CLASSIFICATION OF THIS PAGE (When Data Entered)

REPORT DOCUMENTATION PAGE	READ INSTRUCTIONS BEFORE COMPLETING FORM
1. REPORT NUMBER: AFOSR - TR - 77 - 0214	2. GOVT ACCESSION NO. / 3. RECIPIENT'S CATALOG NUMBER
4. TITLE (and Subtitle): Body and Surface Wave Modeling of Observed Seismic Events	5. TYPE OF REPORT & PERIOD COVERED: Final & Semi-Annual Technical Report, 15 Mar.-30 Sept. 1976
	6. PERFORMING ORG. REPORT NUMBER
7. AUTHOR(s): David G. Harkrider, Donald V. Helmberger	8. CONTRACT OR GRANT NUMBER(s): F44620-72-C-0078, ARPA Order-3291
9. PERFORMING ORGANIZATION NAME AND ADDRESS: California Institute of Technology, Seismological Laboratory, Pasadena, California 91125	10. PROGRAM ELEMENT, PROJECT, TASK AREA & WORK UNIT NUMBERS: ARPA Order 1827, Amend.32, 6F10 Program Code
11. CONTROLLING OFFICE NAME AND ADDRESS: ARPA/NMR, 1400 Wilson Blvd., Arlington VA 22209	12. REPORT DATE: 7 December 1976
	13. NUMBER OF PAGES: 163
14. MONITORING AGENCY NAME & ADDRESS (if different from Controlling Office): AFOSR/NP, Bolling AFB, Bldg.#410, Wash DC 20332	15. SECURITY CLASS. (of this report): Unclassified
	15a. DECLASSIFICATION DOWNGRADING SCHEDULE

16. DISTRIBUTION STATEMENT (of this Report)

Approved for public release; distribution unlimited

(9) Semi-Annual technical rept. (Final), 15 Mar-30 Sep 76.

17. DISTRIBUTION STATEMENT (of the abstract entered in Block 20, if different from Report)

320 050

18. SUPPLEMENTARY NOTES

TECH, OTHER

19. KEY WORDS (Continue on reverse side if necessary and identify by block number)

Linear inversion
Seismic earth monopole
Most beneficial azimuth distribution
Synthetic seismograms
Source P & S Wave Histories
Comparison of matrix and generalized ray theory
Limited source regions
Earthquake source scaling
Far & near field comparisons

20. ABSTRACT (Continue on reverse side if necessary and identify by block number)

The major accomplishments during the first four-year-period are summarized under the categories of (1) Application of Lunar Inversion Theory, (2) Seismic Source Theory and (3) Synthetic Body and Surface Wave Modeling of Observed Seismic Events. The details can be found in previous technical reports under the contract. In Section III, a multipole expansion of the divergence and rotations of the linear displacement field from an arbitrary source is used in a multilayer formulation to → next page

DD FORM 1 JAN 73 1473 EDITION OF 1 NOV 65 IS OBSOLETE

Unclassified

SECURITY CLASSIFICATION OF THIS PAGE (When Data Entered)

cont

to obtain teleseismic body waves. As long as the expansion is obtained in a homogeneous region about the source, the source can be extremely complicated. The technique has been used in other contracts for non-linear finite difference simulations of stick-slip earthquake faulting and an explosion in an axesymmetric finite length tunnel.

In Section IV, both generalized ray theory and matrix techniques were used to calculate synthetic body wave seismograms for a point source in a layered elastic medium. Both methods are found to be equivalent and complementary for various model calculations. Ray theory has the advantage of giving a direct physical interpretation to observed phases. Matrix techniques, while exact in terms of including all multipoles, give little insight into the model, but serves as a check on the dominant phases needed in the ray calculations.

In Section V, a data set of forty-one moderate to large earthquakes were used to derive scaling rules for kinimatic fault models. If effective stress and static stress drop are equal, then fault rise time τ, and fault area, S, are related by $\tau = 16\sqrt{S}/(7\pi^{3/2}\beta)$. Fault length and width are empirically related by $L = 2W$. These scaling laws combine to give width and rise-time in terms of fault length. Finally averaging reported rupture velocities yields $V_R = .72\beta$.

CONTENTS

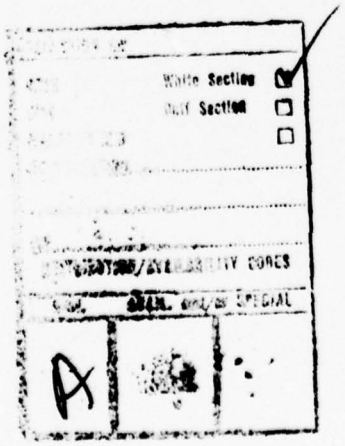

I. SUMMARY

Previous to 14 March 1975, the principal investigator for this contract was Don L. Anderson, with co-investigators C. B. Archambeau, D. G. Harkrider, D. V. Helmberger and H. Kanamori. The title during this period was "Seismic Phenomena Connected with Earthquakes and Explosions."

The major accomplishments during this period can be broadly categorized under the headings of (1) Applications of Linear Inversion Theory,(2) Seismic Source Theory, and (3) Synthetic Body and Surface Wave Modeling of Observed Seismic Events.

(1) Application of Linear Inversion Theory

Linear inversion theory was applied to body wave travel times and free oscillation data to obtain the velocity and density structure of a monopole earth. The theory was adapted to find the set of source parameters which optimally fit the variance weighted data set of spatial and frequency distributed path-corrected Rayleigh waves from the San Fernando earthquake. The interesting side result from this technique is the a priori determination of what azimuth distribution of observations is most beneficial in determining the source parameters. Of the 18 WWSN stations used for this event, two stations contain a total of 30% of the total information in the data set.

(2) Seismic Source Theory

Two different approaches for investigating the characteristics of the seismic source, in particular the determination of corner frequency for P and S waves, were developed. The first uses theoretical volume source models of tectonic release of the Archambeau type and obtains numerically their P- and S-wave spectra. The spectra for these particular models show a definite difference in the P-waves and S-wave corner frequencies. This approach yields theoretical M_S vs m_b curves which can be discussed in terms of scaling by the various source parameters. The second approach is to obtain the earthquake P-wave source history from comparison of theoretical and observed seismograms. This history is then used as the S-wave source history to obtain theoretical seismograms which are compared with S-wave observations of the same events.

The question of the validity of using far-field theory in order to determine source parameters such as moment and corner frequencies at ranges where this assumption is questionable was evaluated. The displacement fields were numerically investigated at a variety of ranges and source histories in order to establish criteria for estimating the minimum far field range in both the time and frequency domain.

The effect of finite source regions on various scaling laws for surface waves from underground explosions were investigated using simple theoretical source models. The scaling laws for simple models were found to be critically influenced by the effective radius of the source region. The strong dependence on radius appears to be related to the perfect symmetry of the source regions and will be investigated later.

3) Synthetic Body and Surface Wave Modeling of Observed Seismic Events

Amplitudes and arrival times of body and Rayleigh waves from NTS events were used to determine an average crustal model from NTS to mid-Arizona. Transversely polarized shear waves (SH) from well located earthquakes were also used to determine an upper mantle shear velocity structure. It was further demonstrated that observations of travel times for vertically polarized shear waves (SV), the most common technique, can lead to erroneous shear structure models due to contamination from P-SV interactions.

In order to study body waves from realistic models of earthquakes, generalized ray theory was extended to a shear dislocation source. Displacements at the surface of layered halfspace produced by a point source dislocation were investigated. Expressing the source in terms of P, SV and SH displacement potentials allows the solution to be expanded in generalized rays. The transient response for each ray is obtained by the Cagniard-deHoop method. First-motion and high-frequency asymptotic approximations of the exact solutions were discussed.

Using a generalized inverse technique WWSSN long-period P and SH waveforms were analyzed from the Koyna earthquake. The effects of local plane-layered earth structure near an imbedded point dislocation source are put in using a modified plane-wave ray theory which includes the standard reflection and transmission coefficients plus source corrections for radiation pattern and geometrical spreading. The generalized inverse compares synthetic seismograms to the observed in the time domain through the use of a correlation function. Using published crustal models of the Koyna region and primarily by modelling the crustal phases P, pP, and sP, the first 25 seconds of the long-period waveforms are synthesized for 17 stations and a focal mechanism obtained for the Koyna earthquake which is significantly different from previous mechanisms.

The technique has also been successfully applied to the Borrego Mountain earthquake of April 9, 1968. Synthetic seismograms computed from the resulting model match in close detail the first 25 seconds of long period seismograms from a wide range of azimuths. The main shock source time function was determined by a new simultaneous short period-long period deconvolution technique as well as by the inversion technique. The duration and shape of this time function indicate that most of the body wave energy was radiated from a surface with effective radius of only 8 km. This is much smaller than the total surface rupture length or the length of the aftershock zone. Along with the moment determination of $M_o = 11.2 \times 10^{25}$ dyne-cm, this radius implies a high stress drop of about 96 bars. Evidence in the amplitude data indicates that the polarization angle of shear waves is very sensitive to lateral structure.

A technique utilizing theoretical wave forms was developed to determine precise shear wave travel times. This technique was applied to long-period World-Wide Standard Seismograph Network and Canadian network seismograms of five large nuclear explosions to obtain a surface focus shear wave data set containing about 100 travel times for distances greater than 30°. Very

little scatter is present in the data from Novaya Zemlya and the Nevada test site, and so a reliable inversion to a lower mantle velocity structure is permitted. This velocity model, based on the 59 travel times from Novaya Zemlya, has significantly more structure than earlier models. The model, S1, has proved to be appropriate for free oscillations as well as for travel times. This model should be useful in studying both lateral inhomogeneities and the mineralogical composition of the earth's mantle.

For the period from 15 March 1975 to 30 September 1976 the principal investigators were D. G. Harkrider and D. V. Helmberger under the title "Body and Surface Wave Modeling of Observed Seismic Events." The following paragraphs are a summary of the semi-annual technical report. The details can be found in sections III through V.

In order to extend teleseismic body wave theory to more generalized sources than a point shear dislocation, it is convenient to express the source in a multipole form. An expansion of an outgoing linear elastic wave field in spherical harmonics provides an equivalent elastic source of quite general character and nearly any seismic source model can be written in this form. As long as the expansion is done in a linear homogenious region, potentials can be used to continue the solution in space and time in the region. In Section III the equivalent source is then embedded in a stack of plane elastic layers representing the near-source crustal structure and expressions are derived for computing the steeply emergent body waves existing at the base of the model. These displacements can then be combined with transfer functions representing the effect of the remainder of the travel path to compute theoretical seismograms for the body waves recorded in the far field. Using this technique teleseismic body waves have been calculated by other investigators for relaxation sources, and for non linear finite difference source calculations such as for a three-dimensional finite difference simulation of a strike-slip earthquake faulting and an explosion in an axisymmetric finite tunnel.

One of the interesting questions concerning the use of matrix methods in the source region is whether the assumption of plane uniform layers implicity requires a source region which is uniformly layered outside of the local source region in which teleseismic body waves are generated in Section IV, both ray theory and propagator matrix techniques were used to calculate synthetic seismograms for a point dislocation in a layered elastic medium. Both methods are equivalent and complementary for various model calculations. Ray theory has the advantage of giving a direct physical interpretation to observed phases. Matrix techniques, while exact in terms of including all multiples, gives little insight into the model but does serve as a check to the ray calculations. It can also be used as a tool for calculating the effect of gradients in the earth model by approximating them with many thin layers.

In Section V, a data set of forty-one moderate and large earthquakes has been used to derive scaling rules for kinematic fault parameters. If effective stress and static stress drop are equal, then fault rise time, τ, and fault area, S, are related by $\tau = 16S^{1/2}/(7\pi^{3/2}\beta)$, where β is shear velocity.

Fault length (parallel to strike) and width (parallel to dip) are empirically related by L - 2W. Scatter for both scaling rules is about a factor of two. These scaling laws combine to give width and rise time in terms of fault length. Length is then used as the sole free parameter in a Haskell type fault model to derive scaling laws relating seismic moment to M_s (20 sec. surface wave magnitude), M_s to S and m_b (1 sec body wave magnitude) to M_s. Observed data agree well with the predicted scaling relation. The "source spectrum" depends on both azimuth and apparent velocity of the phase or mode, so there is a different "source spectrum" for each mode, rather than a single spectrum for all modes. Furthermore, fault width (i.e. the two dimensionality of faults) must not be neglected. Inclusion of width leads to different average source spectra for surface waves and body waves. These spectra in turn imply that m_b and M_s reach maximum values regardless of further increases in L and seismic moment. The m_b:M_s relation from this study differs significantly from the Gutenberg-Richter relation, because the G-R equation was derived for body waves with a predominant period of about 5 sec and thus does not apply to modern 1 sec m_b determinations. Previous investigators who assumed that the G-R relation was derived from 1 sec data were in error. Finally averaging reported rupture velocities yields the relation $V_R = .72\beta$.

II. Abstracts of Publications Not Previously Reported During this Contract Period

Langston, C. A. and R. Butler, "Focal Mechanism of the August 1, 1975, Oroville Earthquake," Bull. Seismo. Soc. Am., 66, p. 1111-1120.

Long period teleseismic P and S waves from the WWSS and Canadian networks are modeled to determine the focal parameters for the main shock in the Oroville earthquake series. Using the techniques of P first motions, waveform synthesis, and phase identification the focal parameters are determined as follows: dip 65^{o}; rake -70^{o}; strike 180^{o}; depth 5.5 ± 1.5 km; moment $5.7 \pm 2.0 \times 10^{24}$ dyne-cm; and a symmetric triangular time function 3 sec. in duration. This is a north-south striking, westward dipping, normal fault with a small component of left-lateral motion. The time separation between the small foreshock and mainshock appears to be 6.5 sec. rather than 8.1 sec. as previously determined.

Chung, W. Y. and H. Kanamori, "Source Process and Tectonic Implications of the Spanish Deep Focus Earthquake of March 29, 1954," Earth and Planet. Sci. Letters, in press, 1976.

The source process of the deep-focus Spanish earthquake of March 29, 1954 (m_b = 7.1, h = 630 km) has been studied by using seismograms recorded at teleseismic distances. Because of its unusual location, this earthquake is considered to be one of the most important earthquakes that merit detailed studies. Long-period body wave records reveal that the earthquake is a complicated multiple event whose waveform is quite different from that of usual deep earthquakes. The total duration of P phases at teleseismic distances is as long as 40 seconds. This long duration may explain the considerable property damage in Granada and Malaga, Spain, which is rather rare for deep earthquakes. Using the azimuthal distribution of the differences between the arrival times of the first, the second and later P phases, the hypocenters of the later events are determined with respect to the first event. The focus of the second event is located on the vertical nodal plane of the first shock suggesting that this vertical plane is the fault plane. This fault plane which strikes in N 2° E and dips 89.1° E defines a nearly vertical dip-slip fault, the block to the west moving downwards. The time interval and spatial separation between the first and the second events are 4.3 sec and 19 km respectively, giving an apparent rupture velocity of 4.3 km/sec which is about 74% of the S wave velocity at the source. A third event occurred about 8.8 sec after the first event and about 35.6 km from it. At least 6 to 10 events can be identified during the whole sequence. The mechanism of some of the later events, however, seems to differ from the first two events. Synthetic seismograms are generated by superposition of a number of point sources and are matched with the observed signals to determine the seismic moment. The seismic moments of the later events are comparable to, or even larger than, that of the first. The total seismic moment is determined to be 7×10^{27} dyne-cm while the moments of the first and the second shocks are 2.1×10^{26} dyne-cm and 5.1×10^{26} dyne-cm respectively. The earthquake may respresent a series of fractures in a detached piece of the lithosphere which sank rapidly into the deep mantle preserving the heterogeneity of material property at shallow depths.

Geller, R. J., "Scaling Relations for Earthquake Source Parameters and Magnitudes," Bull. Seismo. Soc. Am., 66, 1501-1523, 1976.

A data set of 41 modertate and large earthquakes has been used to derive scaling rules for kinematic fault parameters. If effective stress and static stress drop are equal, then fault rise time, τ, and fault area, S, are related by $\tau = 16S^{1/2}/(7\pi^{3/2}\beta)$, where β is shear velocity. Fault length (parallel to strike) and width (parallel to dip) are empirically related by L = 2W. Scatter for both scaling rules is abut a factor of two. These scaling laws combine to give width and rise time in terms of fault length. Length is then used as the sole free parameter in a Haskell type fault model to derive scaling laws relating seismic moment to M_S (20-sec surface-wave magnitude), M_S to S and m_b (1-sec body-wave magnitude) to M_S. Observed data agree well with the predicted scaling relation. The "source spectrum" depends on both azimuth and apparent velocity of the phase or mode, so there is a different "source spectrum" for each mode, rather than a single spectrum for all modes. Furthermore, fault width (i.e. the two dimensionality of faults) must not be neglected. Inclusion of width leads to different average source spectra for surface waves and body waves. These spectra in turn imply that m_b and M_S reach maximum values regardless of further increases in L and seismic moment. The m_b versus M_S relation from this study differs significantly from the Gutenberg-Richter (G-R) relation, because the G-R equation was derived for body waves with a predominant period of about 5 sec and thus does not apply to modern 1-sec m_b determinations. Previous investigators who assumed that the G-R relation was derived from 1-sec data were in error. Finally, averaging reported rupture velocities yields the relation $v_R = 0.72\beta$.

Hart, R. S., D. L. Anderson and H. Kanamori, "Shear Velocity and Density of an Attenuating Earth," Earth and Planet. Sci. Letters, 32, 25-34, 1976.

The dispersion that must accompany absorption is taken into account in many recent body-wave investigations but has been largely ignored in surface-wave and free-oscillation studies. In order to compare body-wave and free-oscillation data a correction must be made to travel times or periods to account for absorption-related physical dispersion. The correction depends on the frequency and Q of the data and can be as high as 1% which is much larger than the uncertainty of the raw data. Corrected toroidal mode data is inverted to obtain shear velocity and density versus depth. The average shear velocity in the upper 600 km is $\sim$ 2% greater than obtained from the uncorrected data. The resulting shear-wave travel times oscillate about the Jeffreys-Bullen values with an average baseline of only +0.5 second. Thus, the discrepancy between body-wave and free-oscillation studies is eliminated.

Hill, D. P. and D. L. Anderson, "A Note on the Earth Stretching Approximation for Love Waves," Bull. Seismo. Soc. Am., in press, 1976.

Earth flattening transformations provide an efficient means for computing Love wave dispersion and torsional normal mode frequencies in radially heterogeneous, spherically symmetric earth models. These transformations involve simple algebraic scaling factors applied to solutions for SH waves in a layered

half-space. They result in considerable computational savings over solutions expressed directly in spherical geometry. Several earth flattening transformations for SH waves are described in the literature (Anderson and Toksoz, 1973; Sato, 1968, Biswas and Knopoff, 1970). Chapman (1973) has examined the general class of power-law earth flattening transformations and their application to body wave problems. In this note we clarify the earth-stretching approximation used by Anderson and Toksoz (1963).

III. The Body Waves Due to a General Seismic Source in a Layered Earth Model:

1. Formulation of the Theory

T. C. Bache and D. G. Harkrider

THE BODY WAVES DUE TO A GENERAL SEISMIC SOURCE IN A LAYERED EARTH MODEL: 1. FORMULATION OF THE THEORY

by

T. C. Bache

and

D. G. Harkrider

ABSTRACT

The radiation field exterior to any kind of volume source in a homogeneous medium can be represented in terms of an expansion in spherical harmonics. Such an expansion then provides an equivalent elastic source representation of quite general character in that nearly any proposed seismic source model, whether obtained using analytical or numerical (finite difference or finite element) methods, can be written in this form. The compatibility of this equivalent source with currently used source models, especially numerical models including detailed computations of the nonlinear processes at the source, is discussed. The equivalent source is then embedded in a stack of plane elastic layers representing the near-source crustal geology and expressions are derived for computing the steeply emergent body waves exiting the base of the model. These displacements can then be combined with transfer functions representing the effect of the remainder of the travel path to compute theoretical seismograms for the body waves recorded in the far field.

INTRODUCTION

A fundamental objective of theoretical seismology is the development of computational methods for accurately simulating the propagation of seismic waves through the earth. The last 10 - 15 years have seen intense activity aimed at the development of techniques for computing elastic waves in layered media. Widespread use is being made of such methods as generalized ray theory (e.g., Gilbert and Helmberger, 1972) and the reflectivity method (e.g., Fuchs and Müller, 1971) which can compute the far field body waves in a spherically stratified elastic earth model to almost any desired precision.

Concurrent with improvements in wave propagation techniques, vastly improved methods for simulating the seismic source (earthquake or explosion) have also come into extensive use. These include complex analytical source theories such as that of Archambeau (1968) as well as the use of numerical finite difference/finite element methods. The numerical methods, particularly the finite difference formulations, are now being applied in attempts to directly simulate the nonlinear processes at the source (e.g., Cherry, et al., 1976b).

Much of the data through which we view the seismic source is recorded in the far field and an important test of any source model is how well it agrees with the far field ground motion data. Therefore, it is necessary to have a bridge between the source calculations and the elastic wave

propagation techniques of theoretical seismology. That is, we need an equivalent elastic source.

An expansion of the outgoing elastic wave field in spherical harmonics provides an equivalent elastic source of quite general character and nearly any seismic source model can be written in this form. Harkrider and Archambeau (1976) derived the expressions for computing surface waves for such a source embedded in a stack of plane elastic layers. In this paper the corresponding theory for the steeply emergent body waves exiting the base of this plane layered model is given. The derivation is closely related to that of Fuchs (1966) and Hudson (1969a,b) who treated a similar problem except that their source was assumed to be given in terms of elementary point forces and their derivatives. Our results are, of course, completely equivalent where the source representations coincide.

In the following section the form of the equivalent elastic source and its compatibility with analytical and numerical source calculations is discussed. Subsequent sections contain the derivation of the far field body waves for such a source in a layered elastic medium. Finally, we briefly discuss the computation of theoretical body wave seismograms, using this formulation for the seismic source and crust in the source vicinity together with other methods for simulating the rest of the travel path. In a companion paper (Bache and Archambeau, 1976), the theoretical seismogram calculations are discussed in greater detail and a number of examples are given.

EQUIVALENT ELASTIC SOURCE

The radiation field exterior to any kind of volume source in a homogeneous medium can be represented in terms of an expansion in spherical harmonics. Archambeau (1968) seems to have been the first to recognize the usefulness of this fundamental result and to apply it to geophysical problems. The expansion in spherical harmonics gives a compact equivalent elastic source representation of quite general character and nearly any proposed seismic source model can be cast in this form. A brief description of this source representation and its compatibility with commonly used source theories is the subject of this section.

The Fourier transformed equations of motion in a homogeneous, isotropic, linearly elastic medium may be written

$$\underset{\sim}{\bar{u}} = -\left(\frac{1}{k_\alpha^2}\right)\nabla\bar{\chi}^{(4)} + \left(\frac{2}{k_\beta^2}\right)\nabla \times \underset{\sim}{\bar{\chi}} \quad , \tag{1}$$

where $\underset{\sim}{\bar{u}}$ is particle displacement and k_α and k_β are the compressional and shear wave numbers. The Cartesian potentials $\bar{\chi}^{(4)}$ and $\underset{\sim}{\bar{\chi}}$ are defined by

$$\begin{aligned} \bar{\chi}^{(4)} &= \nabla \cdot \underset{\sim}{\bar{u}} \quad , \\ \underset{\sim}{\bar{\chi}} &= \frac{1}{2}\nabla \times \underset{\sim}{\bar{u}} \quad , \end{aligned} \tag{2}$$

and may be easily shown to satisfy the wave equation

$$\nabla^2\bar{\chi}^{(j)} + k_i^2\bar{\chi}^{(j)} = 0, \; j = 1, 2, 3, 4, \tag{3}$$

where $k_4 \equiv k_\alpha = \omega/\alpha$ and $k_i \equiv k_\beta = \omega/\beta$ for i = 1,2,3. This equation has as a solution the following expansion in spherical eigenfunctions (e.g., Morse and Feshbach (1953)),

$$\underset{\sim}{\chi}^{(j)}(\underset{\sim}{R},\omega) = \sum_{\ell=0}^{\infty} h_\ell^{(2)}(k_j R) \sum_{m=0}^{\ell} \left[A_{\ell m}^{(j)}(\omega) \cos m\phi + B_{\ell m}^{(j)}(\omega) \sin m\phi \right] P_\ell^m(\cos\theta) \quad , \tag{4}$$

where the $h_\ell^{(2)}$ are spherical Hankel functions of the second kind and the P_ℓ^m are associated Legendre functions. The vector $\underset{\sim}{R}$ has as components the spherical coordinates R,θ,ϕ.

Equations (4), together with (1), provide an elastic point source representation of the (outgoing) displacement field. The values of the multipole coefficients, $A_{\ell m}^{(j)}(\omega)$, $B_{\ell m}^{(j)}(\omega)$, j = 1,2,3,4, prescribe the displacement field at all points in the homogeneous medium where (1) applies. This point source representation can be viewed as a generalized form for a sum of a monopole or center of dilatation (ℓ = 0), a dipole or couple (ℓ = 1), a quadrupole or double-couple (ℓ = 2), etc. For example, a center of dilatation is represented by a single coefficient $A_{00}^{(4)}$, while for a horizontal double-couple the nonzero coefficients are $-A_{21}^{(1)} = B_{21}^{(2)} = A_{22}^{(3)}$ and $B_{22}^{(4)}$.

Description of the character of the elastic field generated by seismic sources is, of course, a basic geophysical problem. For this paper it is convenient to discuss seismic source descriptions in three categories:

1. Those obtained using finite difference/finite element numerical methods.
2. Analytical source models of relaxation type.
3. Dislocation source models.

With numerical methods one can attempt to directly include complexities of the source mechanism in a deterministic computational scheme. For example, finite difference methods have been extensively used to compute the propagating shock wave due to an underground nuclear explosion (e.g., Cherry, et al., 1974). In this case the nonlinear behavior of the rock under high stress loading determines the character of the seismic signal. If the source region can be assumed to be embedded in a medium in which (1) applies, an equivalent elastic source of the form (4) can be obtained from the outgoing displacement field. This is indicated schematically in Figure 1. Briefly, the procedure is to monitor the outgoing displacement field or, alternatively, the potentials, $\bar{\chi}^{(j)}$, on a spherical surface of radius $\hat{R}$. Using the orthogonality of the spherical harmonics, these potentials are related to the multipole coefficients by

$$\begin{Bmatrix} A_{\ell m}^{(j)}(\omega) \\ B_{\ell m}^{(j)}(\omega) \end{Bmatrix} = \frac{C_{\ell m}}{h_\ell^{(2)}(k_j \hat{R})} \int_0^{2\pi} \int_0^{\pi} \bar{\chi}^{(j)}(\hat{R},\omega)\, P_\ell^m(\cos\theta) \begin{Bmatrix} \cos m\phi \\ \sin m\phi \end{Bmatrix} \sin\theta d\theta d\phi, \tag{5}$$

where

$$C_{\ell m} = \frac{(2\ell+1)(\ell-m)!}{2\pi(\ell+m)}, \quad m \neq 0,$$

$$C_{\ell_0} = (2\ell+1)/4\pi .$$

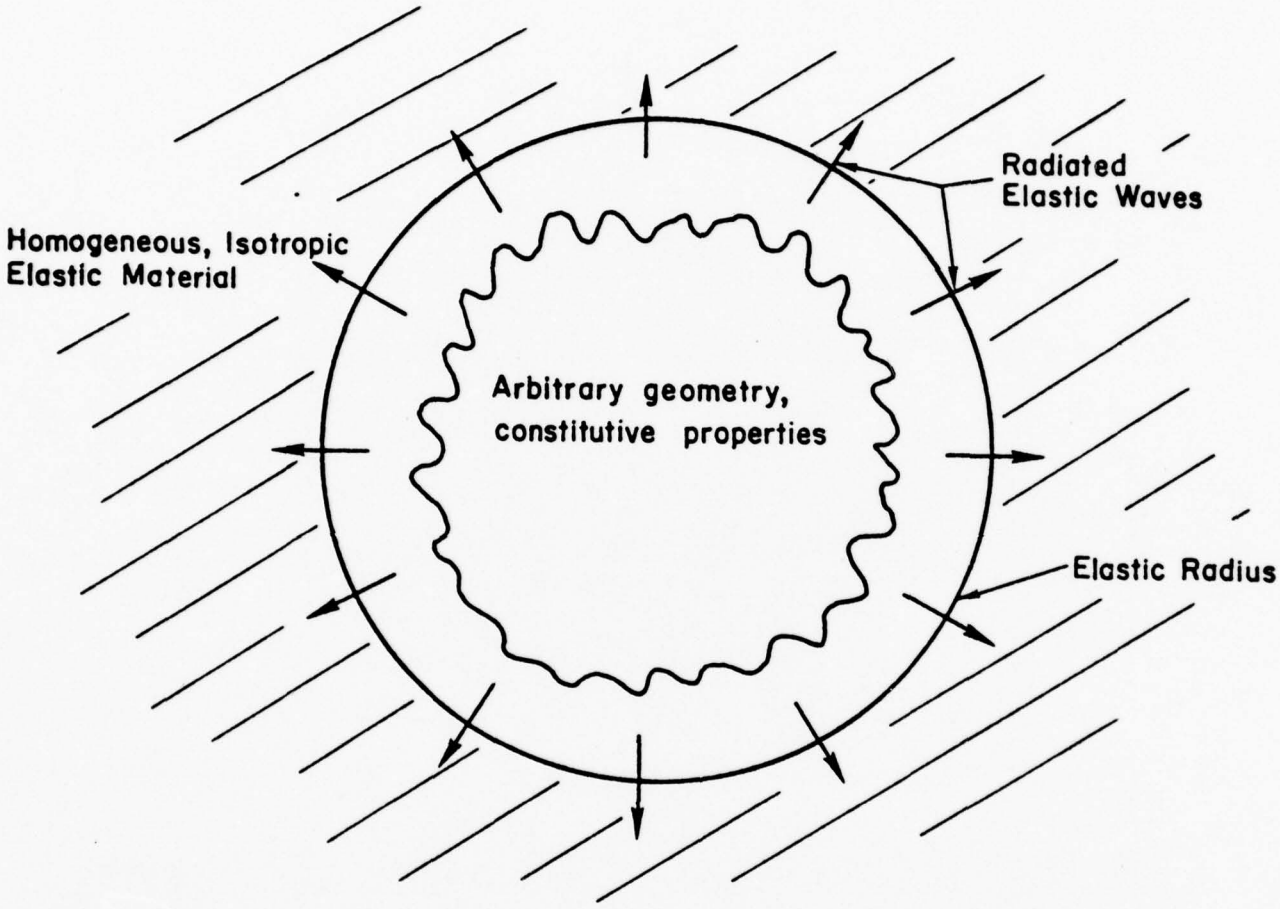

Figure 1. Schematic display of the determination of an equivalent elastic representation for an arbitrary volume source.

Use of this procedure for linking nonlinear finite difference source calculations with analytical wave propagation techniques was suggested to the first author by Archambeau (1973, personal communication), and has since been implemented for a number of complex explosion geometries (Cherry, et al., 1975, 1976a), and for a three-dimensional finite difference simulation of stick-slip earthquake faulting (Cherry, et al., 1976b). The number of terms required for the expansion (4) to converge depends on the symmetry of the source radiation at frequencies of interest. The most elementary application of the method is for one-dimensional (spherically symmetric) explosion source calculations. For such problems the elastic field is often described by a reduced displacement potential defined by

$$U(R,t) = \frac{\partial}{\partial R}\left[\frac{\Psi(t-R/\alpha)}{R}\right] . \qquad (6)$$

Applying the Fourier transform and comparing to (1) together with (4), it is easily derived that

$$A_{00}^{(4)}(\omega) = -i\, k_\alpha^3\, \overline{\Psi}(\omega) , \qquad (7)$$

which shows the equivalence between the reduced displacement potential and the monopole. For more complex sources such as an explosion in an axisymmetric tunnel (Cherry, et al., 1975) or several explosions detonated simultaneously (Cherry, et al., 1976a) quadrupole and higher order terms occur in the expansion. When an earthquake source is computed, the

leading term is, as expected, the quadrupole (Cherry, et al., 1976b).

Three-dimensional relaxation models of the seismic source mechanism have been developed by Archambeau (1968, 1972) and Minster (1973). These authors present their results in terms of an expansion in spherical harmonics. One form of Archambeau's model has been used in a number of studies of induced tectonic stress release by underground nuclear explosions (Archambeau and Sammis, 1970; Archambeau, 1972; Bache, 1976). In this symmetric problem only the quadrupole term occurs in the expansion. When the Archambeau/Minster model is used to represent propagating ruptures (earthquakes), many terms may be required for the expansion (4) to converge, depending on fault length, rupture velocity and frequency.

The most common approach to earthquake source theory is to assume that dislocation theory is applicable (e.g., Haskell, 1964; Savage, 1966). Such theories generally represent the source in terms of a double-couple with frequency content depending on the dislocation time history assumed. Harkrider (1976) has given the expressions relating dislocation source theories to the expansion in spherical harmonics (4). For a horizontal double-couple (normal strike-slip fault) Harkrider (1976), Equation (36), gives the Cartesian potentials as

$$\bar{\Phi} = -i \frac{\mu \bar{D}(\omega)}{4\pi\rho\omega^2} k_\alpha^3 \sin 2\phi \frac{P_2^2(\cos\theta)}{3} h_2^{(2)}(k_\alpha R) ,$$

$$\bar{\Psi}_1 = -i \frac{\mu \bar{D}(\omega)}{4\pi\rho\omega^2} k_\beta^3 \cos\phi \frac{P_2^1(\cos\theta)}{3} h_2^{(2)}(k_\beta R) ,$$

$$\bar{\Psi}_2 = i \frac{\mu \bar{D}(\omega)}{4\pi\rho\omega^2} k_\beta^3 \sin\phi \frac{P_2^1(\cos\theta)}{3} h_2^{(2)}(k_\beta R) , \qquad (8)$$

$$\bar{\Psi}_3 = i \frac{\mu \bar{D}(\omega)}{4\pi\rho\omega^2} k_\beta^3 \cos 2\phi \frac{P_2^2(\cos\theta)}{3} h_2^{(2)}(k_\beta R) ,$$

where ρ and μ are the density and shear modulus, and $\bar{D}(\omega)$ represents the Fourier transformed dislocation time history. The implied dimensions of these potentials are per unit fault area. The results can be generalized to finite faults by introducing an integration over the fault surface. For fault models on which the dislocation history is invariant and the variation of phase between dislocation points and observer is negligible over the fault plane, (8) multiplied by the fault area are the potentials for a normal strike-slip fault.

The Cartesian potentials ($\bar{\Phi}$, $\bar{\underset{\sim}{\Psi}}$) are related to the displacements by

$$\bar{\underset{\sim}{u}} = \nabla\bar{\Phi} + \nabla \times \bar{\underset{\sim}{\Psi}} . \qquad (9)$$

Comparing to (1), we see that

$$\bar{\chi}^{(4)} = -k_\alpha^2 \bar{\Phi} ,$$

$$\bar{\underset{\sim}{\chi}} = \frac{k_\beta^2}{2} \bar{\underset{\sim}{\Psi}} . \qquad (10)$$

Using (10) and comparing (8) to (4), the multipole coefficients for the normal strike-slip dislocation are:

$$B_{22}^{(4)}(\omega) = \frac{i\mu\,\bar{D}(\omega)\,k_\alpha^3}{12\pi(\lambda+2\mu)}\,,$$

$$A_{21}^{(1)}(\omega) = \frac{-i\,\bar{D}(\omega)\,k_\beta^3}{24\pi}\,, \qquad (11)$$

$$B_{21}^{(2)}(\omega) = A_{22}^{(3)}(\omega) = -A_{21}^{(1)}(\omega)\,.$$

Expressions from which the multipole coefficients for a double-couple at arbitrary orientation can be obtained are given by Harkrider (1976), Appendix A.

Whether the seismic source is modeled by numerical methods or analytical theories, the multipole coefficients provide a computationally convenient equivalent elastic source. Thus far, the discussion has been restricted to the multipolar expansion with respect to a coordinate system fixed with respect to the source. Minster (1973) gives the transformation matrices by which the multipole coefficients in a standard coordinate system (e.g., fixed with respect to the surface of the earth) may be obtained from any rotated system. Using these results, multipole coefficients can be computed in a convenient source related system and then rotated to a fixed geographical system.

In the following section the equivalent elastic source in the form discussed here will be embedded in a multilayered medium and we will derive the expressions for computing the steeply emergent, far field body waves.

THE EQUIVALENT ELASTIC SOURCE IN A MULTILAYERED HALFSPACE

A number of authors have investigated the elastic waves radiating from point sources in a multilayered medium overlying a homogeneous halfspace. Most of these studies have relied on Thomson-Haskell matrix theory (Thomson, 1950; Haskell, 1953) as will our derivation. Harkrider (1964) developed solutions for surface waves due to elementary point forces at depth. Fuchs (1966) derived transfer functions which include the effect of the layered crustal model on the far field P waves from three types of sources: a center of dilatation, a couple and a double-couple. Hudson (1969a,b) extended Fuchs' body wave results to apply to quite general sources of finite extent and derived the analogous theory for surface waves. However, in all these theories the source representation is in terms of elementary point forces and their derivatives. The representation in this form of complicated sources (including terms of higher order than the double-couple) at arbitrary orientation would appear to be an arduous task. Thus, the usefulness of these previous results, especially for routine numerical computations, seems to be limited by the inherent complexity of the source representation.

The multipolar expansion discussed in the previous section provides a unique, compact and convenient numerical representation for seismic sources of arbitrary complexity and orientation. Harkrider and Archambeau (1976) have computed the

surface waves for a source given in this form embedded in a multilayered medium. This required the formulation of the displacement field in terms of integrals over wave number, k. The surface waves are then given by the residue contribution to these integrals. For the body waves it is necessary to evaluate the branch line contribution to similar integrals and this is the main result presented here. Derivation of the k integrals in the appropriate form follows closely the derivations of Harkrider (1964) and Harkrider and Archambeau (1976) and the notation is, for the most part, the same. It should be pointed out that our results are completely equivalent to those of Hudson (1969a,b). The difference is, of course, in the source representation.

Consider a semi-infinite elastic medium made up of n parallel, homogeneous, isotropic elastic layers. Number the layers from 1 at the free surface to n for the underlying halfspace. Place the origin of a cylindrical coordinate system (r,ϕ,z) at the free surface and denote the layer interfaces by z_i, $i = 1,2, \ldots, n-1$. This geometry is depicted in Figure 2. Let $(\bar{q}_i, \bar{v}_i, \bar{w}_i)$ be the components of the Fourier transformed displacements in the (r,ϕ,z) directions in the ith layer. Then, following Harkrider (1964), the cylindrical potentials $\bar{\phi}_i$, $\bar{\psi}_i$, $\bar{\Omega}_i$ are defined by

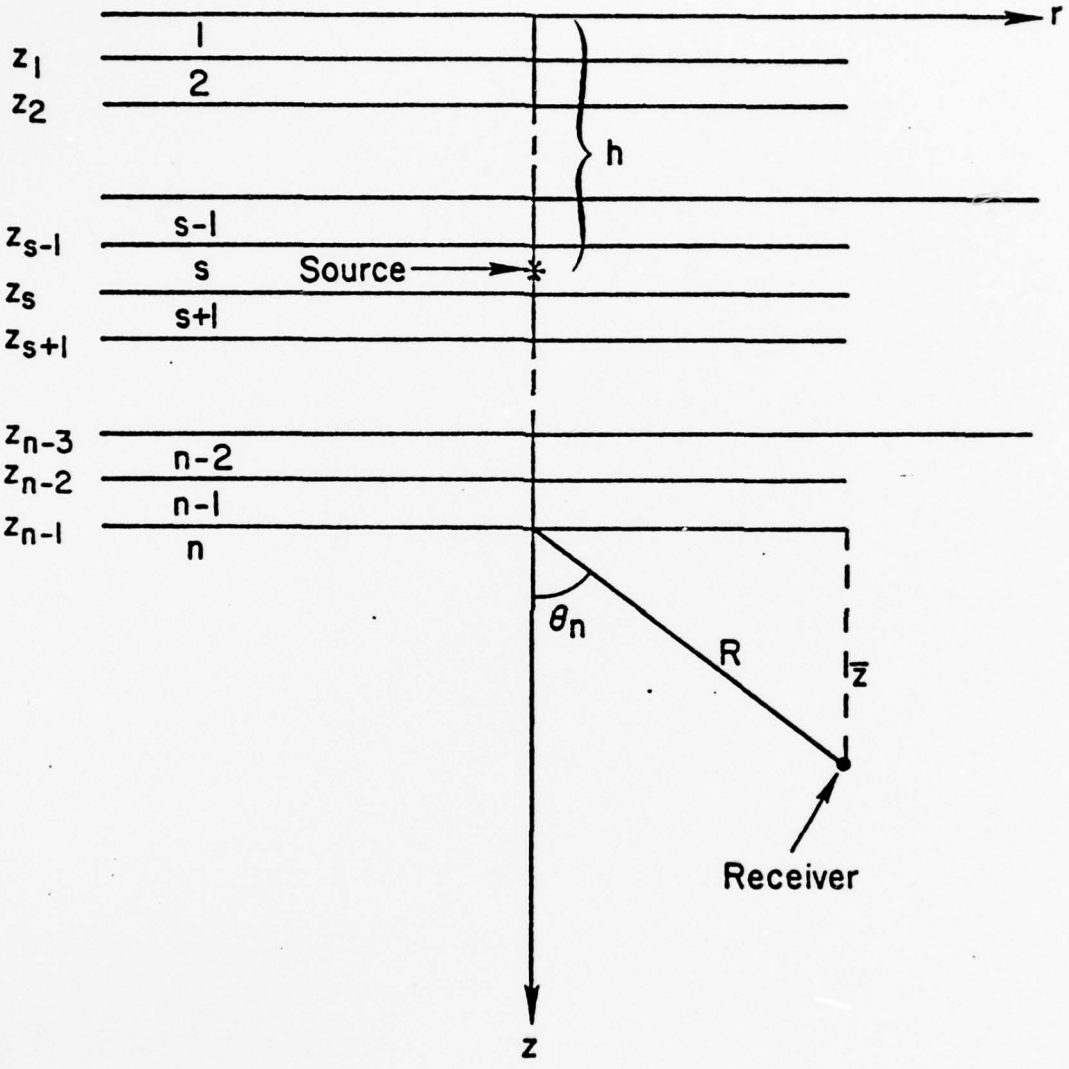

Figure 2. The geometry and coordinate system for a source at depth h in a multilayered halfspace.

$$\bar{q}_i(r,\phi,z) = \frac{\partial \bar{\Phi}_i}{\partial r} + \frac{\partial^2 \bar{\Psi}_i}{\partial r \partial z} + \frac{1}{r}\frac{\partial \bar{\Omega}_i}{\partial \phi} ,$$

$$\bar{v}_i(r,\phi,z) = \frac{1}{r}\frac{\partial \bar{\Phi}_i}{\partial \phi} + \frac{1}{r}\frac{\partial^2 \bar{\Psi}_i}{\partial z \partial \phi} - \frac{\partial \bar{\Omega}_i}{\partial r} . \qquad (12)$$

$$\bar{w}_i(r,\phi,z) = \frac{\partial \bar{\Phi}_i}{\partial z} + \frac{\partial^2 \bar{\Psi}_i}{\partial z^2} + k_{\beta_i}^2 \bar{\Psi}_i, \quad i = 1,2, \ldots, n.$$

We will subsequently be interested in an equivalent elastic point source at a depth z = h. Let the source layer be denoted by a subscript s; that is, $z_s < h < z_{s-1}$. It is necessary to express the cylindrical potentials ($\bar{\Phi}_s$, $\bar{\Psi}_s$, $\bar{\Omega}_s$) in the source layer in terms of the spherical potentials, $\bar{\chi}^{(j)}$, from (4). The equivalence is given by Harkrider and Archambeau (1976) and is as follows:

$$\bar{\Phi}_s = \sum_{m=0}^{\ell} \int_0^{\infty} \left\{ \bar{A}_m \cos m\phi + \bar{B}_m \sin m\phi \right\} \frac{e^{-ikr_\alpha |z-h|}}{r_\alpha} J_m(kr)\,dk ,$$

$$\bar{\Psi}_s = \sum_{m=0}^{\ell} \int_0^{\infty} \left\{ \bar{E}_m \cos m\phi + \bar{F}_m \sin m\phi \right\} \frac{e^{-ikr_\beta |z-h|}}{r_\beta} J_m(kr)\,dk , \qquad (13)$$

$$\bar{\Omega}_s = \sum_{m=0}^{\ell} \int_0^{\infty} \left\{ \bar{C}_m^{(3)} \cos m\phi + \bar{D}_m^{(3)} \sin m\phi \right\} \frac{e^{-ikr_\beta |z-h|}}{r_\beta} \frac{J_m(kr)}{k^2}\,dk ,$$

where

$$\bar{A}_m = -\frac{1}{k_\alpha^3} \sum_{\ell=m}^{\infty} (i)^{m-n}[\mathrm{sgn}(h-z)]^{m+\ell} A_{\ell m}^{(4)} (-1)^{m+n} P_\ell^m\left(\frac{kr_\alpha}{k_\alpha}\right) ,$$

$$\bar{B}_m = -\frac{1}{k_\alpha^3} \sum_{\ell=m}^{\infty} (i)^{m-n}[\mathrm{sgn}(h-z)]^{m+\ell} B_{\ell m}^{(4)} (-1)^{m+n} P_\ell^m\left(\frac{kr_\alpha}{k_\alpha}\right) , \tag{14}$$

$$\bar{C}_m^{(j)} = \frac{2}{k_\beta^3} \sum_{\ell=m}^{\infty} (i)^{m-n}[\mathrm{sgn}(h-z)]^{m+\ell} A_{\ell m}^{(j)} (-1)^{m+n} P_\ell^m\left(\frac{kr_\beta}{k_\beta}\right) ,$$

$$\bar{D}_m^{(j)} = \frac{2}{k_\beta^3} \sum_{\ell=m}^{\infty} (i)^{m-n}[\mathrm{sgn}(h-z)]^{m+\ell} B_{\ell m}^{(j)} (-1)^{m+n} P_\ell^m\left(\frac{kr_\beta}{k_\beta}\right) ,$$

where $j = 1,2,3$ *in the definitions of* $\bar{C}_m^{(j)}$, $\bar{D}_m^{(j)}$, *and*

$$k = \omega/c,\ k_\gamma = \omega/\gamma ,$$

$$r_\gamma = (c^2/\gamma^2 - 1)^{1/2} ,\ \gamma = \alpha \text{ or } \beta , \tag{15}$$

c = horizontal phase velocity.

The coefficients $\bar{E}_m$, $\bar{F}_m$ in the expression for $\bar{\psi}_s$ are related to the $\bar{C}_m^{(j)}$, $\bar{D}_m^{(j)}$ by:

$$2k\bar{E}_0 = \bar{C}_1^{(2)} - \bar{D}_1^{(1)} ,\ \bar{F}_0 = 0 ,$$

$$2k\bar{E}_1 = \bar{C}_2^{(2)} - \bar{D}_2^{(1)} - 2\bar{C}_0^{(2)} , \tag{16}$$

$$2k\bar{F}_1 = \bar{C}_2^{(1)} + \bar{D}_2^{(2)} + 2\bar{C}_0^{(1)} ,$$

and, taking $\bar{C}_m^{(i)} = D_m^{(j)} = 0$ for $m > \ell$,

$$2k\bar{E}_m = \bar{C}_{m+1}^{(2)} - \bar{C}_{m-1}^{(2)} - \bar{D}_{m+1}^{(1)} - \bar{D}_{m-1}^{(1)} \quad ,$$

$$2k\bar{F}_m = \bar{C}_{m+1}^{(1)} + \bar{C}_{m-1}^{(1)} + \bar{D}_{m+1}^{(2)} - \bar{D}_{m-1}^{(2)} \quad , \quad 2 \leq m \leq \ell \ .$$

Since the location of material boundaries depends only on z, the dependence on r and ϕ will be everywhere the same as in the source layer. Therefore, separate the potentials in the layers as follows:

$$\begin{Bmatrix} \bar{\Phi}_i(r,\phi,z) \\ \bar{\Psi}_i(r,\phi,z) \\ \bar{\Omega}_i(r,\phi,z) \end{Bmatrix} = \sum_{m=0}^{\ell} \int_0^{\infty} \begin{Bmatrix} \Phi_i^{(m)}(\phi,z) \\ \Psi_i^{(m)}(\phi,z) \\ \Omega_i^{(m)}(\phi,z) \end{Bmatrix} J_m(kr)dk \ , \qquad (17)$$

$i = 1, 2, \ldots, n.$

The potentials $\Phi_i^{(m)}$, $\Psi_i^{(m)}$, $\Omega_i^{(m)}$ satisfy wave equations for which the general solutions may be written:

$$\Phi_i^{(m)}(\phi,z) = \tilde{\Delta}_i^{(m)} e^{-ikr_{\alpha_i}z} + \tilde{\Delta}_i^{(m)'} e^{ikr_{\alpha_i}z} \ ,$$

$$\Psi_i^{(m)}(\phi,z) = \tilde{\omega}_i^{(m)} e^{-ikr_{\beta_i}z} + \tilde{\omega}_i^{(m)'} e^{ikr_{\beta_i}z} \ , \qquad (18)$$

$$\Omega_i^{(m)}(\phi,z) = \tilde{\varepsilon}_i^{(m)} e^{-ikr_{\beta_i}z} + \tilde{\varepsilon}_i^{(m)'} e^{ikr_{\beta_i}z} \ .$$

In (18) and subsequent equations subscripts i, $i = 1,2, \ldots, n$, denote quantities in the ith layer.

Then, define

$$\hat{\Delta}_i^{(m)} = - k^2 \left(\frac{c}{\alpha_i}\right)^2 e^{-kr\alpha_i z_{i-1}} \tilde{\Delta}_i^{(m)} ,$$

$$\hat{\omega}_i^{(m)} = \frac{ik^3}{\gamma_i} e^{-ikr\beta_i z_{i-1}} \tilde{\omega}_i^{(m)} , \qquad (19)$$

$$\hat{\varepsilon}_i^{(m)} = k\, e^{-ikr\beta_i z_{i-1}} \tilde{\varepsilon}^{(m)} .$$

We will subsequently be interested in the values of the potential in the halfspace (i = n). Applying the radiation condition at infinity, (18) and (19) give

$$\phi_n^{(m)}(\phi,z) = - \frac{1}{k_{\alpha_n}^2} e^{-ikr\alpha_n \bar{z}} \hat{\Delta}_n^{(m)} ,$$

$$\psi_n^{(m)}(\phi,z) = - \frac{i\gamma_n}{k^3} e^{-ikr\beta_n \bar{z}} \hat{\omega}_n^{(m)} , \qquad (20)$$

$$\Omega_n^{(m)}(\phi,z) = \frac{1}{k} e^{-ikr\beta_n \bar{z}} \hat{\varepsilon}_n^{(m)} ,$$

where

$$\bar{z} = z - z_{n-1} ,$$

$$\gamma_i = 2\beta_i^2/c^2 . \qquad (21)$$

Now, combining (17) and (20), we have:

$$\bar{\Phi}_n(r,\phi,z) = \sum_{m=0}^{\ell} \int_0^{\infty} \left(-\frac{1}{k_{\alpha_n}^2}\right) \hat{\Delta}_n^{(m)} \, e^{-ikr_{\alpha_n}\bar{z}} \, J_m(kr)dk \, ,$$

$$\bar{\Psi}_n(r,\phi,z) = \sum_{m=0}^{\ell} \int_0^{\infty} -\frac{i}{k}\left(\frac{2}{k_\beta^2}\right) \hat{\omega}_n^{(m)} \, e^{-ikr_{\beta_n}\bar{z}} \, J_m(kr)dk, \tag{22}$$

$$\bar{\Omega}_n(r,\phi,z) = \sum_{m=0}^{\ell} \int_0^{\infty} \frac{1}{k} \hat{\varepsilon}_n^{(m)} \, e^{-ikr_{\beta_n}\bar{z}} \, J_m(kr)dk \, .$$

In equations (22) we now have the cylindrical potentials $\bar{\Phi}_n$, $\bar{\Psi}_n$, $\bar{\Omega}_n$, in the nth layer (halfspace) in terms of a sum of integrals of the Sommerfeld type. The coefficients $\hat{\Delta}_n^{(m)}$, $\hat{\omega}_n^{(m)}$, $\hat{\varepsilon}_n^{(m)}$ depend on azimuth, ϕ, as well as wave number, k, and include the modification of the source generated pulse by the material discontinuities in the layered halfspace. Following Harkrider (1964, Eqs. (62) and (122)), these coefficients are solutions of the matrix equations:

$$\begin{bmatrix} \hat{\Delta}_n^{(m)} \\ \hat{\Delta}_n^{(m)} \\ \hat{\omega}_n^{(m)} \\ \hat{\omega}_n^{(m)} \end{bmatrix} = J^R \left\{ \begin{bmatrix} \dot{u}_{R_1}(0)/c \\ \dot{w}_{R_1}(0)/c \\ 0 \\ 0 \end{bmatrix} + A_{R_{S1}}^{-1} \begin{bmatrix} \delta U_m \\ \delta W_m \\ \delta Z_m \\ \delta X_m \end{bmatrix} \right\} ,$$

$$\begin{bmatrix} \hat{\varepsilon}_n^{(m)} \\ \hat{\varepsilon}_n^{(m)} \end{bmatrix} = J^L \left\{ \begin{bmatrix} \dot{v}_{L_1}(0)/c \\ 0 \end{bmatrix} + A_{L_{S1}}^{-1} \begin{bmatrix} \delta V_m \\ \delta Y_m \end{bmatrix} \right\} , \tag{23}$$

where the J^R and J^L are given by Equations (61) and (124) of Harkrider (1964). The matrix $A_{R_{S1}}$ is defined by Harkrider and is the layer product matrix which gives the displacement-stress vector for P - SV motion at the source depth in terms of the displacement-stress vector at the surface. Similarly, $A_{L_{S1}}$ is the transfer matrix for the displacement-stress vector associated with SH motion.

The source terms in (23) are given by Harkrider and Archambeau (1976) as follows:

$$
\begin{aligned}
\delta U_m &= \delta \left(\frac{\dot{u}_s}{c} \right)_m^c \cos m\phi + \delta \left(\frac{\dot{u}_s}{c} \right)_m^s \sin m\phi \quad , \\
\delta W_m &= \delta \left(\frac{\dot{w}_s}{c} \right)_m^c \cos m\phi + \delta \left(\frac{\dot{w}_s}{c} \right)_m^s \sin m\phi \quad , \\
\delta Z_m &= \delta \sigma_m^c \cos m\phi + \delta \sigma_m^s \sin m\phi \quad , \\
\delta X_m &= \delta \tau_{Rm}^c \cos m\phi + \delta \tau_{Rm}^s \sin m\phi \quad , \\
\delta V_m &= \delta \left(\frac{\dot{v}_s}{c} \right)_m^c \cos m\phi + \delta \left(\frac{\dot{v}_s}{c} \right)_m^s \sin m\phi \quad , \\
\delta Y_m &= \delta \tau_{Lm}^c \cos m\phi + \delta \tau_{Lm}^s \sin m\phi \quad ,
\end{aligned}
\tag{24}
$$

where

$$\delta\left(\frac{\dot{u}_s}{c}\right)^c_m = 2k^2\left[\frac{\overline{A}^o_m}{r_\alpha} - ik\,\overline{E}^e_m\right] ,$$

$$\delta\left(\frac{\dot{u}_s}{c}\right)^s_m = 2k^2\left[\frac{\overline{B}^o_m}{r_\alpha} - ik\,\overline{F}^e_m\right] ,$$

$$\delta\left(\frac{\dot{w}_s}{c}\right)^c_m = 2k^2\left[\overline{A}^e_m + ik\,\frac{\overline{E}^o_m}{r_\beta}\right] ,$$

$$\delta\left(\frac{\dot{w}_s}{c}\right)^s_m = 2k^2\left[\overline{B}^e_m + ik\,\frac{\overline{F}^o_m}{r_\beta}\right] ,$$

$$\delta\sigma^c_m = 2\rho c^2k^2\left[(\gamma-1)\,\frac{\overline{A}^o_m}{r_\alpha} - ik\gamma\,\overline{E}^e_m\right] ,$$

$$\delta\sigma^s_m = 2\rho c^2k^2\left[(\gamma-1)\,\frac{\overline{B}^o_m}{r_\alpha} - ik\gamma\,\overline{F}^e_m\right] ,$$

$$\delta\tau^c_{Rm} = 2\rho c^2k^2\left[-\gamma\overline{A}^e_m - ik(\gamma-1)\,\frac{\overline{E}^o_m}{r_\beta}\right] ,$$

$$\delta\tau^s_{Rm} = 2\rho c^2k^2\left[-\gamma\overline{B}^e_m - ik(\gamma-1)\,\frac{\overline{F}^o_m}{r_\beta}\right] \qquad (25)$$

$$\delta\left(\frac{\dot{v}_s}{c}\right)^c_m = i2k^2_\beta\,\frac{\overline{C}^{(3)o}_m}{r_\beta} ,$$

$$\delta\left(\frac{\dot{v}_s}{c}\right)^s_m = i2k^2_\beta\,\frac{\overline{D}^{(3)o}_m}{r_\beta} ,$$

$$\delta\tau^c_{Lm} = -\,i2k^2_\beta\mu\,\overline{C}^{(3)e}_m ,$$

$$\delta\tau^s_{Lm} = -\,i2k^2_\beta\mu\,\overline{D}^{(3)e}_m .$$

The quantities r_α, r_β, ρ, μ, γ, k_β refer to the layer in which the source occurs, with ρ and μ being the density and shear modulus. The coefficients $\bar{A}_m$, $\bar{B}_m$, etc. are given by (14) with the following modification. The series are separated into two parts;

$$\bar{A}_m = \bar{A}_m^e + \bar{A}_m^o \ , \tag{26}$$

with the e superscript denoting a series made up of terms with $m + \ell$ even and the o superscript denoting a similar series from terms with $m + \ell$ odd.

Equations (23) may be viewed as a set of simultaneous linear algebraic equations and solved for $\hat{\Delta}_n^{(m)}$, $\hat{\omega}_n^{(m)}$, $\hat{\varepsilon}_n^{(m)}$ in terms of known quantities. The result is:

$$\begin{aligned}
2\hat{\Delta}_n^{(m)} &= \left\{ R_1\left(J^R_{11}+J^R_{21}\right) - R_2\left(J^R_{12}+J^R_{22}\right) + J^R_{13}+J^R_{23} \right\} Y_m \\
&\quad + \left\{ R_3\left(J^R_{11}+J^R_{21}\right) - R_4\left(J^R_{12}+J^R_{22}\right) + J^R_{14}+J^R_{24} \right\} Z_m \ , \\
2\hat{\omega}_n^{(m)} &= \left\{ R_1\left(J^R_{31}+J^R_{41}\right) - R_2\left(J^R_{32}+J^R_{42}\right) + J^R_{33}+J^R_{43} \right\} Y_m \\
&\quad + \left\{ R_3\left(J^R_{31}+J^R_{41}\right) - R_4\left(J^R_{32}+J^R_{42}\right) + J^R_{34}+J^R_{44} \right\} Z_m \ , \\
\hat{\varepsilon}_n^{(m)} &= L_1 X_m \ ,
\end{aligned} \tag{27}$$

where

$$F_{R}R_{1} = \left(J^{R}_{13} - J^{R}_{23}\right)\left(J^{R}_{32} - J^{R}_{42}\right) - \left(J^{R}_{12} - J^{R}_{22}\right)\left(J^{R}_{33} - J^{R}_{43}\right) \quad ,$$

$$F_{R}R_{2} = \left(J^{R}_{13} - J^{R}_{23}\right)\left(J^{R}_{31} - J^{R}_{41}\right) - \left(J^{R}_{11} - J^{R}_{21}\right)\left(J^{R}_{33} - J^{R}_{43}\right) \quad ,$$

$$F_{R}R_{3} = \left(J^{R}_{14} - J^{R}_{24}\right)\left(J^{R}_{32} - J^{R}_{42}\right) - \left(J^{R}_{12} - J^{R}_{22}\right)\left(J^{R}_{34} - J^{R}_{44}\right) \quad ,$$

$$F_{R}R_{4} = \left(J^{R}_{14} - J^{R}_{24}\right)\left(J^{R}_{31} - J^{R}_{41}\right) - \left(J^{R}_{11} - J^{R}_{21}\right)\left(J^{R}_{34} - J^{R}_{44}\right) \quad ,$$

$$F_{R} = \left(J^{R}_{12} - J^{R}_{22}\right)\left(J^{R}_{31} - J^{R}_{41}\right) - \left(J^{R}_{11} - J^{R}_{21}\right)\left(J^{R}_{32} - J^{R}_{42}\right) \quad ,$$

$$L_{1} = \left(J^{L}_{11}J^{L}_{22} - J^{L}_{12}J^{L}_{21}\right) \Big/ \left(J^{L}_{11} - J^{L}_{21}\right) \quad ,$$

and

$$Y_{m} = \left(A_{R_{S1}}\right)_{42}\delta U_{m} - \left(A_{R_{S1}}\right)_{32}\delta W_{m} + \left(A_{R_{S1}}\right)_{22}\delta Z_{m} - \left(A_{R_{S1}}\right)_{12}\delta X_{m} \quad ,$$

$$Z_{m} = -\left(A_{R_{S1}}\right)_{41}\delta U_{m} + \left(A_{R_{S1}}\right)_{31}\delta W_{m} - \left(A_{R_{S1}}\right)_{21}\delta Z_{m} + \left(A_{R_{S1}}\right)_{11}\delta X_{m} \quad , \tag{28}$$

$$X_{m} = -\left(A_{L_{S1}}\right)_{21}\delta V_{m} + \left(A_{L_{S1}}\right)_{11}\delta Y_{m} \quad .$$

Equations (27) give $\hat{\Delta}_{n}^{(m)}$, $\hat{\omega}_{n}^{(m)}$, $\hat{\varepsilon}_{n}^{(m)}$ in terms of the multipole coefficients specifying the source and the Haskell-Thomson layer matrices. Then (22) together with (12) give closed form solutions for the displacements in the nth layer or halfspace. In the following section we evaluate the integrals in (22) to extract the solutions for the steeply emergent body waves of primary interest here.

COMPUTATION OF BODY WAVES

To compute the displacement potentials from (22), it is necessary to evaluate integrals of the form

$$I_m = \int_0^\infty f_m(k,\omega)\, e^{-ikr_\gamma \bar{z}}\, J_m(kr)\, dk \,, \qquad (29)$$

$$\gamma = \alpha_n \quad \text{or} \quad \beta_n \,, \; m = 0, 1, 2, \ldots \,.$$

For $m = 0$ the dilatational potential, $\bar{\Phi}_n$, was evaluated at large distances from the source by Fuchs (1966) using saddle point methods. Hudson (1969a,b) encountered integrals very similar to those in (22) when solving for the body waves due to a point source of general form in a layered medium. As mentioned in the previous section, Hudson's solution is analogous to that obtained here, with the difference being in the specification of the source.

Hudson solved for the far field body waves given by integrals like (29) by using contour integration in the complex plane and approximating the branch line contribution using the saddle point method. The details of this integration may be found in the works of Fuchs and Hudson and will not be reproduced here. It will suffice to give the results which are:

$$I_m = i^{m+1} f_m(k,\omega)\, r_\gamma \frac{e^{-ik_\gamma R}}{R} \qquad (30)$$

where $R^2 = r^2 + \bar{z}^2$. The geometry is shown in Figure 2. The saddle point approximation is valid as long as $R >> r$; that is,

as long as the receiver is sufficiently far from the base of the stack of plane layers. Alternatively, since $r/R = \sin\theta_n$, this approximation is valid for steeply emergent body waves.

With the solution (30), we may now write the far field body wave contribution to the potentials (22):

$$\bar{\Phi}_n(r,\phi,z) = \sum_{m=0}^{\ell} \left(-\frac{1}{k_{\alpha_n}^2}\right) i^{m+1} r_{\alpha_n} \hat{\Delta}_n^{(m)} \frac{e^{-ik_{\alpha_n}R}}{R} ,$$

$$\bar{\Psi}_n(r,\phi,z) = \sum_{m=0}^{\ell} \left(\frac{2}{k_{\beta_n}^2}\right) \frac{i^m}{k} r_{\beta_n} \hat{\omega}_n^{(m)} \frac{e^{-ik_{\beta_n}R}}{R} , \qquad (31)$$

$$\bar{\Omega}_n(r,\phi,z) = \sum_{m=0}^{\ell} \frac{i^{m+1}}{k} r_{\beta_n} \hat{\varepsilon}_n^{(m)} \frac{e^{-ik_{\beta_n}R}}{R} .$$

The cylindrical displacements $(\bar{q}_n, \bar{v}_n, \bar{w}_n)$ then result from substituting (31) into (12). It is more convenient to deal with the displacement components in spherical coordinates where they are identified as the P, SV and SH components of the propagating wave. In the far field, these components are given by

$$\bar{U}_P = \sin\theta_n \frac{\partial\bar{\Phi}_n}{\partial r} + \cos\theta_n \frac{\partial\bar{\Phi}_n}{\partial z} ,$$

$$\bar{U}_{SV} = \cos\theta_n \frac{\partial^2\bar{\Psi}_n}{\partial r\partial z} - \sin\theta_n k^2\bar{\Psi}_n , \qquad (32)$$

$$\bar{U}_{SH} = -\frac{\partial\bar{\Omega}_n}{\partial r} .$$

Then carrying out the indicated differentiations and retaining only terms of $O(R^{-1})$, the displacements are:

$$\bar{U}_P = \sum_{m=0}^{\ell} \left(-\frac{1}{k_{\alpha_n}} \right) i^m r_{\alpha_n} \hat{\Delta}_n^{(m)} \frac{e}{R}^{-ik_{\alpha_n} R} ,$$

$$\bar{U}_{SV} = \sum_{m=0}^{\ell} \left(\frac{2}{k_{\beta_n}} \right) i^{m-1} r_{\beta_n} \hat{\omega}_n^{(m)} \frac{e}{R}^{-ik_{\beta_n} R} , \qquad (33)$$

$$\bar{U}_{SH} = \sum_{m=0}^{\ell} i^m r_{\beta_n} \hat{\varepsilon}_n^{(m)} \frac{e}{R}^{-ik_{\beta_n} R} .$$

These are the far field body waves propagating into the underlying halfspace at specified horizontal phase velocity c. Equations (33), together with (27), provide a straightforward computational algorithm for computing these displacements. A summary of the computational procedure is given below.

Assume that we have a seismic source specified in terms of multipole coefficients. We then wish to compute the P and S waves propagating into the halfspace at takeoff angle θ_n, in which case a different horizontal wave speed is required for the P and S computations. Alternatively, we wish to compute the displacements propagating at a fixed phase velocity, c.

Having the multipole coefficients, c and the azimuth ϕ, the following steps are carried out for each frequency, ω.

1. Compute the source layer potentials $\bar{\Phi}_s$, $\bar{\Psi}_s$, $\bar{\Omega}_s$ from (13 - 16).
2. Compute the displacement-stress discontinuity quantities δU_m, δW_m, etc., from (24 - 25) for each m.
3. Compute the layer product matrices $A_{R_{Sl}}$, $A_{L_{Sl}}$, J^R, J^L. The latter two matrices are independent of the source, while the first two depend only on source depth.
4. Compute the source terms Y_m, Z_m, X_m from (29).
5. Compute $\hat{\Delta}_n^{(m)}$, $\hat{\omega}_n^{(m)}$, $\hat{\varepsilon}_n^{(m)}$ from (27).
6. Compute the displacement spectra at a selected distance R from (33).

Formulation of the solution in terms of Haskell-Thomson matrices is convenient for various modifications that may be of interest. For example, Haskell (1953) and Dorman (1962) show how to modify the layer matrices to account for the presence of a fluid layer and this modification can easily be carried through the algebra leading to (23) and (27).

COMPUTATION OF THEORETICAL SEISMOGRAMS

Our objective is to develop improved methods for computing theoretical seismograms at large (say greater than 1500 km) distances. Equations (33) give the P, SV, SH waves emanating into a homogeneous halfspace underlying a stack of plane layers in which a seismic source is embedded. If this plane layered model is used to represent the crust in the source vicinity, (33) represents the waves propagated into the upper mantle. The major restriction on the use of (33) is to situations for which the saddle point approximation is valid; that is, to small angles of emergence.

To compute theoretical seismograms we need to combine (33) with other methods for computing the remainder of the travel path to the receiver. There are a number of computational schemes that could be chosen but we have found it convenient to use generalized ray theory (Wiggins and Helmberger, 1974) for the upper mantle and Haskell-Thomson matrices (Haskell, 1962) for the crust in the vicinity of the receiver. Thus we break the travel path into three pieces:

1. The crust at the source down to a depth D.
2. The crust at the receiver to the same depth D.
3. A laterally homogeneous upper mantle extending from D to depths greater than the deepest turning point of interest.

The travel path segments are linked by requiring that the velocities at D be the same in all three structures. This scheme gives a great deal of computational flexibility in that portions of the travel path can be varied without repeating the entire calculation. The actual implementation is described in a companion paper (Bache and Archambeau, 1976) where a number of examples are presented.

Methods similar to those outlined here have been used by a number of investigators. Most closely related is the work by Douglas and colleagues (e.g., Douglas, et al., 1972, 1974; Cullen and Douglas, 1975) which uses the method of Hudson (1969a,b) for embedding a seismic source in a plane layered model of the source crustal structure. Also, these authors represent the geometric spreading effect of the upper mantle by a constant which is a function only of epicentral distance (Carpenter, 1966) rather than the detailed generalized ray theory method we prefer. We note that beyond the triplications the upper mantle effect does essentially reduce to a distance dependent constant, though its value depends on the earth model used. Other authors who have used similar techniques include Kogeus (1968) and Hasegawa (1972, 1973) who used Fuchs (1966) formulation for the source crustal transfer function and Julian and Anderson's (1968) geometric spreading factor.

For simple point sources (center of dilatation, couple or double-couple) generalized ray theory can be directly applied to compute theoretical seismograms (e.g., Wiggins and

Helmberger, 1974; Müller, 1971). Another successful theoretical seismogram computing technique is the reflectivity method (Fuchs, 1975; Fuchs and Müller, 1971; Kind and Müller, 1975) though it too is restricted to elementary point source representations.

The major difference between the method presented in this paper and the others mentioned above is in the source representation. Our method is essentially independent of the complexity of the source as long as the outgoing elastic wave field can be expanded in spherical harmonics.

ACKNOWLEDGMENTS

This research was supported by the Advanced Research Projects Agency of the Department of Defense and was monitored by the Air Force Office of Scientific Research under Contract No. F44620-74-C-0063 with Systems, Science and Software, and Contract No. F44620-72-C-0078 with the California Institute of Technology.

T. C. Bache
Systems, Science and Software
P. O. Box 1620
La Jolla, California 92038

D. G. Harkrider
Seismological Laboratory
California Institute of Technology
Pasadena, California 91125
Contribution No. 2736, Division of Geological and Planetary Science

REFERENCES

Archambeau, C. B. (1968), General theory of elastodynamic source fields, Rev. Geophys., 6, 241-288.

Archambeau, C. B. and C. Sammis (1970), Seismic radiation from explosions in prestressed media and the measurement of tectonic stress in the earth, Rev. Geophys., 8, 473-499.

Archambeau, C. B. (1972), The theory of stress wave radiation from explosions in prestressed media, Geophys. J., 29, 329-366.

Bache, T. C. (1976), The effect of tectonic stress release on explosion P wave signatures, BSSA, (in press).

Bache, T. C. and C. B. Archambeau (1976), The body waves due to a general seismic source in a layered earth model: 2. Computation of theoretical seismograms for a propagating earthquake source, to be submitted for publication.

Carpenter, E. W. (1966), A quantitative evaluation of teleseismic explosion records, Proc. Roy. Soc., Lond., A., 290, 396-407.

Cherry, J. T., T. C. Bache, C. B. Archambeau and D. G. Harkrider (1974), A deterministic approach to the prediction of teleseismic ground motion from nuclear explosions, Systems, Science and Software Final Contract Report, DNA 3321F.

Cherry, J. T., T. C. Bache and D. F. Patch (1975), The teleseismic ground motion generated by a nuclear explosion in a tunnel and its effects on the M_s/m_b discriminant, Systems, Science and Software Final Contract Report, DNA 3645F.

Cherry, J. T., T. C. Bache, W. O. Wray and J. F. Masso (1976a), Teleseismic coupling from the simultaneous detonation of an array of nuclear explosions, Systems, Science and Software Report SSS-R-76-2865.

Cherry, J. T., T. C. Bache and J. F. Masso (1976b), A three dimensional finite difference simulation of earthquake faulting, to be submitted for publication.

Cullen, E. A. and A. Douglas (1975), P-wave seismograms from three seismic sources in SW USSR, Geophys. J., 41, 11-28.

Dorman, J. (1962), Period equation for waves of Rayleigh type on a layered, liquid-solid half space, BSSA, 52, 389-397.

Douglas, A., J. A. Hudson and C. Blamey (1972), A quantitative evaluation of seismic signals at teleseismic distances – III. Computed P and Rayleigh wave seismograms, Geophys. J., 28, 385-410.

Douglas, A., J. B. Young and J. A. Hudson (1974), Complex P wave seismograms from simple earthquake sources, Geophys. J., 37, 141-150.

Fuchs, K. (1966), The transfer function for P waves for a system consisting of a point source in a layered medium, BSSA, 56, 75-108.

Fuchs, K. and G. Müller (1971), Computation of synthetic seismograms with the reflectivity method and comparison with observations, Geophys. J., 23, 417-433.

Fuchs, K. (1975), Synthetic seismograms of PS-reflections from transition zones computed with the reflectivity method, J. Geophys., 41, 445-462.

Gilbert, F. and D. V. Helmberger (1972), Generalized ray theory for a layered sphere, Geophys. J., 27, 57-80.

Harkrider, D. G. (1964), Surface waves in multilayered media. I. Rayleigh and Love waves from sources in a multilayered half-space, BSSA, 54, 627-679.

Harkrider, D. G. and C. B. Archambeau (1976), Theoretical Rayleigh and Love waves from an explosion in prestressed source regions, to be submitted for publication.

Harkrider, D. G. (1976), Potentials and displacements for two theoretical seismic sources, Geophys. J., (in press).

Haskell, N. A. (1953), The dispersion of surface waves on multilayered media, BSSA, 43, 17-34.

Haskell, N. A. (1962), Crustal reflection of plane P and SV waves, JGR, 67, 4751-4767.

Haskell, N. A. (1964), Total energy and energy spectral density of elastic wave radiation from propagating faults, BSSA, 54, 1811-1841.

Helmberger, D. V. (1974), Generalized ray theory for shear dislocations, BSSA, 64, 45-64.

Hudson, J. A. (1969a), A quantitative evaluation of seismic signals at teleseismic distances--I. Radiation from point sources, Geophys. J., 18, 233-249.

Hudson, J. A. (1969b), A quantitative evaluation of seismic signals at teleseismic distances--II. Body and surface waves from an extended source, Geophys. J., 18, 353-370.

Julian, B. R. and D. L. Anderson (1968), Travel times, apparent velocities and amplitudes of body waves, BSSA, 58, 339-366.

Kind, R. and G. Müller (1975), Computations of SV waves in realistic earth models, J. Geophys., 41, 149-172.

Kogeus, K. (1968), A synthesis of short-period P wave records from distant explosion sources, BSSA, 58, 663-680.

Minster, J. B. (1973), Elastodynamics of failure in a continuum, Ph.D. thesis, California Institute of Technology, Pasadena.

Morse, P. M. and H. Feshbach (1953), Methods of theoretical physics, McGraw-Hill, New York.

Müller, G. (1971), Approximate treatment of elastic body waves in media with spherical symmetry, Geophys. J., 23, 435-449.

Savage, J. C. (1966), Radiation from a realistic model of faulting, BSSA, 49, 337-367.

Thomson, W. T. (1950), Transmission of elastic waves through a stratified solid medium, J. Appl. Phys., 21, 89-93.

Wiggins, R. A. and D. V. Helmberger (1974), Synthetic seismogram computation by expansion in generalized rays, Geophys. J., 37, 73-90.

FIGURE CAPTIONS

1. Schematic display of the determination of an equivalent elastic representation for an arbitrary volume source.
2. The geometry and coordinate system for a source at depth h in a multilayered halfspace.

IV. The April 29, 1965 Puget Sound Earthquake and the Crustal and Upper Mantle Structure of Western Washington

C. A. Langston and D. E. Blum

The April 29, 1965, Puget Sound Earthquake and the Crustal and Upper Mantle Structure of Western Washington

by

Charles A. Langston and David E. Blum

Seismological Laboratory, California Institute of Technology

Pasadena, California 91125

Contribution No. 2822 , Division of Geological and Planetary Sciences, California Institute of Technology, Pasadena, California 91125.

Abstract

Simultaneous modelling of source parameters and local layered earth structure for the April 29, 1965, Puget Sound earthquake was done using both ray and layer matrix formulations for point dislocations imbedded in layered media. The source parameters obtained are: dip 70° to the east, strike 344°, rake -75°, 63 km depth, average moment of $1.4 \pm 0.6 \times 10^{26}$ dyne-cm, and a triangular time function with a rise time of 0.5 sec and fall-off of 2.5 sec. An upper mantle and crustal model for southern Puget Sound was determined from inferred reflections from interfaces above the source. The main features of the model include a distinct 15 km thick low velocity zone with a 2.5 km/sec P wave velocity contrast lower boundary situated at approximately 56 km depth. Ray calculations which allow for sources in dipping structure indicate that the inferred high contrast value can trade off significantly with interface dip provided the structure dips eastward. The crustal model is less than 15 km thick with a substantial sediment section near the surface. A stacking technique using the instantaneous amplitude of the analytic signal is developed for interpreting short period teleseismic observations. The inferred reflection from the base of the low velocity zone is recovered from short period P and S waves. An apparent attenuation is also observed for pP from comparisons between the short and long period data sets. This correlates with the local surface structure of Puget Sound and yields an effective Q of approximately 65 for the crust and upper mantle.

Introduction

A previous paper dealt with the problem of trying to deduce source parameters from an extremely shallow earthquake, the Koyna event of December, 1967 (Langston, 1976a). The interference of the direct waves and surface reflections was very severe due to the depth of the Koyna hypocenter. Some speculations were made to the origin of some of the reverberations after the reflections but these were hampered by both ignorance of the Koyna crustal structure and the interference with the major phases. If, however, an earthquake is deep enough so that the surface reflections and the direct wave are well separated, perhaps layer interfaces between the hypocenter and free surface can be resolved by intermediate reflected arrivals. It is exactly this supposition which will be used to explain the shape of long period P waves from the Puget Sound earthquake. A crust model for southern Puget Sound will be deduced by identifying arrivals between P and pP as underside reflections from crustal layers. A major compressional and shear wave low velocity zone (LVZ) in the uppermost mantle will be proposed by modelling the time, amplitude, and polarity of these reflected arrivals.

Simultaneously, care will be taken to model the source parameters as well.

Geologic and Tectonic Setting

Puget Sound is located in northwestern Washington and is part of a major north-south geologic and physiographic province, the Puget-Willamette depression (Figure 1) (Snavely and Wagner, 1963). The geologic development of this area has been controlled by Tertiary sedimentation and volcanism in a north-south trending eugeosyncline shown in Figure 1 (Snavely and Wagner, 1963; Snavely et al., 1968). The Puget-Willamette depression may be fault controlled with major faults occurring on the eastern margin of Puget Sound and the western side of the Willamette Valley (Algermissen and Harding, 1965; Bromery and Snavely, 1964).

Of seismic refraction profiles which have been made on land, perhaps the most significant is the one by Berg et al. (1966). They obtain a very thin (16 km) crust and a Pn velocity of 8.0 km/sec for the Coast Ranges of Oregon and southern Washington. Tatal and Tuve (1955), who did some of the first crustal refraction studies in the Pacific northwest, reached a similar conclusion for the southern Puget Sound area obtaining a crustal thickness of about 19 km and Pn velocity of 8.0 km/sec. Because of the conspicuous lack of pre-Tertiary granitic basement within the margins of the Tertiary eugeosyncline (Figure 1) and from the velocity and thickness values obtained in this refraction profile some authors have suggested that the area is a large embayment of oceanic crust in the North American continent (Hamilton and Myers, 1966; Dickinson, 1970).

Through detailed gravity and magnetic modelling Danes, et al. (1965) deduced some of the major structures of southern Puget Sound. Their principal results include the discovery of a large northwest trending igneous horst structure with flanking deep sedimentary basins. They infer sediment thicknesses of 4 km and 10 km for the southern Tacoma basin and northern Seattle basin, respectively. The large observed gravity gradients suggest major faults bounding this horst with inferred throws on the order of several kilometers. It may be significant that the April 1965 event occurred under the eastern edge of this structure. Danes (1969) has also suggested that Puget Sound is a great isostatic depression with an isostatic anomaly greater than -100 mgal.

The theory of plate tectonics forms the basis for current thinking on the tectonic framework of the Pacific Northwest. Interpretation of the magnetic anomalies of Raff and Mason (1961) by Vine and Wilson (1965), Wilson (1965), and Vine (1966) and other subsequent work by Tobin and Sykes (1968), Atwater (1970), Dickinson (1970), Silver (1971a, 1971b, 1972), Crosson (1972), and Chandra (1974), among others, have led to a hypothesis relating the geophysical and geologic data into one plate tectonic scheme. The model states that subduction of

oceanic crust and upper mantle is taking place north of Cape Mendocino to Vancouver Island. A small offshore ridge system, the Gorda-Juan de Fuca rise, is still producing oceanic lithosphere which is the remnant of the previously more extensive Farallon plate (Atwater, 1970). Spreading at a half-rate of about 2.5 cm/year, this small plate may still be underthrusting the continent as the association of andesitic vulcanism in the Cascades seems to require (Dickenson, 1970) and as inferred from offshore geologic evidence (Silver, 1971a,1972). Against the normal assumptions of plate tectonics, this small plate does not appear to be rigid, but seems to be experiencing internal deformation (Silver,1971b; Crosson, 1972).

Perhaps the most serious problem with this scheme is the conspicuous absence of a seismic Benioff zone. The general seismicity level of the area is low other than at the offshore fracture zones (Tobin and Sykes, 1968; Chandra, 1974). Puget Sound has a moderate background of diffuse seismicity, however, and a few events have occurred at depths of up to 70 km (Crosson, 1972). The magnitude 6.5 Puget Sound earthquake of April 1965 was located at 60 km depth, see Figure 1 (Algermissen and Harding, 1965), and the somewhat larger April 1949 event, at 70 km (Nuttli, 1952). Although these events are not extremely deep for other island and continental arcs, they are very unusual compared to all other continental U. S. earthquakes. Because of this, they have been cited as evidence for

a remnant of a subducting plate, or perhaps, a very slowly subducting plate under Washington (Isacks and Molnar, 1971; Crosson, 1972). Other geophysical evidence supporting this plate model comes from travel time anomalies determined from P residuals for the 1965 event (McKenzie and Julian, 1971) and from an array processing study using teleseismic P arrivals at Puget Sound (Lin, 1974). Both of these studies reach the similar conclusion that a high wave velocity plate dips to the east with an angle of about 50 degrees.

The unusual depth of the April 1965 event and the interesting geologic and geophysical problems this area presents motivates the detailed waveform study that this paper reports. The original purpose of this study was to find a detailed source model for the earthquake, but as it turned out, much more interesting information could be found by modelling the local source structure as well.

The Puget Sound Earthquake

On April 29, 1965, at 15:28:44 GMT a magnitude 6.5 earthquake shook the environs of southern Puget Sound causing moderate damage in Seattle and Tacoma. The location of the epicenter was midway between these two cities and the hypocentral depth estimated to be at 60 km (Algermissen and Harding, 1965). Consistent focal mechanisms for the event done by several authors show predominantly normal dip-slip movement on a 70° eastward dipping plane striking approximately 15° west of north

(Algermissen and Harding, 1965; Isacks and Molnar, 1971; Chandra, 1974). The auxiliary plane is only poorly constrained because of sparse local station coverage, a common occurrence for this type of orientation. Because of excellent teleseismic coverage, however, the first nodal plane is extremely well determined and serves as a very useful constraint in the waveform modelling.

Data and Data Processing

The gathering and processing of long period P and SH waveforms were done as described in Langston (1976a). Table 1 lists the WWSSN stations utilized for this study. Unfortunately, there was only one station in which the horizontal components were naturally rotated with respect to the ray direction. As a result, only a few SH waveforms could be salvaged for waveshape analysis and even these may be contaminated by the rotation process.

Most of the stations in Table 1 were equipped with the longer period 30-100 instrument instead of the 15-100 instrument used in the Koyna study. A few stations, ANT, QUI, SJG, and BEC had just been changed to the standard 15-100 instrument, however, so these

were equalized to be consistent with the rest of the data set. An operator was constructed and convolved with these data to effectively make them 30-100 observations. The 30-100 instrument response was calculated using Hagiwara's (1958) formulation.

Data Inversion and Interpretation

As a starting point, it would be most convenient to present the final inferred earth and source models and P waveform fits. The complex interactions of the earth and source models will then be examined point by point and the reasoning behind each effect presented in a coherent manner.

Figure 2 displays the results of trial and error waveform modelling to find a source and earth model most consistent with the long period data. A standard first motion plot (bottom hemisphere) is given in the center of the diagram with the P nodal planes inferred from this study. In this determination, pP as well as P first motions were incorporated. Lines are drawn from each observed-synthetic waveform pair to the appropriate spot on the focal sphere which represents the downgoing P ray at that station. For each seismogram pair the observed is plotted above the synthetic. The source orientation parameters are given in the corner of Figure 2 In this model the source is assumed to be a single point dislocation

with a triangular time function characterized by a rise and fall-off time δt_1 and δt_2 equal to 0.5 and 2.5 sec, respectively. The final plane-layered earth model is presented in Figure 3 and is under the heading of 'PS-9' in Table 2. The source is situated at a depth of 63 km for this model.

Both ray theory (Langston and Helmberger, 1975) and propagator matrix techniques (Haskell, 1953; Harkrider, 1964; Fuchs, 1966) were used to calculate synthetic seismograms for a point dislocation in a layered elastic medium. Both methods are equivalent and complementary for various model calculations. Ray theory has the advantage of giving a direct physical interpretation to observed phases. Matrix techniques, while exact in terms of including all multiples, gives little insight into the model but does serve as a check to the ray calculations. It can also be used as a tool for calculating the effect of gradients in the earth model by approximating them with many thin layers.

Two striking features are apparent in Figures 2 and 3. The first is the quality of the waveform fits over the entire azimuth range. The observed waveforms have a tremendous variation in shape as a function of azimuth and take-off angle which the model approximates quite nicely for nearly all stations. Secondly, the earth model presented in Figure 3 is quite unusual. The major features of PS-9 include a very distinct and large low-velocity zone between 41 and 56 km depth. This structure is sandwiched between what appears to be mantle velocity material. The crustal section at the top is very thin, less than 15 km, and has very low velocity materials near the free surface. This model was inferred entirely from the long period P waves and will be discussed by closely examining which characteristics of the P waves control its various details.

Let us first look at what effects a simple earth model, a layer over a halfspace, gives for the long period P response. Figure 4 compares the simple one layer model (Table 2) with PS-9 for representative P waveforms. The major phases P, pP, and sP are quickly apparent in these waveform comparisons although there are significant differences in the interval between the direct P wave and pP. The small arrival several seconds before pP in the one layer model is the P reflection from the bottom of the layer except at GUA where it is an S-P conversion at reflection. The first 18 sec of the P-wave for the simple model is just the convolution of the source time function with the Q operator and the instrument response since there are no distortions due to near source structure.

For COP and stations like it in the northeast (see Figure 2) the first 18 sec of the observed P wave show at least two arrivals after the dilatational direct P. First there is an equal sized compression, arrival A (Figure 4) approximately two seconds after P with another dilatational arrival, arrival B, 2 seconds after that. Examination of the one layer model of COP demonstrates that the overswing of the instrument response is not a factor here. At PTO the direct wave and arrival A have the same sign and add constructively because of the change in the P radiation pattern. This shows up as an increase in the P amplitude, relative to pP, at PTO and at other similar stations. Arrival B is plainly the same polarity as at COP. The interpretation of these arrivals is based on the assumption that they represent underside reflections from discontinuities above the source and not from source complications. It is entirely reasonable to assume that there are major discontinuities between a 60 km deep

source and the free surface, but it is obviously extremely hard to prove, unequivocally, that small arrivals are from such reflections and not source effects. The seismograms of Figure 2 suggest that these arrivals are associated with pP rather than the direct P wave by the observation that when direct P changes polarity the A and B arrivals remain constant.

Assuming that these arrivals came from reflectors above the source, what can be said about their properties? Since the strength of up-going P determines the amplitude of the reflection as well as the material contrasts, an approximate determination of the velocity contrast can immediately be made. At the northeastern P nodal stations upgoing SV radiation is at minimum because of fault orientation so that only P interactions can be considered. A cursory examination of the waveforms gives a minimum amplitude estimate for reflection A of about 0.15. This is clearly an underestimate since interference with the direct wave knocks it down considerably. There must be interference since the width of the first swing changes as a function of P amplitude and azimuth. Compare STU and TOL, Figure 2, for example. The type of contrast can immediately be deduced because of the known polarity of pP. Since upgoing P is dilatational and the reflection is compressional, the reflection coefficient must be negative, which implies a higher to lower velocity contrast. Simultaneously modelling the time function, relative timing, and relative amplitudes of direct P and phase A for

the northeastern and southeastern stations yields the high contrast of 8.0 to 5.5 km/sec for the lowermost boundary of PS-9, Figure 3.

Continuing this line of reasoning one step further to phase B gives some remarkable results. Using the same process for finding the sign of the reflection coefficient, the polarity of B suggests that it comes from a lower to higher velocity contrast. Phase B, therefore, delimits the top of a low velocity zone. Figure 5 demonstrates this explicitly for the station KEV. Ray number one is normalized to unity and all other ray amplitudes referenced to it. The top of the LVZ was modelled with two interfaces in order to increase the width of the reflected pulse. This particular model explains the azimuthal variation of wave shapes for the first eighteen seconds remarkably well (Figure 2).

The uncertainty in orientation (see Figure 2) is not a major factor in the modelling. The first motion data constrain the north-south nodal plane to within a degree. Since all of the stations are near the center of the plot and most are close to the nodal plane, relatively large variations in the rake (-90 ±20°) do little to affect the relative amplitudes of P and pP. Upgoing SV is more sensitive so there is some basis for assigning the particular value used, although it is a small effect and will be discussed later. The velocity assigned to the source layer is a value typically found for these depths in upper mantle studies. Variations in this velocity, of up to ± 0.5 km/sec, don't significantly affect the results since

we are looking at relative amplitudes and velocity contrasts only. This does point out that the absolute values of velocity for any part of the inferred model are somewhat ambiguous.

The phase pP and sP control and constrain the top of model PS-9. For the source function inferred from the direct P wave, it is evident that pP in a simple one-layer model (Figure 4) starts too sharply. The small arrival before pP suggests that a number of small reflections in the upper crust could give the desired effect of producing a smooth ramp before the main pP peak. Further evidence for this type of model occurs in the western stations HNR, GUA, and ANP. The predicted sP phase for the one layer model is much too large and is not affected by small changes in the radiation pattern. The easiest way to cut down this amplitude is to lower the reflection coefficient by using low velocities near the top of the model. This implies many contrasts also, since there must be some kind of transition from mantle to sediment velocities. This is the basis for modelling the upper crust in model PS-9. It is interesting to note that the crustal section had to be kept thin since thicker crustal models caused spurious arrivals from the Moho before the arrival time of pP. The absolute velocities for the top are not too well constrained. These values were determined by using the local refraction results of Berg et al. (1966) and Tatel and Tuve (1955). The

lowest velocities are appropriate for Tertiary clastic rocks as reported in Press (1966). The mantle velocity above the LVZ of 7.8 km/sec was based on the data of Dehlinger et al. (1965) and McCollum and Crosson (1975).

The S wave velocity is one of the least constrained parameters in the model. The average S time is only constrained by sP, a phase which is distorted and reduced in size by the model. However, there is some evidence that large S wave contrasts exist in the LVZ. At the western azimuth stations S-P reflections were needed to reduce the backswing of the direct P (see GUA, Figure 4, for a comparison) and theoretical arrivals after sP were only obtained after increasing the shear velocity contrast at the boundaries of the LVZ. These arrivals are shown as 'C' and 'D' in Figure 4 and are crustal multiples with substantial S to P conversions. Figure 2 shows that these multiples can help explain the arrivals after sP at these stations.

These multiples bring up interesting questions concerning the arrivals after pP at the northeastern and eastern stations. PS-9 predicts a few crustal multiples after pP but nothing like those in some of the observations. Figure 6 shows the long period P wave from the station KEV with a synthetic produced from the PS-9 model above and one made from a preliminary model, PS-1 (Table 2), below. The PS-1 model did not predict the LVZ interference effects very well nor the shape of pP for most observations. Because of the

low shear velocities and higher contrasts this model has, compared to PS-9, crustal reverberations after pP are quite pronounced and fit the observations quite nicely for this azimuth. However, since it did not fit the front part of the record very well, in general, it was not used. This exercise demonstrates that the arrivals after pP could conceivably be explained by large velocity contrasts although lateral inhomogeneity would probably be needed to match them. These crustal and mantle reverberations sample larger portions of the model and at distances further away from the epicenter as relative arrival times increase. Lateral changes over a scale length of 50 km, not inconceivable for the region, coupled with the substantial depth of the source could be responsible for such effects. It must be mentioned that an added ambiguity inherent in this modelling is the lack of receiver characteristics. For the same reasons cited in the Koyna study (Langston, 1976[a]) no receiver responses were evaluated. Presumably, the effect for the vertical P wave is small but could be on the same order as the small arrivals behind pP. As such, these unknowns have to be considered a source of error in the study.

The evidence for constraining the rake angle of the north-south nodal plane comes from the relative amplitude of the reflection from the bottom of the LVZ. The observations of Figure 3.2 suggest that the reflection is more pronounced for the northern stations

(KEV, NUR, etc.) compared to the southern stations (QUI, NNA, LPB, ANT). Rather than invoke extreme lateral heterogeneity for this interface, a simple explanation can be made for the effect using fault orientation. If the fault was pure dip-slip ($\lambda = -90°$) the northern and southern stations should be identical since the radiation pattern would be symmetric about a line perpendicular to the fault plane. Varying the rake angle strongly affects only the upgoing SV radiation since it is near a node for eastern azimuths and this type of orientation. It was found that the interference of S-P conversions with the P reflections decreased the amplitude of the LVZ phases where upgoing SV was comparatively large. Using this effect the rake angle was deduced to be approximately -75° rather than pure dip-slip.

Because the extremely high velocity contrasts found for the LVZ of PS-9, it might prove interesting to perform a parameter study which includes one more level of structure complication by including layer dip. Figure 7 is the result of such a calculation. The bottom interfaces of PS-9 which include the LVZ were simply tilted towards the east preserving all layer thicknesses and velocities. A ray theoretical approach was used to calculate the response for this three dimensional model and is described elsewhere (Langston, 1976c). Since all interfaces are parallel, the method, in this case, simply consists of assigning each ray an amplitude corresponding to a new incident angle and azimuth at the source and tracing it through the plane parallel model with a 'local' ray parameter determined by the station azimuth and distance and structure dip.

An eastward dipping model is shown because of the suggestions made by McKenzie and Julian (1971) and Lin (1974) for an eastward dipping slab.

Figure 7 shows the first 18 seconds of eight representative P waves of Figure 2. The effect of layer dip manifests itself primarily in those very stations which were important in resolving the LVZ, e.g., KEV, IST, COP, and NNA. Stations in which direct P is predominant, such as ATL and GUA, show little change with increasing dip. The main effect of layer dip for all eastern azimuths is to have up-going rays start from the focal sphere in a more easterly direction. Differences between the focal area azimuth and station azimuth can be up to 30°.

This change in the relative amplitude between down- and up-going rays due to the modified radiation pattern coupled with changes in the reflection coefficie for this particular source and structure model produces the effect of a direct tradeoff between layer dip (to the east) and LVZ interface contrasts. Although there is no way of knowing from these data whether planar dipping structure exists at Puget Sound it is very evident that it could have a very important effect on the particular velocity contrasts inferred from the horizontally layered model. A 50% reduction could easily be possible, say for the $\delta = 20°$ case, but the general characteristics of the LVZ must still be included in the earth model.

Modelling the rotated SH waves revealed little about the source or structure. Figure 8 shows the six observed SH waves with corresponding synthetic seismograms computed by ray techniques using the PS-9 model. Basically, the observed SH waves are very simple showing only the direct S. Most of the "glichiness" of these waves is due to digital noise in the rotation process. Since upgoing S is relatively small for these stations none of the major discontinuities of PS-9 are directly observable except for the free surface. The phase sS is not readily apparent in the observations although it is theoretically small. Several possibilities can be presented. First, the S-velocity structure of PS-9 may be completely wrong so that sS time is significantly different. However, examination of the SH observations yields no consistent arrival at any other time. A second possibility is that local receiver crustal effects such as S-coupled PL waves may contaminate the tangential component. S-waves are notorious for this and the position of sS relative to S makes this possibility very probable (Helmberger and Engen, 1974). A third and very likely possibility is that the earth model near the source is deficient. It could be that anelastic attenuation plays an important role. Some short period results will be presented below which support this speculation.

Scaling the synthetic direct P and SH waves to the long period data yields a moment determination for the Puget Sound event. A value of $1.3 \pm 0.6 \times 10^{26}$ dyne-cm is obtained from 21 P waves (see Figure 3.2). The uncertainty given is the standard error. The six SH waves, Figure 8, yield an average value of $1.7 \pm 0.6 \times 10^{26}$ dyne-cm,

slightly higher than the P waves but well within the uncertainties of the geometrical spreading correction and assumptions on attenuation. The average moment including both P and S waves, is $1.4 \pm 0.6 \times 10^{26}$ dyne-cm. The scatter in amplitudes, yet not in waveshape, can be considerable even for nearby stations. For example, compare IST and ATU, Figure 2.

An attempt was made to utilize the many short period observations from this event to determine timing and amplitude information to help pin down the inferred structural discontinuities. Although the attempt eventually fell short of its original goals some interesting effects between the direct and reflected phases were observed.

An easy way to change a short period record into a form suitable for stacking is to compute an envelope of the signal. Once the envelope is found for several records a suitable amplitude normalization is performed and the traces averaged with all seismograms lined up with respect to their first arrivals. A convenient way to compute the type of envelope needed here is to take the instantaneous amplitude of the analytic signal (Farnbach, 1975). The analytic signal is defined by (Bracewell, 1965)

$$\begin{aligned} \hat{S}(t) &= f(t) - iF_{Hi}(t) \\ &= |\hat{S}(t)|\, e^{i\alpha(t)} \end{aligned} \qquad (1)$$

where,

$f(t)$ = observed time series

$\hat{S}(t)$ = analytic signal

$F_{Hi}(t)$ = Hilbert transform of $f(t)$

$\alpha(t)$ = time varying phase

$|\hat{S}(t)|$ = instantaneous amplitude.

The Hilbert Transform in equation (1) can simply be thought of as a convolution of $-1/\pi t$ with $f(t)$. Figure 9 shows an example of taking the instantaneous amplitude, $|\hat{S}(t)|$, of a short period vertical P wave recorded at AFI. This method preserves the times and relative amplitudes of the arrivals and even makes the record a little easier

to visually interpret. By no means does it purport to add any information; it simply makes the sesimograms easier to work with. The normalization was done by setting the area of the first 10 seconds of the envelope to unity. This tended to boost the relative amplitude of sharp arrivals to that of emergent arrivals.

Figure 10 shows the results obtained from a stacking experiment. The traces labelled 'P' are stacked envelopes of short period vertical P waves grouped as a function of range. The range interval is indicated under each group name and the number in parentheses represents the number of seismograms used per group. Table 1 indicates the particular stations used in this grouping. The P wave stacked traces show several interesting effects. In the first 10 sec two prominent arrivals are usually evident and are designated P and p_mP in the diagram. The first arrival is interpreted to be the direct P wave with p_mP being the reflection from the bottom of the LVZ. The timing agrees with the long period result. This is not too useful except to show that the reflection has approximately the same frequency content as the direct wave. This implies that the contrast at this boundary must be sharp, probably less than 2 km in transition. The most striking effect these traces demonstrate, however, is the very conspicuous absence of pP, especially at the smaller epicentral distances. A simple glance at the long period waveforms in Figure 2 reveals that, except for the western stations, pP

is at least as big as direct P and usually two or three times bigger. The relative amplitude of pP in groups a, b, and c of Figure 10 is at least half that of direct P. Not until stations with ranges greater than 75° are considered does pP start becoming apparent. This effect can be inferred to come from earth structure by using the information gleaned from p_mP. Because the frequency content of upgoing rays is similar to that of the downgoing rays a source effect, such as directivity, can automatically be eliminated. All reflections should be apparent unless structure or attenuation effects cancel the arrivals.

An explanation for this observation can be found in the geologic and structural framework of Puget Sound. Figure 11 is a map of southern Puget Sound with the epicenter plotted near the center (after Algermissen and Harding, 1965). The concentric circles are contours of the position pP hits the surface for a particular station distance. These were computed from ray theory for model PS-9 using the expression

$$x_r = \sum_{j=1}^{n} \frac{p}{\eta_{\alpha_j}} Th_j \qquad (2)$$

where

x_r = radius from epicenter

p = ray parameter considered

$$\eta_{\alpha_j} = \left(\frac{1}{\alpha_j^2} - p^2 \right)^{1/2}$$

Th_j = thickness of the j^{th} layer

The summation is for all layers between the hypocenter and the free surface. The hachured lines across Figure 11 represent a simplified version of structural discontinuities from the gravity and magnetic interpretation of Daneš et al. (1965). They are dashed where questionable. The tick marks are on the down-thrown side of the inferred fault. The large numbers in parentheses are inferred depths to crystalline basement from the surface. This map readily demonstrates the great structural relief and complexity in the near-surface geology. The contours of pP are only approximate when considered from this approach since they were calculated using a plane layered model, an assumption which clearly breaks down for the near surface layers. Nevertheless, they should be useful to first order. Comparing the distance ranges and the structure gives a possible explanation for the amplitude behavior of short period pP. For all stations at distances less than 75° pP bounces at points which have thick sections of sediment. For stations with ranges greater than that, pP bounces within the boundaries of the large horst or near its edge where sediment thicknesses are presumably smaller. This observation seems to correlate with the effects seen in the traces of Figure 10. Possibly, then, the attenuation of pP

relative to P comes from either structurally disturbed sediments causing wave scattering or perhaps from anelastic attenuation. Either mechanism is feasible. An effective 'Q' can be computed from these observations by using equation (3). A conservative estimate of the amplitude attenuation factor, a, is about 1/3 for a .75 sec short period sinusoid, and with a total travel time, T, of 17 sec gives

$$Q_{eff} = \frac{-\omega T}{2 \ln a} \qquad (3)$$

$$= 65$$

This amounts to convolving pP with another Q operator on top of the first (T/Q = 1.0) with a travel-time to Q ratio of 0.3. This particular Q operator would have negligible effect on a long period P waveform.

The realization that Puget Sound is structurally heterogeneous can explain why the shape details of pP are not fit by PS-9 for all azimuths (see Figure 2). In fact, it is surprising that the model works at all. Perhaps the pathological case of GDH, Figure 2, can have an explanation in this light.

Returning to Figure 10 one last point can be made using the short period stacking procedure. The bottom trace, labeled 'S', is the average of both horizontal short period S wave components at seven stations (Table 1). The result of the averaging revealed

two arrivals roughly 3 sec apart. The first is interpreted to be direct S. Comparisons with each corresponding long period component revealed that the short period S started after any long period S-P precursors and correlated with where the long period arrival was sharpest. The second arrival, because of its timing, is interpreted to be the reflection from the bottom of the LVZ. This arrival did not occur at all stations and there were significant waveform variations between stations to make this a tentative conclusion. It does give weak evidence against multiple source complications through the agreement in travel times for the inferred reflected S phase.

Discussion of the earthquake results

The source model presented here is an exceedingly simple one. The orientation agrees with previous studies and the time function is short and uncomplicated. It is certainly quite possible that there are other source complications but an earth model has been presented which, if anything, demonstrates the problems one has to deal with in order to discern these effects.

The earth model, on the other hand, is relatively complicated. In some respects it is heartening to see how some parts of the model agree with the geology and previous geophysics. For example, the inferred crustal thickness is about 15 km. The refraction results are consistent with this including a recent study using

local mine blasts recorded by the Puget Sound seismic array. This particular study also obtained a shallow depth to Moho of 15 to 20 km (H. Zuercher, 1975). The low velocity layers at the top of the model, needed to widen pP and attenuate sP, correlate nicely with the thick sections of presumably Tertiary sediments under the blanket of glacial till.

On the other hand, discovery of the massive LVZ in the uppermost mantle by these means presents many problems in uniqueness, although the model produces a good fit to all the P waves. Clearly, a check on this conclusion is desirable. One way to do this would be to examine another earthquake to see if the same structure effects are observable. The 1949 event would be the logical choice since it occurred nearby and at a depth of 70 km. The records, however, are not easily available and the orientation of the event, relative to the station coverage, might not be appropriate for observing these effects. Because the inferred structural boundaries of the LVZ are so distinct they should be directly observable from upcoming phase conversions and reverberations using teleseismic sources for stations situated over the structure. Fortunately, there are several long period WWSS and Canadian network stations nearby to test the model. The WWSSN station at Corvallis, Oregon, was studied in this manner (Langston, 1976, this volume) and although the details of the earth model are different from PS-9, the distinct LVZ was again found.

It is interesting to note that in a recent set of papers on earthquake travel times in Puget Sound, Crosson (1976) found a possible LVZ although he states it may not be resolvable from his data. Further discussion will be given in Langston (1976 b, this volume).

Conclusions

A major, distinct low velocity zone is inferred in the uppermost mantle under Puget Sound by modelling reflected arrivals in the long period P waveforms from the 1965 Puget Sound earthquake. The LVZ occurs in the depth interval of 41 to 56 km and is sandwiched between layers having mantle velocities. The velocity contrast at the bottom interface of the LVZ must be on the order of 2.5 km/sec as inferred from the theoretical relative P amplitudes from the point dislocation source, assuming horizontal structure. If eastward dipping structure is allowed, the velocity contrasts in the LVZ trade-off directly with dip.

The crust of southern Puget Sound is thin, less than 15 km, and has a thick sediment section near the surface as inferred from the shapes of the pP and sP phases. This is consistent with other geophysical studies.

The earthquake source parameters determined by the P and SH waveform study are the following: 70° dip to the east; 344° strike; -75° rake, making it a normal dip-slip fault, consistent with previous studies; seismic moment of $1.4 \pm 0.6 \times 10^{26}$ dyne-cm; 63 km depth; and a simple time history represented by a triangular far-field source function with a rise time of 0.5 sec and a fall off of 2.5 sec. The depth is constrained by pP and sP travel times.

The synthetic P and SH waveforms computed from the given source and earth models reproduce the major azimuthal variations which occur in the data waveforms.

A short period stacking procedure utilizing the instantaneous amplitude of the analytic signal is presented and used to find reflected

arrivals. An apparent attenuation is found for short period versus long period pP and is correlated with sediment thickness at the reflection point. The amplitude discrepancy yields an effective Q of about 65 for the earth structure above the earthquake.

Acknowledgments

This research was supported by the Advanced Research Projicts Agency of the Department of Defense and was monitored by the Air Force Office of Scientific Research under Contract F44620-72-C-0078 and F44620-72C-0083.

REFERENCES

Algermissen, S. T. and S. T. Harding (1965). Preliminary Seismological Report, in The Puget Sound, Washington Earthquake of April 29, 1965, U. S. Department of Commerce, Coast and Geodetic Survey, U. S. Government Printing Office, Washington, 51 pages.

Atwater, T. (1970). Implications of plate tectonics for the Cenozoic tectonic evolution of Western North America, Bull., Geol. Soc. Am., 81, 3513-3536.

Berg, J. W., L. T. Trembly, D. A. Emilla, J. R. Hutt, J. M. King, L. T. Long, W. R. McKnight, S. K. Sarmah, R. Souders, J. V. Thiruvathukal, D. A. Vossler (1966). Crustal refraction profile, Oregon Coast Range, Bull. Seism. Soc. Am., 56, 1357-1362.

Bracewell, R. (1965). The Fourier Transform and Its Applications, McGraw-Hill Book Co., New York, 381 pages.

Bromery, R. W. and P. D. Snavely, Jr. (1964). Geologic interpretation of reconnaissance gravity and aeromagnetic surveys in northwestern Oregon, U. S. Geological Survey Bull. 1181-N.

Chandra, U. (1974). Seismicity, earthquake mechanisms, and tectonics along the western coast of North America, from 42°N to 61°N, Bull. Seism. Soc. Am., 64, 1529-1549.

Crosson, R. S. (1972). Small earthquakes, structure, and tectonics of the Puget Sound Region, Bull. Seism. Soc. Am., 62, 5, 1133-1171.

Crosson, R. S. (1976). Crustal structure modeling of earthquake data, 2, velocity structure of the Puget Sound Region, Washington, J. Geophys. Res. 81, 3047-3054.

Danes, Z. F. (1969). Gravity results in western Washington, EOS, 50, 348-350.

Daneš, Z. F., M. M. Bonno, E. Brau, W. D. Gilham, T. F. Hoffman, D. Johnson, M. H. Jones, B. Malfait, J. Masten, and G. O. Teague, (1965). Geophysical investigation of the southern Puget Sound area, Washington, J. Geophys. Res., 70, 5573-5580.

Dehlinger, P., E. F. Chiburis, and M. M. Collver (1965). Local travel-time curves and their geologic implications for the Pacific Northwest States, Bull. Seism. Soc. Am., 55, 587-607.

Dickinson, W. R. (1970). Relations of andesites, granites, and derivative sandstones to arc-trench tectonics, Rev. Geophys., Space Phys., 8, 813-860.

Farnbach, J. S. (1975). The complex envelope in seismic signal analysis, Bull. Seism. Soc. Am., 65, 951-962.

Fuchs, K. (1966). The transfer function for P-waves for a system consisting of a point source in a layered medium, Bull. Seism. Soc. Am., 56, 75-108.

Hamilton, W., and W. B. Myers (1966). Cenozoic tectonics of the Western United States, Rev. Geophys. and Space Physics, 4, 509-549.

Harkrider, D. G. (1964). Surface waves in multilayered elastic media I. Rayleigh and Love waves from buried sources in a multilayered elastic half-space, Bull. Seism. Soc. Am., 54, 627-679.

Haskell, N. A. (1953). The dispersion of surface waves on multilayered media, Bull. Seism. Soc. Am., 43, 17-34.

Helmberger, D. V. and G. R. Engen (1974). Upper mantle shear structure, J. Geophys. Res., 79, 4017-4028.

Isacks, B. and P. Molnar (1971). Distribution of stresses in the descending lithosphere from a global survey of focal-mechanism solutions of mantle earthquakes, Rev. Geophys. Space Phys., 9, 103-174.

Langston, C. A. (1976a). A body wave inversion of the Koyna, India, earthquake of 10 December 1967 and some implications for body wave focal mechanisms, J. Geophys. Res., 81, 2517-2529.

Langston, C. A. (1976b). Corvallis, Oregon, Crustal and upper mantle structure from teleseismic P ans S waves, in preparation.

Langston, C. A. (1976c). The effects of planar dipping structure on source and receiver responses for constant ray parameter, in preparation.

Langston, C. A. and D. V. Helmberger (1975). A procedure for modelling shallow dislocation sources, Geophys. J. R. astr. Soc., 42, 117-130.

Lin, J. W. (1974). A study of upper mantle structure in the Pacific Northwest using P waves from teleseisms, Ph.D. Thesis, University of Washington, 98 pp.

McCollom, R. L., and R. S. Crosson (1975). An array study of upper mantle velocity in Washington state, Bull. Seism. Soc. Am., 65, 467-482.

McKenzie, D., and B. Julian (1971). Puget Sound, Washington, earthquake and the mantle structure beneath the northwestern United States, Geol. Soc. Am. Bull., 82, 3519-3524.

Nuttli, O. W. (1952). The western Washington earthquake of April 13, 1949, Bull. Seism. Soc. Am., 42, 21-28.

Press, F., (1966). Seismic velocities, in Handbook of Physical Constants, Geol. Soc. Am. Mem. 97.

Raff, A. D., and R. G. Mason (1961). Magnetic survey off the west coast of North America, 40°N latitude to 52°N latitude, Geol. Soc. America Bull., 72, 1267-1270.

Silver, E. A. (1971a). Transitional tectonics and late Cenozoic structure of the continental margin off northernmost California, Geol. Soc. Am. Bull., 82, 1-22.

Silver, E. A. (1971b). Small plate tectonics in the northeastern Pacific, Geol. Soc. Am. Bull., 82, 3491-3496.

Silver, E. A. (1972). Pleistocene tectonic accretion of the continental slope of Washington, Mar. Geol., 13, 239-249.

Snavely, P. D. and H. C. Wagner (1963). Tertiary geologic history of western Oregon and Washington, Div. Mines Geol. Report of Invest. #22, 25 pages.

Snavely, P. D., N. S. MacLeod, H. C. Wagner (1968). Tholeiitic and alkalic basalts of the Eocene Siletz River volcanics, Oregon Coast Range, Am. J. Sci., 266, 454-481.

Tatel, H. E. and M. A. Tuve (1955). Seismic exploration of a continental crust, Geol. Soc. Am. Spec. Paper 62, 35-50.

Tobin, D. G., and L. R. Sykes (1968). Seismicity and tectonics of the northeast Pacific Ocean, J. Geophys. Res., 73, 3821-3845.

Vine, F. J. (1966). Spreading of the ocean floor: New evidence, Science, 154, 1405-1414.

Vine, F. J. and J. T. Wilson (1965). Magnetic anomalies over a young oceanic ridge off Vancouver Island, Science, 150, 485-489.

Wilson, J. T. (1965). Transform faults, oceanic ridges and magnetic anomalies southwest of Vancouver Island, Science, 150, 482-485.

Zuercher, H. (1975). A study of the crust in Puget Sound using a fixed seismic source, M. S. thesis, University of Washington, 62 pages.

Table 1

Station Information

Station	$\Delta^{(0)}$	$AZ^{(0)}$	$BAZ^{(0)}$	Components
AFI	75.3	229.7	32.3	P, p(d)
AKU	53.2	30.1	304.7	p(b)
ANP	87.8	305.5	37.6	P
ANT	84.8	133.6	327.5	P, p(d)
ARE	78.2	130.5	327.5	s
ATL	31.8	102.2	307.4	P, p(a)
ATU	89.8	26.2	337.7	P, p(d)
BEC	45.7	87.6	306.7	P, p(b)
CAR	59.2	109.5	319.4	P, p(b), s
COP	70.5	25.3	329.2	P, S
ESK	65.6	33.3	319.3	p(c)
GDH	39.4	31.6	272.9	P, p(a), S
GEO	33.7	87.8	299.5	P, p(a)
GIE	55.5	140.0	334.1	p(b)
GUA	82.0	281.2	43.3	P
HNR	88.7	254.7	41.6	P, p(d)
IST	88.3	21.3	340.9	P, p(d)
KEV	61.0	11.7	336.6	P, p(c)
KON	66.3	24.4	326.5	P
KTG	49.5	25.9	298.4	P, p(b), S
LPB	80.0	127.8	326.0	P, p(d), s

Table 1 (continued)

Station	$\Delta^{(0)}$	$AZ^{(0)}$	$BAZ^{(0)}$	Components
MAL	79.5	46.2	322.4	P
NNA	71.7	132.7	329.3	P, S
NOR	45.7	11.4	293.8	s
NUR	69.2	16.8	336.6	P, p(c), s
OGD	34.3	82.8	297.0	p(a)
PDA	67.4	58.6	313.0	P
PTO	74.1	46.0	319.7	P, p(c), S
QUI	60.8	127.5	327.4	P
SCP	32.2	85.2	296.9	P
SHA	31.0	110.2	312.3	P
SJG	54.1	102.8	315.8	P
STU	75.4	30.8	328.3	P, p(d)
TOL	77.2	44.0	322.1	P, s
TRN	62.6	104.7	318.1	P, p(c)
UME	65.3	17.3	332.9	p(c), s
VAL	65.3	39.2	316.1	p(c), S
WES	35.9	78.8	295.9	P, p(a)

P: long period vertical P waveform or first motion

p(a): short period vertical P waveform. Letter in parenthesis designates stacking group.

S: long period tangential S waveform

s: short period horizontal S waveforms used in stacking

Table 2

Structure Models

	Layer #	V_p	V_s	ρ	Th
1) PS-1	1	3.0	1.2	1.8	2.0
	2	4.0	2.0	2.0	2.0
	3	5.0	2.5	2.2	1.0
	4	6.0	3.0	2.3	1.0
	5	7.0	3.5	2.4	1.0
	6	7.8	4.0	3.2	28.0
	7	6.5	3.0	2.7	10.0
	8	5.5	2.7	2.6	10.0
	9	8.0	4.3	3.2	-
2) PS-9	1	2.0	1.0	2.5	1.2
	2	3.0	1.5	2.5	1.2
	3	4.5	2.3	2.5	2.5
	4	6.8	3.9	2.9	4.0
	5	7.4	4.2	3.0	4.5
	6	7.8	4.3	3.2	27.3
	7	6.5	3.1	2.9	7.0
	8	5.5	2.9	2.7	8.0
	9	8.0	4.6	3.2	-
3) Layer Over Halfspace	1	6.0	3.5	2.7	10.0
	2	8.0	4.6	3.2	-

Figure Captions

Figure 1. Index map of western Washington and Oregon showing the epicenter of the 1965 Puget Sound event and WWSSN stations used in the receiver structure determination. The dashed line is the approximate extent of the Tertiary eugeosyncline, after Snavely and Wagner (1963).

Figure 2. Comparison of synthetic and observed P waveforms for the final source and earth structure models. The observed is displayed directly above the synthetic at each station with the calculated moment indicated next to the traces (x 10^{26} dyne-cm). The focal plot is for the bottom hemisphere.

Figure 3. PS-9 earth model for Puget Sound.

Figure 4. Comparison of P wave synthetic seismograms at five representative stations for the one layer model (top) and PS-9 (bottom). The phase identifications are referred to in the text.

Figure 5. KEV ray summation showing the effects caused by reflections from interfaces bounding the inferred LVZ.

Figure 6. Comparison of P wave synthetic seismograms computed using the PS-1 and PS-9 earth models (Table 2) with the observation at KEV (middle).

Figure 7. Parameter study in which the horizontal layer interfaces at the LVZ of PS-9 are allowed to dip. At each station the top trace is the observed P wave and just below it is the synthetic for PS-9. Below this waveform are two synthetics for a 10° E and 20° E dipping LVZ.

Figure 8. Comparison of the observed and final synthetic SH waves. Same scheme as in Figure 2.

Figure 9. Example of finding the envelope of a short period record using the instantaneous amplitude of the analytic signal.

Figure 10. Stacked envelopes of short period P and S waves. The arrows point directly to the phase being identified except for the pP arrow, which designates the theoretical arrival time.

Figure 11. Map of the southern Puget Sound area showing the epicenter for the 1965 event (after Algermissen and Harding, 1965). The concentric circles are contours of pP reflection points as a function of epicentral distance. The hachured lines are faults inferred by gravity and magnetics from Danes et al. (1965) with the tick marks on the downthrown side. The numbers in parenthesis are depth to basement in km.

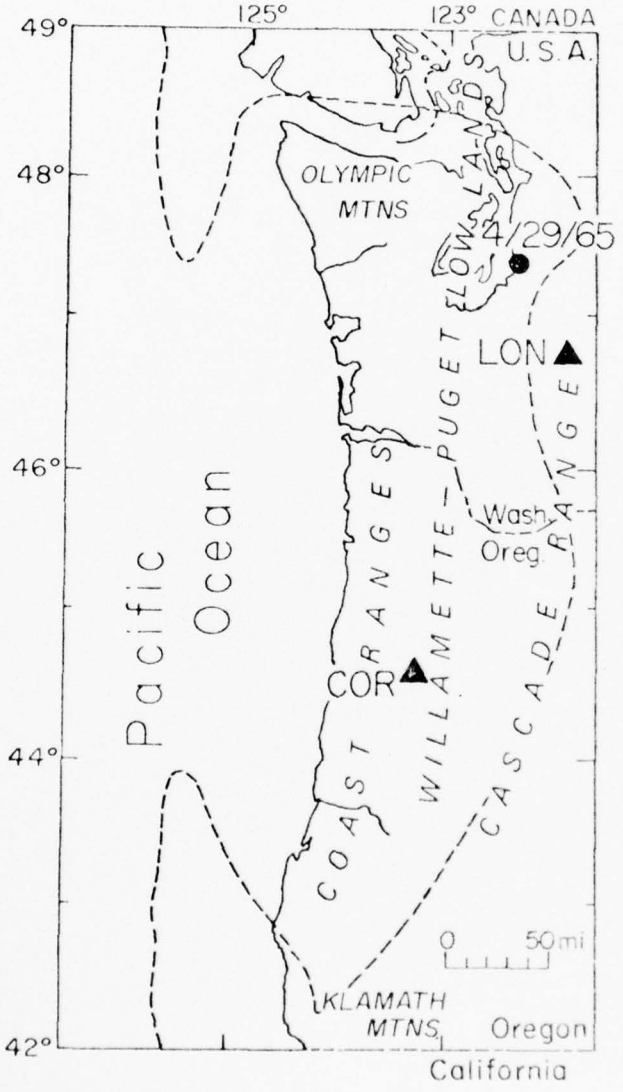
49°
125°
123°
CANADA
U.S.A.
48°
OLYMPIC
MTNS
4/29/65
LOWLAND
LON
PUGET
46°
Pacific
Ocean
COAST RANGES
WILLAMETTE
Wash.
Oreg.
CASCADE RANGE
COR
44°
0
50 mi
KLAMATH
MTNS.
Oregon
California
42°

Fig. 1

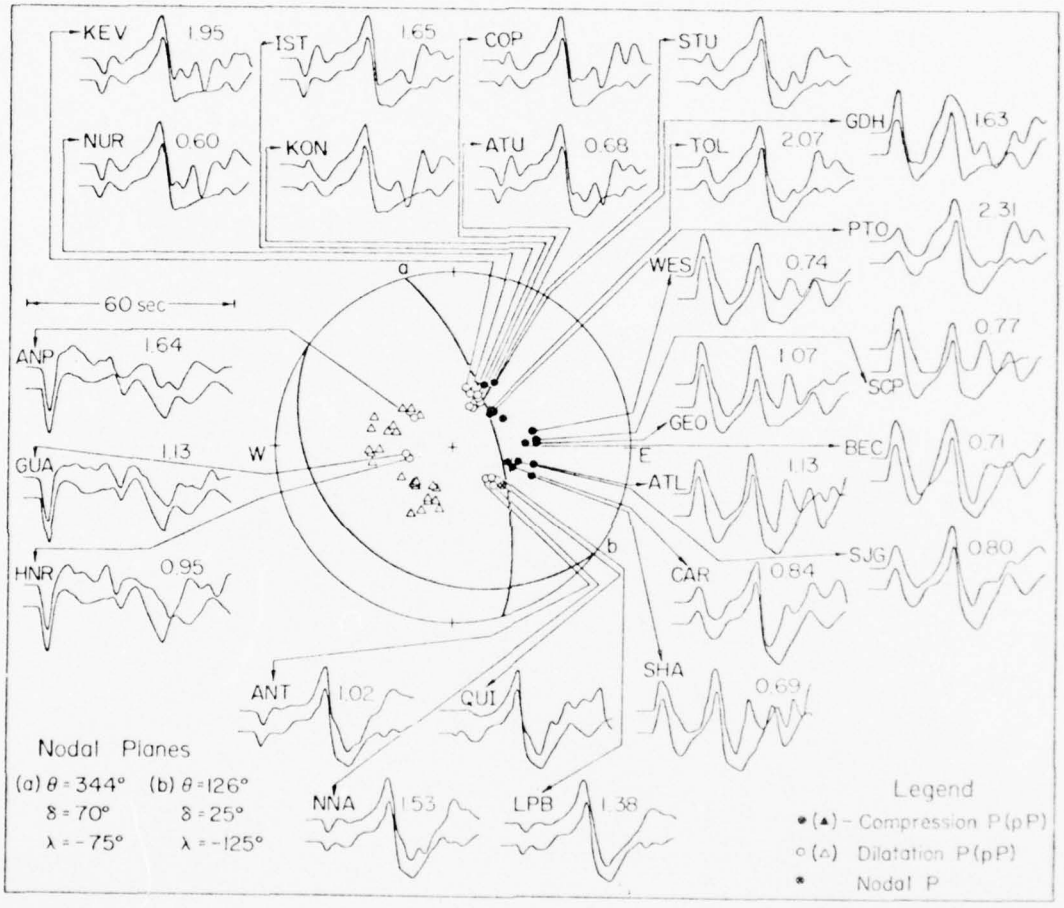
KEV 1.95
IST 1.65
COP
STU
NUR 0.60
KON
ATU 0.68
TOL 2.07
GDH 1.63
PTO 2.31
WES 0.74
60 sec
ANP 1.64
1.07
0.77
SCP
GEO
GUA 1.13
W
E
BEC 0.71
ATL 1.13
HNR 0.95
b
CAR 0.84
SJG 0.80
SHA 0.69
ANT 1.02
GUI
NNA 1.53
LPB 1.38
Nodal Planes
(a) θ = 344° (b) θ = 126°
δ = 70° δ = 25°
λ = -75° λ = -125°
Legend
● (▲) - Compression P (pP)
○ (△) Dilatation P (pP)
* Nodal P

Fig. 2

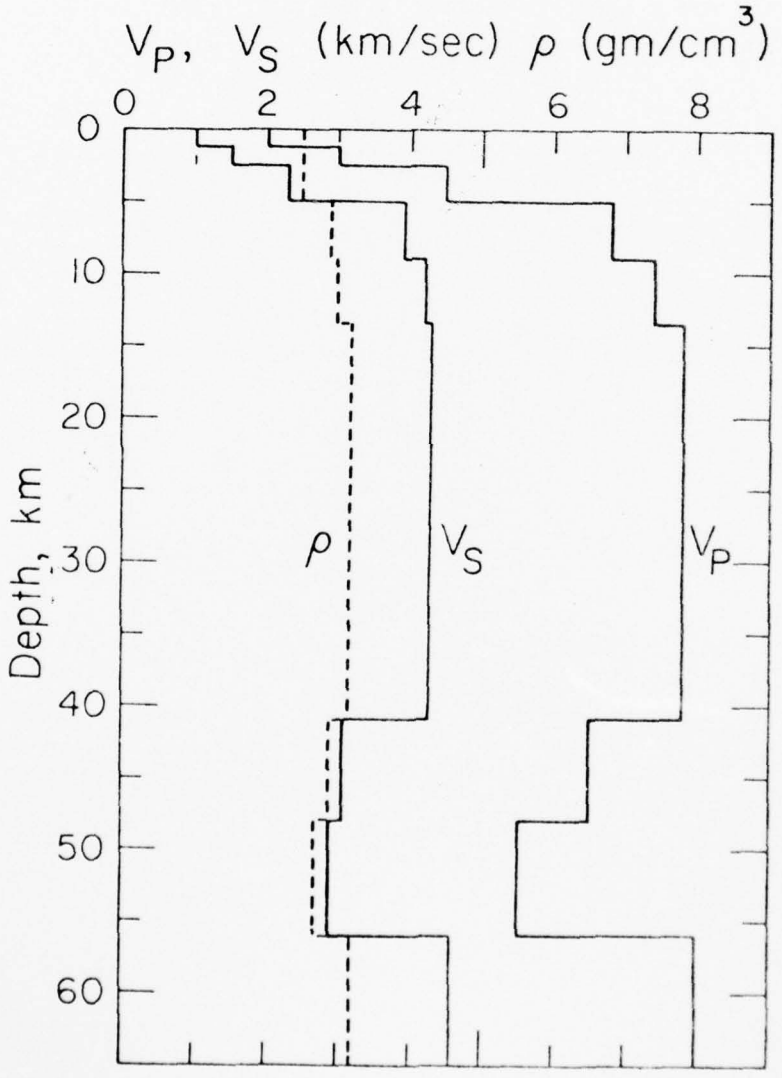

Fig. 3

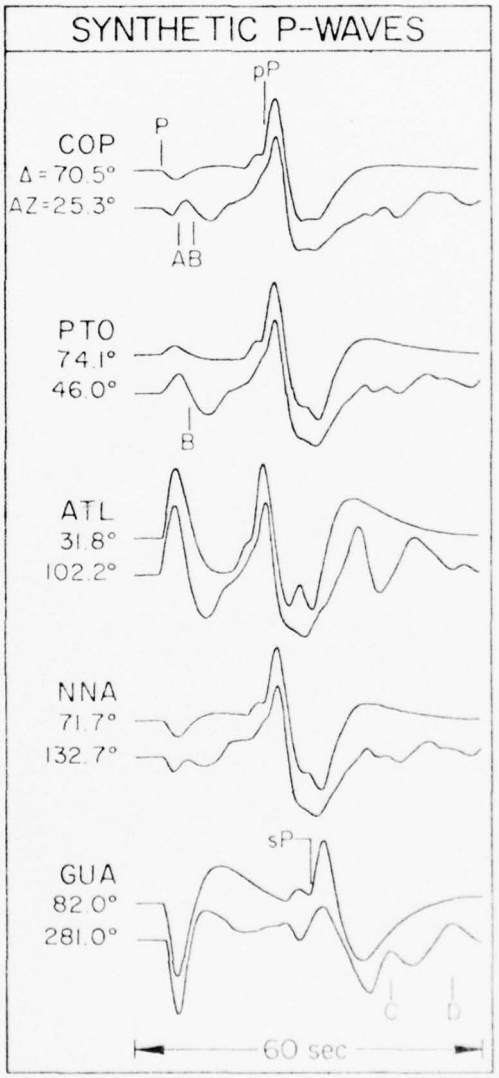
SYNTHETIC P-WAVES
pP
P
COP
Δ = 70.5°
AZ = 25.3°
AB
PTO
74.1°
46.0°
B
ATL
31.8°
102.2°
NNA
71.7°
132.7°
sP
GUA
82.0°
281.0°
C
D
60 sec

Fig. 4

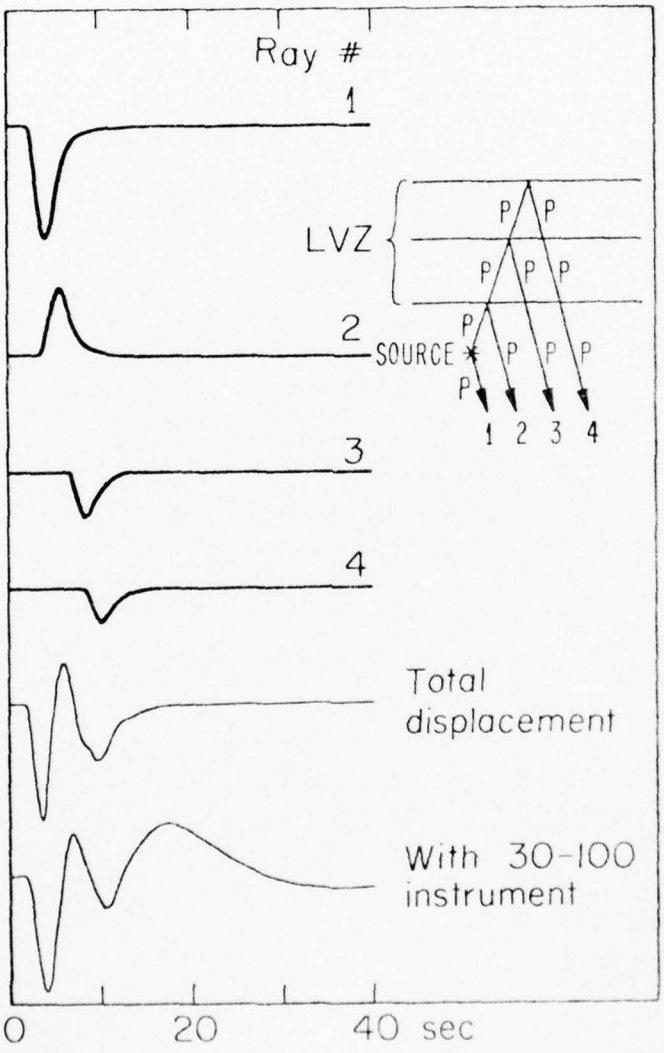
Ray #
1
LVZ
2
SOURCE
3
4
P
1 2 3 4
Total displacement
With 30-100 instrument
0
20
40 sec

Fig. 5

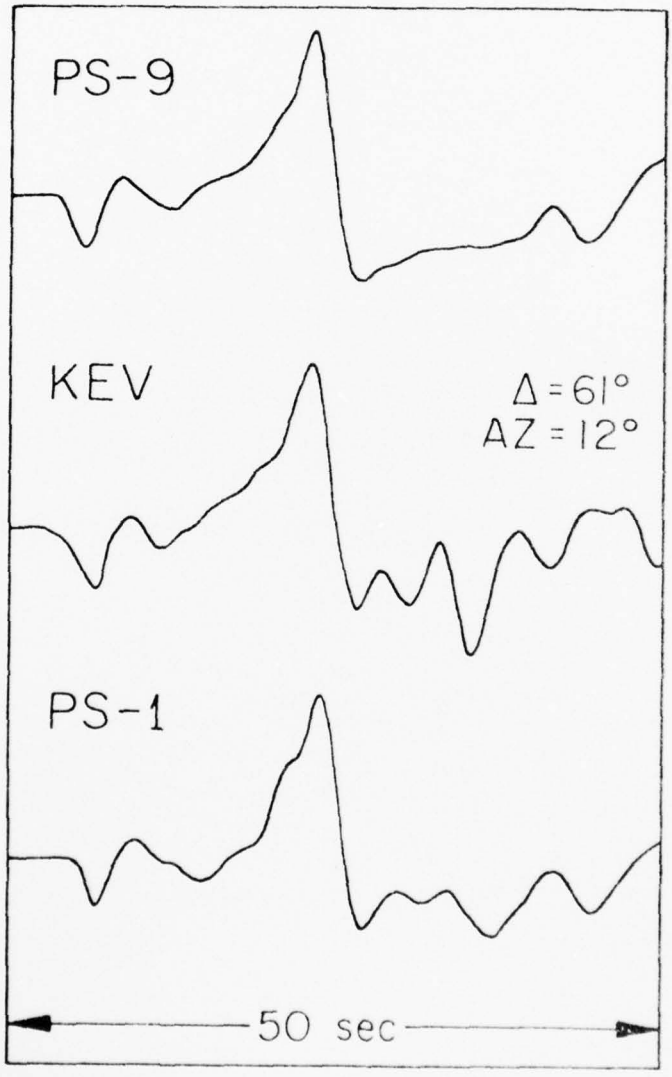

Fig 6

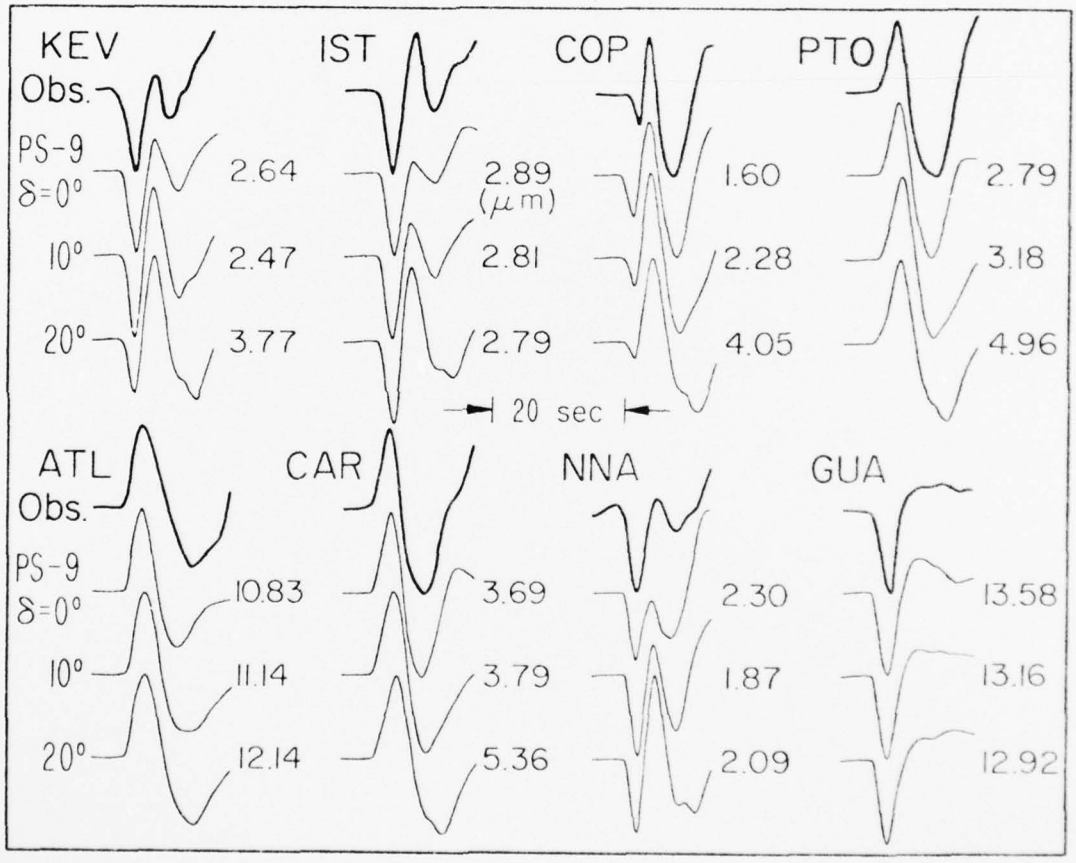
KEV
Obs.
PS-9
δ=0°
10°
20°
2.64
2.47
3.77
IST
2.89
(μm)
2.81
2.79
COP
1.60
2.28
4.05
PTO
2.79
3.18
4.96
20 sec
ATL
Obs.
PS-9
δ=0°
10°
20°
10.83
11.14
12.14
CAR
3.69
3.79
5.36
NNA
2.30
1.87
2.09
GUA
13.58
13.16
12.92

Fig. 7

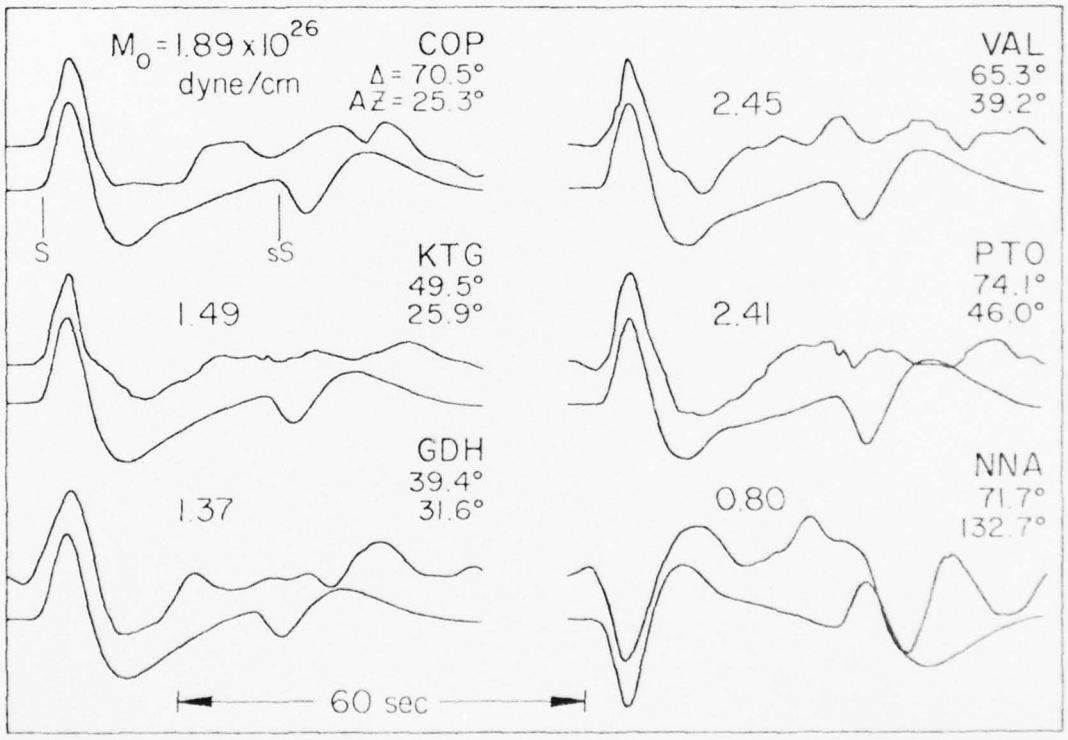
$M_o = 1.89 \times 10^{26}$ dyne/cm
COP
Δ = 70.5°
AZ = 25.3°
S
sS
VAL
65.3°
39.2°
2.45
KTG
49.5°
25.9°
1.49
PTO
74.1°
46.0°
2.41
GDH
39.4°
31.6°
1.37
NNA
71.7°
132.7°
0.80
60 sec

Fig 8

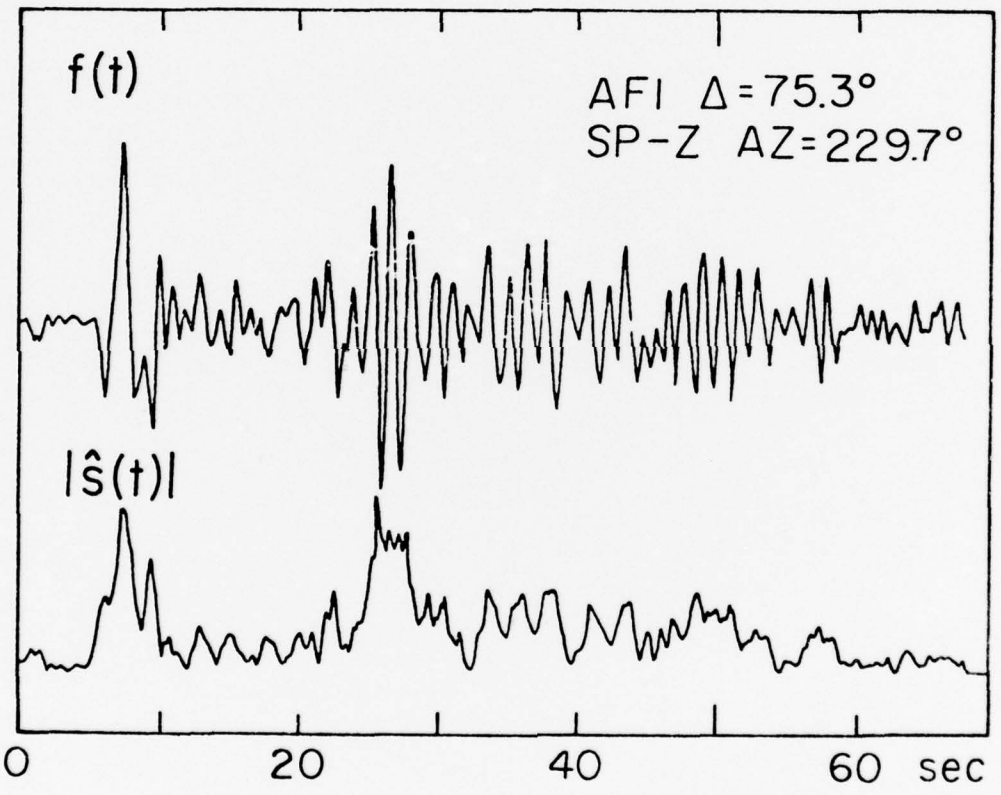

Fig. 9

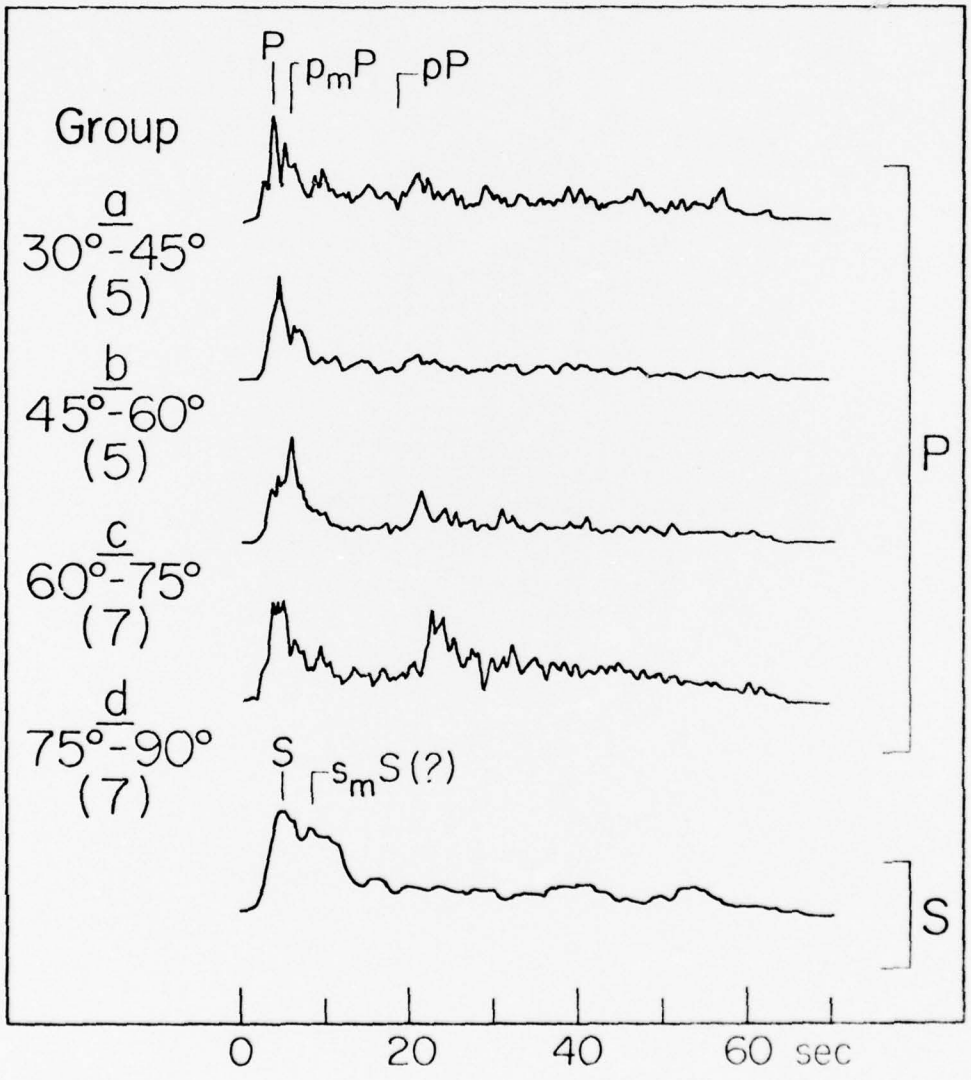
P
pmP
pP
Group
a
30°-45°
(5)
b
45°-60°
(5)
c
60°-75°
(7)
d
75°-90°
(7)
P
S
smS(?)
S
0
20
40
60 sec

Fig. 10

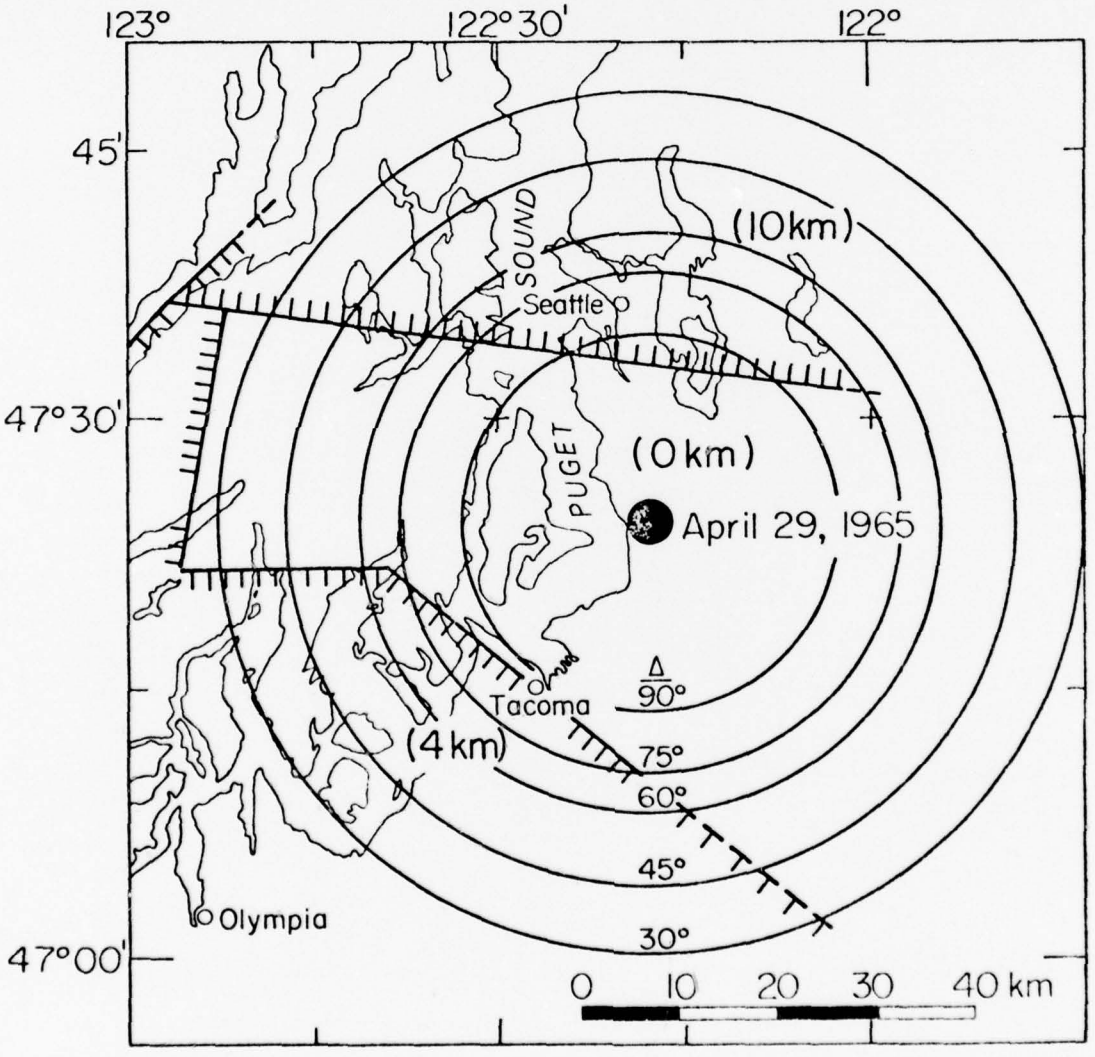
123°
122°30'
122°
45'
47°30'
47°00'
SOUND
PUGET
Seattle
Tacoma
Olympia
(10km)
(0km)
(4km)
April 29, 1965
Δ
90°
75°
60°
45°
30°
0 10 20 30 40 km

Fig. 11

V. Scaling Relations for Earthquake Source Parameters and Magnitudes

R. J. Geller

SCALING RELATIONS FOR EARTHQUAKE SOURCE PARAMETERS AND MAGNITUDES

Robert J. Geller

ABSTRACT

A dataset of forty-one moderate and large earthquakes has been used to derive scaling rules for kinematic fault parameters. If effective stress and static stress drop are equal, then fault rise time, τ, and fault area, S, are related by $\tau = 16S^{1/2}/(7\pi^{3/2}\beta)$, where β is shear velocity. Fault length (parallel to strike) and width (parallel to dip) are empirically related by $L = 2W$. Scatter for both scaling rules is about a factor of two. These scaling laws combine to give width and rise time in terms of fault length. Length is then used as the sole free parameter in a Haskell type fault model to derive scaling laws relating seismic moment to M_S (20 sec. surface wave magnitude), M_S to S and m_b (1 sec body wave magnitude) to M_S. Observed data agree well with the predicted scaling relation. The "source spectrum" depends on both azimuth and apparent velocity of the phase or mode, so there is a different "source spectrum" for each mode, rather than a single spectrum for all modes. Furthermore, fault width (i.e. the two dimensionality of faults) must not be neglected. Inclusion of width leads to different average source spectra for surface waves and body waves. These spectra in turn imply that m_b and M_S reach maximum values regardless of further increases in L and seismic moment. The m_b:M_S relation from this study differs significantly from the Gutenberg-Richter relation, because the G-R equation was derived for body waves with a predominant period of about 5 sec and thus does not apply to modern 1 sec m_b determinations. Previous

investigators who assumed that the G-R relation was derived from 1 sec data were in error. Finally averaging reported rupture velocities yields the relation $V_R = .72\beta$.

INTRODUCTION

The purpose of this paper is to examine empirical relations between gross fault parameters and the agreement of these relations with theoretical models of seismic sources. The gross parameters to be studied are fault length, width and rise time, rupture velocity m_b and M_s, and seismic moment. Data from other investigators' studies of individual earthquakes are used to study scaling of source parameters in an approximate way. In general the data are consistent with fault width scaling proportionately to fault length and rise time scaling proportionately to the square root of fault area. This scaling can then be used to find $m_b - M_s$, $\log M_o - M_s$ and $\log S - M_s$ relations. Some of those relations have been studied by Kanamori and Anderson (1975b),who provided a theoretical basis for many of the empirical relationships used in seismology.

Tsuboi (1956) was the first investigator to utilize similarity, the concept of relating earthquakes of different sizes by a one parameter model. By assuming that the horizontal dimensions of the earthquake source volume were three times larger than the vertical dimension, Tsuboi derived from the relation $E = \mu\varepsilon^2 A^{1.5}/6$, where E is released energy, μ is average rigidity, ε is average strain drop and A is aftershock area. Such approximate scaling relations, as first pointed out by Tsuboi, require that the physics of material failure be identical for large and small earthquakes. If that assumption is generally true and

if earthquakes tend to be geometrically similar, then it follows that fault length and width, and final dislocation all will scale together. Differences in material properties will weaken the exactness of the similarity when earthquakes from two different regions are compared, but, in an approximate sense, similarity, as is shown by the data presented below, is a valid concept.

The first paper to systematically relate observed gross seismic source parameters to the source spectrum was the now classic work of Aki (1967). Although the results presented in this paper modify his results, the methodology and basic outlook are similar to Aki's. Later Brune (1970, 1971) contributed to the understanding of seismic source spectra.

Similarity between earthquakes is a dynamic as well as a static concept. Not only the final static parameters, but also the spectral shape of the equivalent source time function, scales with fault length. Spectral similarity can best be demonstrated by comparing two earthquakes with identical location and focal mechanism, but different magnitude. Such a comparison ensures that seismograms from both events will be affected equally by the medium response, so that all differences between the records will be from the source effects.

Observational studies of similar pairs of earthquakes have been made by Berckhemer (1962) whose results were interpreted by Aki (1967) to support Aki's ω^{-2} model. Tsujiura (1973) studied groups of events from various regions, concluding that most data were in accord with Aki's ω^{-2} model, but that some were better fit by an ω^{-1} or ω^{0} model.

One cannot directly compare spectral characteristics of source mechanisms from different regions without first correcting the seismograms for transmission effects. Removing the effects of medium response will usually require use of synthetic seismogram methods. We assume however that one can compare logarithmic fault parameters, such as m_b, M_S or log L, for events in different regions. These comparison are made with the intention of looking at order of magnitude relationships rather than details.

In this paper we will look at scaling relations between five sets of such logarithmic parameters: log L vs. log W (fault length vs. width), log τ vs. log S (fault rise time vs. area), M_S vs. log M_o (surface wave magnitude vs. seismic moment), m_b vs. M_S and log S vs. M_S. What will be shown are not exact correlations, but rather trends which appear to be applicable to most earthquakes. Agreement between the simple model used in this paper and the data are quite good. (Long narrow transform faults, such as the San Andreas, are a separate class of faults which are not considered in this paper.)

OBSERVATIONAL DATASET

The earthquake data shown in Table 1 are from the same forty-one shallow events used by Kanamori and Anderson (1975b). All values for M_S are from their paper; the sources for all other observational parameters are given in the table of references. Except for minor differences which are primarily due to the use of slightly different references, data for M_o and S are equivalent to Kanamori and Andersons'. Each

numbered entry in the table of references corresponds to the earthquake with the same number in Table 1. All but two of the columns are observational data; τ^*, predicted rise time, and $\Delta\sigma$, calculated stress drop, will be discussed below. Length and width have been taken from the references, or in some cases estimated. Length always refers to length along the strike, regardless of focal mechanism; width refers to width along the dip. Average dislocation comes either from field measurements or from dividing the moment (determined from seismograms) by the area and an assumed value of the shear modulus.

For all events since August 1963 the m_b value is either taken directly from the PDE Monthly Summary, or calculated from the data in Earthquake Data Reports. As reported by L. M. Murphy in Båth (1969), USCGS (later NOAA and now USGS) asks for the amplitude of the largest pulse (with period less than three seconds) in the first five cycles of the teleseismic P or P_n arrival. The values of A and T are then used in the Gutenberg-Richter formula

$$m_b = \log_{10}(A/T) + Q, \qquad (1)$$

to derive m_b for each station. Values more than 0.7 magnitude units from the mean are deleted and the final average is then taken.

Estimates of rise times typically were made by fitting the first upswing on long-period local records to synthetic seismograms calculated using the Haskell (1969) whole space model at one or two stations.

Clearly it would be desirable to use synthetics made for more realistic models of earth structure, but they have not yet been calculated for these events. Uncertainties due to the tradeoff between rise time and rupture velocity and due to the model may combine to cause errors which cannot be estimated. In some cases, such as the Tottori earthquake (Kanamori, 1972b), rupture velocity and rise time are independently constrained.

LENGTH VERSUS WIDTH

Fault length is plotted against fault width in Figure 1. It can be seen that (with considerable scatter) observational data demonstrate that L = 2W. In Figure 1, the numbers refer to earthquakes in Table 1. Intraplate events are plotted as open circles and interplate events as solid circles. (This convention is also used in all later figures.) There is not any clear difference between the interplace and intraplate groups. Abe (1976) has independently found L = 2W for a dataset of Japanese earthquakes.

The Haskell model uses L as the direction in which rupture propagates, while L was measured along the direction of the strike for Figure 1. It is implicitly assumed, then, that for these 41 events rupture propagated parallel to the strike. This almost certainly false for some thrust events such as San Fernando (Boore and Zoback (1974), Trifunac (1974), Mikumo (1973b)),and may well be false for events like Nemuro-Oki L < W. In spite of these exceptions it seems that rupture usually propagates parallel to the strike, especially for strike-slip faults.

RISE TIME VERSUS THEORETICAL PREDICTIONS

Kanamori (1972b) showed that

$$\dot{D} = \frac{\bar{D}}{\tau} \cong \sigma_{e,o} \frac{\beta}{\mu} \tag{2}$$

where $\dot{D}$ is dislocation velocity, $\bar{D}$ is average dislocation, τ is rise time, and $\sigma_{e,o}$ is effective stress. If one assumes that effective dynamic stress is equal to static stress drop, $\Delta\sigma$, this assumption can be tested by comparing observed rise times to the theoretically predicted rise time

$$\tau^* = \frac{\mu\bar{D}}{\beta\Delta\sigma} \quad . \tag{3}$$

One can obtain stress drop in closed form for only a few simple models. The most straightforward of these is the circular crack with constant stress drop discussed by Keiles-Borok (1959). For that model stress drop is given by

$$\Delta\sigma = 7\pi^{3/2}\mu\bar{D}/(16\sqrt{S}) = 7M_o/(16(LW/\pi)^{3/2}) \tag{4}$$

Although this formula does not give the exact stress drop for the rectangular fault model, it follows from the work of Sato (1972) that this is a good approximation. If we substitute (4) in (3), where S is the area of the rectangular fault and $\bar{D}$ is average dislocation, we obtain

$$\tau^* = 16S^{1/2}/(7\pi^{3/2}\beta) \qquad (5)$$

The values of $\Delta\sigma$ and τ^* in Table 1 were calculated using (4) and (5), respectively.

Figure 2 is a plot of observed versus predicted (from (5)) rise times for a number of earthquakes. It can be seen that, again with considerable scatter, observational and theoretical rise times are in agreement. Abe (1975b) reached a similar conclusion from a dataset of five Japanese earthquakes.

The agreement between theoretical and observed rise times has important implications for engineering seismology. The only observational parameter required in (5) is fault area, which frequently can be estimated from geological data. If total dislocation can also be determined from geological field work, then particle velocity near the fault, an important parameter in engineering seismology, can be reliably estimated. This is potentially of great values in areas lacking in historical seismicity or good instrumental data.

RUPTURE VELOCITY

Table 1 lists rupture velocities reported by various investigators. These values were determined from matching synthetic seismograms to local records or from surface wave analysis. To a certain extent then, these values are model dependent. Some also may be affected by the difficulty in resolution between rise time and rupture velocity. Nevertheless, these measurements probably represent a good average sample of

rupture velocity measurements. If one picks values of β ranging from 3.5 km/sec for shallow crustal events to 4.5 km/sec for events breaking the entire lithosphere, one then can calculate that the average value of (V_R/β) is 0.72.

Archuleta and Brune (1975) found $V_R/\beta = 0.7$ in experiments on fracture of prestressed foam rubber. Their measured value was for the surface of the foam rubber, but if one assumes infinite rupture velocity along the dip, their result agrees very well with the result $V_R/\beta = 0.72$ observed for earthquakes. (Their minimum possible value for V_R/β at depth is 0.63β.) Agreement between the earthquake and foam rubber rupture velocities may be fortuitous or may be caused by a common physical friction mechanism.

CHOICE OF FAULT MODELS

All "deterministic" source models specify some (nearly always kinematic) conditions at the source, which then fix via the representation theorem of de Hoop (1958) and Burridge and Knopoff (1964), the complete time history at every point in the medium. (Aki (1967, 1972) and Haskell (1966) proposed "statistical" models in which only the amplitude spectrum at the source function is specified. Since we will be looking at dislocation rise times, these statistical models are not appropriate choices.) Typically the source theory papers calculate seismograms for an isotropic homogeneous whole space. Since our interest is in logarithmic source parameters, we will assume the whole space models are adequate.

In most deterministic source models, either fault dislocation (e.g., Haskell (1969), Mikumo (1973b)) or stress drop (and therefore fault dislocation, e.g., Burridge and Willis (1969), Richards (1973), Sato and Hirasawa (1973)),is specified, which in turn gives displacement at other points in the medium. Other authors, e.g., Hanson *et al.* (1974) and Andrews (1975),have studied numerical models with friction between the fault surfaces.

All of these models predict far-field pulses which scale linearly with fault dimensions. Also they all yield flat spectra at low frequencies and ω^{-n} high frequency asymptotes ($n \geq 2$). Thus all of the models have at least one "corner frequency" (and some have several). For these models the static or low frequency level, which is proportional to seismic moment, grows as L^3.

We will continue to use the Haskell (1964, 1969) model of a rectangular fault (shown in Fig. 3) in this paper. Most studies have used this model in the determination of rise times from local seismograms. The basic Haskell model is a fault with length L, width W, rise time τ (linear ramp time function), final dislocation $\bar{D}$ and rupture velocity V_R. Rupture is instantaneous in the width direction and propagates (starting at one end) along the length with velocity V_R. Some investigators have made the natural extension to bilateral rupture propagation.

Haskell's (1964) expressions are for a "one-dimensional" model in which width is included only as a weighting factor in the moment. Hirasawa and Stauder (1965) and Mikumo (1969) included the complete

effect of the width to obtain an expression for spectral source amplitude.

$$\left|U_c(\omega)\right| = \frac{M_o R^C_{\theta\phi}}{4\pi\rho r c^3} \left|\frac{\sin(\omega\chi_\tau)}{\omega\chi_\tau}\right| \left|\frac{\sin(\omega\chi_L)}{\omega\chi_L}\right| \left|\frac{\sin(\omega\chi_W)}{\omega\chi_W}\right| \tag{6}$$

In (6) M_o is moment, ρ is density, r is distance, c is either P or S velocity and $R^C_{\theta\phi}$ is the radiation pattern (given by Haskell, 1964). χ_L and χ_W are duration times associated with length and width, respectively and determined by fault geometry and position of the observer.

$$\chi_L = \left|L(1/v_R - \cos\theta/c)/2\right| \tag{7}$$

$$\chi_W = \left|W(\cos\phi \sin\theta)/(2c)\right| \tag{8}$$

$$\chi_\tau = \tau/2 \tag{9}$$

SPECTRAL CHARACTERISTICS

For the present, let us adopt (in slightly modified form) the similarity relations given by Kanamori and Anderson (1975b).

$$\frac{W}{L} = C_1 = \text{const} \tag{10}$$

$$\frac{\bar{D}}{L} = C_2 = \text{const} \tag{11}$$

$$\frac{\beta\tau}{L} = C_3 = \text{const} \tag{12}$$

(10) is the condition of the geometrical similarity; (11) and (12) imply constant stress drop and constant effective stress.

We will select values of the constants which seem to be good averages of observational data. We found that

$$L = 2W \tag{13}$$

seemed to be the approximate average of the empirical data. When we substitute $L = 2W$ into (5) and set $\beta = 4.0$ km/sec we get

$$\tau = [16\sqrt{L^2/2} \;/\; (7\pi^{3/2} \cdot 4)] = .0726L \tag{14}$$

where τ is in seconds and L is in kilometers.

We could use (11) directly to get a scaling relation between fault displacement and length. In practice though, most estimates of $\bar{D}$ in Table 1 come from dividing M_o by μS, so it seems better to relate moment directly to length. Setting $L = 2W$ in (4) gives moment in terms of fault length and stress drop.

$$M_o = L^3\Delta\sigma \cdot 16/(7(2\pi)^{3/2}) = (1.45 \times 10^{20})\, L^3\Delta\sigma \tag{15}$$

where M_o is in dyne cm, L is in km and $\Delta\sigma$ in bars.

From (6) we can isolate a spectral factor, dependent only on fault parameters and frequency.

$$A(\omega) = L^3 \left| \frac{\sin(\omega\chi_T)}{\omega\chi_T} \right| \left| \frac{\sin(\omega\chi_L)}{\omega\chi_L} \right| \left| \frac{\sin(\omega\chi_W)}{\omega\chi_W} \right| \qquad (16)$$

The L^3 term follows from the similarity relation $M_o \sim L^3$. When $A(\omega)$ is multiplied by stress drop and the constant in similarity equation (15) we get the source moment rate spectrum.

Equation (16) and the factors (7)-(9) are well known results for the case of a rectangular fault in a whole space. These expressions can also be applied directly to the case of a rectangular fault with horizontal rupture propagation in the earth. The form of the expressions remains identical, but c now should be interpreted as the apparent velocity along the earth's surface.

For body waves $c = v_c/\sin i$, where v_c is the near-field P or S velocity and i is the takeoff angle of the teleseismic ray from the focal sphere. This can be understood physically by invoking reciprocity. Signals from a source at the position of the teleseismic receiver would be picked up $(L \cos \theta)/(2c)$ sooner at the end of the fault than at the center. Thus for the case of infinite rupture velocity, this is the difference between arrivals at the receiver from the end and center of the fault. This type of geometrical interpretation can be applied to both (7) and (8), so that these factors are seen to be the difference in arrival times obtained from geometrical optics. Ben-Menahem (1962) gives a more rigorous derivation of this result.

For surface waves (7) is the well known directivity factor first given by Ben-Menahem (1961). If we neglect the variation of the excitation function with depth, (8) is the factor for the effect of fault width on the surface wave spectrum. In both (7) and (8), c is the (frequency dependent) surface wave phase velocity. The geometrical interpretation of (7) and (8) as phase delay between "arrivals" from the center of the fault and the ends is the same as for body waves.

Typical values of c for teleseismic P waves might be 14 km/sec, while for surface waves 4 km/sec is appropriate. If rupture velocity, v_R = 2.5 km/sec, then for surface waves 1/c will be of the same order of magnitude as $1/v_R$. As θ varies from 0 to 2π, χ_L will range from 0.15L to 0.65L. Thus a horizontally propagating rupture will cause a large directivity effect. On the other hand, for body waves from the same source, $\cos\theta = \sin i$, so because of the relatively steep takeoff angles of teleseismic rays, it is reasonable to assume $|\cos\theta| < 0.5$.

This assumption leads to the conclusion that χ_L will vary only from 0.36L to 0.44L. There will be only a small azimuthal dependence (i.e. directivity effect) of the teleseismic body wave pulse. This implies that one can infer the nature of a horizontal rupture propagation much more easily from surface waves than teleseismic body waves.

Because c is the apparent velocity, rather than the near-field P or S velocity, it is inadequate to present only a single spectrum representing the effect of the seismic source, as was done, for example, by Aki (1967,1972). There is a separate "source spectrum," $A(\omega)$, for each body wave phase or surface wave mode, because of the different values of c. The source spectrum depends on azimuth, source dimensions, and the phase velocity, c. Both the length factor, (7) and the width factor, (8), are different for

each mode. In the next section we will average χ_L and χ_W over all azimuths. In these averages, the value of c will affect only χ_W, even though both factors are affected at nearly every particular azimuth.

Both (6) and (16) completely neglect the effect of the earth's transfer function on observed seismic waves. If one were to calculate synthetic seismograms for an individual earthquake, it would be necessary to consider the earth's response and the earthquake source parameters, e.g., Langston and Helmberger (1975) for body waves or Harkrider (1964, 1970) for surface waves. Langston and Helmberger (1975) have demonstrated that sP and pP phases play a crucial role in the "P wave" from shallow earthquakes. Similarly one must consider the surface wave excitation functions and the source mechanism to calculate accurate Rayleigh and Love amplitudes.

In this paper we consider trends among events, rather than accurate determination of parameters of particular events. Therefore, we assume that the effect of the earth structure averages out when we construct scaling relations. Thus we will use (16) to get relations between m_b and M_s, log L and M_s, log M_o and M_s.

AVERAGE SPECTRA

We now want to find average asymptotic forms for log $A(\omega)$ from (16). In particular we require expressions for teleseismic P phases (from which m_b will be determined) and for 20-second Rayleigh waves (from which we find M_s). For both cases we will find average values of χ_L and χ_ω which take the direction of radiation into account. In making our approximation, we will replace $|(\sin X)/X|$ by one for $X < 1$ and by X^{-1} for $X \geq 1$.

Takeoff angles of teleseismic body waves are nearly vertical. We will adopt the approximation that the rays takeoff straight down. Thus, for body waves, we set $\theta = \frac{\pi}{2}$ in (7) and (8). Also, in that case, $|\cos \phi| = \sin \delta$, where δ is dip angle of the fault plane. Using these values, average spectral factors for body waves are

$$\langle \chi_L \rangle_{body} = L/(2V_R) \tag{17}$$

and

$$\langle \chi_W \rangle_{body} = W \sin \delta/(2c) \ . \tag{18}$$

For surface waves we will average χ_L and χ_W for $\theta = 0$ to $\theta = 2\pi$. On the earth's surface we get $|\cos \phi| = \cos \delta$. Thus we get

$$\langle \chi_L \rangle_{surf} = L/(2V_R) \tag{19}$$

and

$$\langle \chi_W \rangle_{surf} = W \cos \delta/(\pi c). \qquad (20)$$

Comparison of (17) and (18) with (19) and (20) shows that the average corner frequency due to fault length will be the same for body waves and surface waves, but that the corner frequencies due to width will be different. This difference affects the high frequency spectrum only since the average corner frequency for width is higher than that for rise time or length. Note that we have assumed that rupture propagates parallel to the earth's surface to obtain (17)-(20).

Before calculating numerical values for (17)-(20) we must fix V_R, δ and c. Also we will use (13) to relate L to W. We will set V_R = 2.88 km/sec, δ = 45°, c = 14 km/sec for body waves and c = 3.9 km/sec for surface waves. (For the earth, c must be the appropriate phase velocity, not the S wave velocity. Neglecting the frequency dependence of surface wave phase velocity is a reasonable approximation.)

From (9) and (14)

$$\chi_\tau = 0.0363\ L = C_\tau L \qquad (21)$$

(17) and (19) both give

$$\langle \chi_L \rangle = 0.174\ L = C_L L \qquad (22)$$

The width factor for body waves is

$$\langle \chi_W \rangle_{body} = 0.0126\ L = C_{Wb} L \qquad (23)$$

For surface waves we get

$$\langle \chi_W \rangle_{surf} = 0.0289\ L = C_{W_s} L \tag{24}$$

We now can approximate the logarithm of $A(\omega)$ from (16).

$$\begin{aligned}
&\log A(\omega) = 3 \log L && \text{for } \omega < (C_L L)^{-1} \\
&\log A(\omega) = 2 \log L - \log \omega - \log C_L && \text{for } (C_L L)^{-1} < \omega < (C_\tau L)^{-1} \\
&\log A(\omega) = \log L - 2 \log \omega - \log (C_L C_\tau) && \text{for } (C_\tau L)^{-1} < \omega < (C_W L)^{-1} \\
&\log A(\omega) = -3 \log \omega - \log (C_L C_\tau C_W) && \text{for } (C_W L)^{-1} < \omega
\end{aligned} \tag{25}$$

The spectra from these relations are plotted in Figure 4. Note that the body wave spectra have a much longer interval of ω^{-2} decay than the surface wave spectra. Calibration of these curves with M_s and M_o is discussed below. Also, note that ω is in radians in (25), but in hz in Figure 4.

The asymptotic spectral amplitudes given by (25) are very similar to the results obtained by Kanamori and Anderson (1975b). They used the same asymptotic approximation for sin X/X in conjunction with Haskell's (1964) spectral expression. Since Haskell's expression ignores the effect of width on the spectrum, the results of this paper differ from Kanamori and Andersons' only at frequencies above the corner frequency for width. For example, the model in this paper predicts

constant 20 sec spectral amplitude for faults longer than 110 km while Kanamori and Andersons' predicts amplitudes which increase linearly with L. As a result, their model predicts $M_S \sim \log L$ for large events, while this paper predicts M_S = const.

Even though both spectra in Figure 4 have an eventual ω^{-3} asymptote, they are quite different than Aki's (1967) ω-cube model. Aki's models, as a result of his assumption that $vk_L = k_T$, had only a single corner frequency. His ω-cube model makes a fairly abrupt transition from ω^0 to ω^{-3} behavior. The spectra presented here, particularly the body wave spectrum, show a gradual transition from ω^0 to ω^{-3} asymptotes.

m_b-M_s RELATION

Changes in the definition of the body wave magnitude scale have resulted in a large amount of confusion today. Gutenberg and Richter (1942) extended the body wave magnitude scale from local events to fairly distant events which were recorded on Wood-Anderson and strong motion torsion instruments.

Gutenberg (1945) introduced a scheme for m_b differing only in minor details from the summary in Richter (1958). He determined m_b from the instruments available in 1945, which were mostly broadband mechanical types. Gutenberg (1945) stated that "the average period of P waves in teleseisms is about 4-6 seconds." In general, Gutenberg did not publish the period of the P waves he used in determining m_b, but from a preliminary examination of his unpublished data it seems that many of his amplitudes were obtained at periods of 4-10 sec.

Gutenberg and Richter (1956) published their final version of the relation between m_b and M_s:

$$m_b = 0.63\ M_s + 2.50 \qquad (26a)$$

$$M_s = 1.59\ m_b - 3.97 \qquad (26b)$$

Their primary reason for deriving this relation was to facilitate the construction of a "unified magnitude scale." Investigators at that time apparently viewed the discrepancy between the two magnitude scales as an experimental error, rather than a fundamental effect of the seismic source spectrum. This view was not unreasonable at the

time because m_b was measured at periods differing only by a factor of 2 to 5 from M_s and modern source theories had not yet been developed. In any case, Gutenberg and Richter found the (body wave) magnitude m_s, corresponding to a given M_s, by using (26a). They then took a weighted average of m_b, the actual body wave magnitude, and m_s to obtain m, the unified magnitude. Later Richter (1958) published values of unified (surface wave) magnitude, M, which he obtained by converting m to M using (26b). In retrospect, unified magnitude was inappropriate, since it now is clear that for all seismic source theories m_b and M_s represent different parts of the spectrum which are not related by a factor independent of fault length.

m_b determinations by the USCGS (later NOAA and now the USGS) differ markedly from those used by Gutenberg and Richter. USCGS values for m_b use (1), but A and T are measured on the WWSSN short period instrument, which is sharply peaked at 0.5 sec. T nearly always is about 1 sec in WWSSN magnitude determinations. Thus WWSSN magnitudes are based roughly on 1 sec spectral amplitude. On the other hand, Gutenberg and Richter determined m_b for many events at about 5 sec, with even larger T for the largest events. Therefore, it is wrong to take the Gutenberg-Richter m_b as being related to spectral amplitude at any one particular period.

MODELING m_b-M_s

Aki (1967) proposed two statistical models of seismic sources, an "ω-square" model (which decayed as ω^{-2} at high frequencies) and an "ω-cube" model, after Haskell (1966) (which decayed as ω^{-3}). Aki

compared these two models by calculating spectral ratios for similar events and by calculating the relation of m_b to M_s predicted by each model.

Aki calculated M_s by adding a constant to the logarithm of spectral amplitudes at 20 sec. The constant was chosen to give the best agreement between theoretical and observational spectral ratios of pairs of similar earthquakes studied by Berckhemer (1962). After fixing the additive constant for M_s, Aki then defined a similar relation for m_b. He set m_b = const + (.71 ~ .83) log A(1 sec) and found the constant which would make $m_b = M_s$ when M_s = 6.75. The coefficient of log A(1 sec) comes from a correction for duration.

Aki (1967) calibrated his curves for the ω-square and ω-cube models in this way. He then compared the m_b-M_s curves predicted by the models to the Gutenberg-Richter m_b-M_s relation (26). He suggested that the excellent agreement of the ω-square model with (26) strongly supported it, over the ω-cube model. Unfortunately, his theoretical m_b-M_s curve was based on 1-sec spectral amplitudes, while (26) was derived from mostly 4 to 10 sec data. Actually it seems that Aki's support for the ω-square model was incorrect. The WWSSN m_b-M_s data (based on 1 sec m_b), discussed below, disagree with the ω-square model.

The approach in this paper is to match m_b-M_s, log S-M_s, log M_o-M_s and spectral ratio data simultaneously, adjusting the two free parameters to get good overall agreement with the data. A least squares solution is not particularly appropriate

because of the large number of parameters and the lack of similarity (e.g., different stress drops) found when earthquakes are examined in detail.

m_b is approximated by a constant plus log A(1 sec) and M_s by another constant plus log A(20 sec). $A(\omega)$ was found using (25) with the constants in (21)-(24). After several trials the additive constants for m_b and M_s were determined to be $C_{m_b} = 4.30$ and $C_{M_s} = 2.97$. To obtain seismic moment as a function of L, it was necessary to assign $\Delta\sigma$ for use in (15). Kanamori and Anderson (1975b) found that stress drops are 10-30 bars for most interplate earthquakes and 30-100 bars for most intraplate earthquakes, so $\Delta\sigma = 50$ bars was used.

Clearly it is not exactly correct to get m_b and M_s directly from spectral amplitudes. A more accurate approach would be computing synthetic seismograms and then measuring m_b and M_s as it is done for data. For this study, using spectral amplitudes seems to be an acceptable approximation. We plan to measure m_b and M_s directly from synthetic seismograms in a future study.

Archambeau (1975) thoroughly discusses the differences between time domain and frequency domain estimates of m_b and M_s. His study stressed the very small differences which are crucial in the context of seismic discrimination. In general though, his study supports the applicability of using spectral amplitudes to estimate m_b of small and moderate events. Probably any discrepancy between spectral amplitudes and time domain amplitudes is most severe for larger events. In later work we will calculate the size of that effect.

m_b-M_s DATA

Two kinds of m_b-M_s data are plotted in Figure 5. Points below the solid line midway up the figure are from a study of almost one thousand events by Evernden (1975). Each point is the average value of M_s for all earthquakes with that m_b value. Because Evernden's m_b values are an average of 0.3 lower than the USGS values, 0.3 is added to the m_b values before plotting them. Points above the line are values for individual events since mid-1963 as listed in Table 1.

Data shown in Figure 5 are in general agreement with a study of the m_b-M_s relation by Nagamune (1972). Nagamune fitted two straight lines to two years of WWSSN m_b-M_s data. He found

$$M_s = 1.89\ m_b - 4.62 \qquad M_s > 5.73$$

and

$$M = 1.05\ m - 0.02 \qquad M < 5.73$$

The latter equation comes from a study of small events mostly in Hokkaido. Magnitudes in the latter equation are very similar to m_b and M_s.

m_b-M_s curves from two models are plotted in Figure 5. The curve on the right is the $m_b - M_s$ relation predicted by Aki (1972), which is based just on log A(1), without any correction for duration. It can be seen that all the data lie substantially to the left (smaller m_b) of the ω-square curve. Inclusion of a duration correction for large

events would not affect the basic conclusion that the ω-square model does not agree at all with the data.

The lefthand curve is derived from the Haskell model presented in this paper. It can be seen that the predicted m_b-M_s curve is generally in good agreement with the data. It would have been better to have averaged the value of m_b for all earthquakes with a particular M_s for all WWSSN events for several years, rather than present just a few data points.

The Evernden data have a slope of one for events with m_b smaller than 5¼ while the predicted m_b-M_s curve has a slope of $\frac{3}{2}$ for $m_b > 4.2$, which clearly disagrees with the data. The large events are too scattered to warrant a definite conclusion, but the predicted maximum m_b of 6.0 is probably 0.3 or 0.4 too small. This discrepancy may be due to use of spectral amplitudes instead of time domain amplitudes. Also, it was assumed above that m_b was always based on 1 sec observations, but this is not strictly true. The Portuguese earthquake of 1969 (number 34 in Table 1) has m_b of 7.3, the largest of any of the events in Table 1. The average T for this event was 1.77 sec; the Haskell model predicts that if m_b had been determined at 1 sec, it would be 0.5 smaller. A systematic variation of T as a function of m_b could account for part of the difference between the theoretical curve and observations. Another possible explanation of the difference may be heterogeneity of the source mechanism. This possibility is discussed later in more detail.

HIGH FREQUENCY SPECTRA

The Haskell model, which has ω^{-3} high frequency decay, moment proportional to L^3 and "corner frequency", ω_c, (for fixed source-receiver geometry, source similarity and source mechanism) proportional to L^{-1}, is a particular member of a general class of models having those properties. Following an argument first suggested by Savage (1972), note that for many source models the area radiating energy to a far-field observer will appear to grow as t^2 and dislocation from that area will grow linearly with t. The far-field pulse, which is the time derivative of the moment function will grow as t^2, giving (Bracewell, 1965, p. 144) ω^{-3} high frequency spectral decay (assuming the t^2 onset is the most abrupt discontinuity). Many models will also have a "corner frequency" proportional to L^{-1}, where L is some characteristic source dimension of that model. Finally, most models give $M_o \sim L^3$, where L is a source dimension. For all models meeting the above three requirements, high frequency spectral amplitudes will behave as

$$A(\omega) \sim M_o(\omega_c/\omega)^3 \sim L^3(L^{-1}/\omega)^3 \sim \omega^{-3} \quad .$$

Thus, all events with fixed geometry and source type will share a common high frequency asymptote which is independent of L. Therefore the conclusion that m_b, and for much larger events, M_s, will have a maximum value, applies to a more general class of models. For example, Minster (1973), derived m_b-M_s curves (with a similar shape to the curve from the Haskell model in Figure 5) from an Archambeau type

(volume) source (also ω^{-3} falloff), although he did not calibrate them against m_b-M_s data. Minster's results also predict maximum values of m_b and M_s.

Many investigators, such as Richards (1973), Dahlen (1974), Sato and Hirasawa (1973) and Madariaga (1975) have outlined crack models for which the initial rupture contributes an ω^{-3} high frequency spectrum while a "stopping phase" caused by simultaneous cessation of fracture everywhere on the fault contributes ω^{-2} and therefore dominates the high frequency spectrum. If such models are applicable, m_b, which is based on the initial rupture, would still have a maximum value, but M_s would not.

M_s VERSUS FAULT AREA

Figure 6 is a plot of fault area, S, (taken from Table 1) and M_s. The predicted M_s-log S curve derived from (21)-(25) agrees quite well with the data. Note that the theoretical curve has four different segments. For small earthquakes, up to $M_s = 6.76$, the slope is $\frac{2}{3}$. From $M_s = 6.76$ to $M_s = 8.12$, the region in which most moderately large earthquakes are clustered, the slope is 1. There is a small section for which the slope is 2, from $M_s = 8.12$ to $M_s = 8.22$. After $M_s = 8.22$, the largest value of M_s for this calibration of the Haskell model, the slope is infinite (e.g., S increases with no further increase in magnitude.)

There is a systematic difference between the interplate (closed circles) and intraplate (open circles) in Figure 6. Half of the

intraplate events fall below the predicted M_s - log S curve, while nearly all interplate earthquakes are above the curve. Kanamori and Anderson (1975b) showed that, at least in the region with slope one, this meant intraplate events had a higher apparent stress.

Utsu and Seki (1954) found the empirical relation log S = 1.02 M-4.01. Their M is Japan Meteorological Agency (JMA) magnitude, which is roughly equivalent to M_s, and S is in km^2. For the unit slope part of the M_s - log S curve in Figure 6 ($M_s > 6.76$) the Utsu-Seki relation predicts about five times the fault area. This may be due to the way Utsu and Seki apparently determined fault area. They used an area encompassing nearly all the aftershocks, rather than the one-day aftershock zone which seems to give much better agreement with observed fault dimensions for earthquakes on continents. Båth and Duda (1964) proposed the relation log S = 1.21 M_s - 5.05, based on a study of six earthquakes from different regions. Båth and Duda used S as aftershock area (in km^2), not fault plane area, so this is basically similar to Utsu and Seki's result. Chinnery (1969) summarizes a number of efforts to find a single linear relation between M_s and the logarithm of other fault parameters.

M_s VERSUS MOMENT

The data of Kanamori and Anderson (1975b) show that $\Delta\sigma$ = 50 bars is a good average, about halfway between values for interplate and intraplate events. Using $\Delta\sigma$ = 50 and (15), we find moment (in dyne cm) is related to fault length (in km) by $M_o = (7.26 \times 10^{21})L^3$ or $\log M_o = 21.9 + 3 \log L$. It was shown above that $M_s \sim n \log L$, where n

varies between 0 and 3, as can be seen from the surface wave spectra in Figure 4. Therefore, for small earthquakes the M_s:log M_o slope is one; for very large events ($M_s \sim$ constant) the slope is infinite (M_o increases but M_s is already at a maximum.).

The log M_o - M_s data from Table 1 are plotted in Figure 7. Most of the moderate sized events (M_s from 6.76 to 8.11) fall on the slope 1.5 portion of the curve (log $M_o \sim \frac{3}{2} M_s$). This part of the curve corresponds to cases where 20 sec spectral amplitudes are measured on the ω^{-1} part of the spectrum. Because the corner frequency for width is only slightly greater than that for rise time, the slope 3 ($M_o \sim 3 \log M_s$) region is very small, extending only from M_s = 8.12 to M_s = 8.22. Beyond that, slope is infinite. The data agree quite well with the theoretical curve. As in Figure 6, intraplate events tend to have smaller M_o for a given M_s, corresponding to higher apparent stress.

Aki (1972) showed that his ω-square model also agreed well with M_s vs. log M_o data. Brune and co-workers (Brune and King, 1967; Brune, 1968; and Brune and Engen, 1969) presented a magnitude scale based on 100 sec surface wave amplitude. They then assumed log $M_o \sim$ log A(100) and fit two segments, each with slope 1, to the data. Because of their different definition of M_o, their results cannot be directly compared to this paper.

Data in this section show that when M_o is larger than about 10^{28} dyne cm, M_s reaches its maximum value. It is important to consider this when discussing the "maximum credible earthquake" likely to occur in a particular area. The earthquake size may be specified in

terms of M_s for most earthquakes, but when the moment approaches 10^{28}, magnitude no longer is a valid parameter for specifying earthquake size. Whenever the maximum credible earthquake is in this range, e.g., as is probably the case in discussing the Alaskan pipeline, moment, not M_s, should be the parameter used.

SPECTRAL RATIOS OF SIMILAR EVENTS

Berckhemer (1962) studied spectral ratios of earthquakes with roughly the same location and mechanism. In theory, the spectral ratio method eliminates the effect of earth structure and leaves only effects due to the difference in source spectra. Aki (1967) used Berckhemer's data to determine the relation between M_s and corner period for the ω-square and ω-cube models.

Berckhemer's original data and Aki's theoretical curves are shown in Figure 8 together with the theoretical curve from the model in this paper. Both models seem to agree fairly well with the data. Perhaps Aki's fits slightly better. Berckhemer presented six pairs of spectra, of which only four are presented here. The remaining two pairs used smaller earthquakes, involving mostly short-period data, which probably are less reliable. No attempt at fitting these two pairs was made.

Tsujiura (1973) published spectral ratio data for many pairs of earthquakes. Most of his events could be fit by both Aki's ω-square model or Aki's (1972) version of Brune's "ω-model", although usually one model or the other fit somewhat better. There were, however, two pairs of events from the Aleutians which had spectral ratios that were

unusually flat and could not be fit by either model. Tsujiura's spectral ratio data have not yet been compared to the model in this paper.

DISCUSSION

The Haskell model with parameters (21)-(24) is in general agreement with m_b-M_s data (Fig. 5), M_s - log S data (Fig. 6), M_s - log M_o data (Fig. 7) and spectral ratio data (Fig. 8). The most serious discrepancy between the data and the model comes in Figure 5. On one hand, the maximum value of m_b is probably several tenths too small. On the other, the data seem to have a slope of about one up to $m_b = 5\frac{1}{4}$, while the curve from the model has slope one only up to $m_b = 4.19$.

This phenomenon could be explained if most earthquakes are complex sources with the first burst of energy coming from a smaller, substantially higher stress drop source, than the average of the whole earthquake. If this is the case, then m_b would be measured on a flat or flatter part of the spectrum than one would expect for the earthquake as a whole.

Burdick and Mellman (1976) have suggested that for the Borrego earthquake of 1968 most of the body wave energy came from a source region with radius of 8 km, giving about half the area shown in Table 1. Since they also found a higher moment, 0.112×10^{27} dyne cm, their stress drop, 96 bars, is about 4 times the value in Table 1, taken from Hanks and Wyss (1972). Tucker and Brune (1975) also suggested that

sources showed a smaller high stress drop event superimposed on the overall average event. The $m_b - M_s$ data in Figure 5 agree with the possibility of the initial fracture having higher stress drop than the bulk event, but certainly do not prove that this happens. Other explanations, e.g., the whole model is wrong, or similarity is wrong for smaller shocks, are equally admissible.

SUMMARY

The following scaling relations relating width and rise time to length and fault area have been given:

$$L = 2W$$

$$\tau = 16S^{1/2} / (7\pi^{3/2}\beta) \quad .$$

The relation for rise time was derived from the assumption that static stress drop and dynamic effective stress are equal; agreement of theoretical rise times with the data tends to support that assumption.

Averages of observed rupture velocities show that $V_R = 0.72\beta$.

The Haskell model predicts that magnitude will reach an upper limit regardless of further increases in fault length and seismic moment. Moment, rather than magnitude should be used to discuss the possible size of great earthquakes.

The "source spectrum" from any source model is a function of apparent (phase) velocity of the mode or phase being considered, as well as of azimuth and source parameters. It is incorrect to speak of a single "source spectrum."

Theoretical relations between m_b and M_s from the Haskell model are:

$$m_b = M_s + 1.33 \qquad M_s < 2.86$$

$$m_b = \frac{2}{3}M_s + 2.28 \qquad 2.86 < M_s < 4.90$$

$$m_b = \frac{1}{3}M_s + 3.91 \qquad 4.90 < M_s < 6.27$$

$$m_b = 6.00 \qquad 6.27 < M_s \ .$$

M_s and fault area (in km^2) are related by

$$\log S = \frac{2}{3} M_s - 2.28 \qquad M_s < 6.76$$

$$\log S = M_s - 4.53 \qquad 6.76 < M_s < 8.12$$

$$\log S = 2M_s - 12.65 \qquad 8.12 < M_s < 8.22$$

$$M_s = 8.22 \qquad S > 6080 \ km^2$$

if L = 2W is used.

If we assume a stress drop of 50 bars, then log M_o (in dyne cm) and M_s are related by

$$\log M_o = M_s + 18.89 \qquad M_s < 6.76$$

$$\log M_o = \frac{3}{2}M_s + 15.51 \qquad 6.76 < M_s < 8.12$$

$$\log M_o = 3M_s + 3.33 \qquad 8.12 < M_s < 8.22$$

$$M_s = 8.22 \qquad \log M_o > 28$$

These scaling relations fit observed data quite well. They should not be used to determine the value of a parameter for any individual earthquake, since these "averages", and the assumptions made to derive them, are not exactly correct for any single event.

A review of work by Gutenberg and Richter reveals that their m_b-M_s relation was derived from m_b data at mostly 5 or 10 second period. Models such as Aki's (1967) ω-square model which fit theoretical 1 sec m_b data to the Gutenberg-Richter relation are probably in error.

ACKNOWLEDGMENT

I have benefited greatly from discussions and comments on the manuscript by Don Anderson, Jerry Frazier, Tom Hanks, David Harkrider, Don Helmberger, Hiroo Kanamori, Dan Kosloff and Kunihiko Shimazaki. Hiroo Kanamori and Don Anderson kindly made their data and manuscript available prior to publication. Hiroo Kanamori called the discrepancy between modern and classical m_b data to my attention. I sincerely thank the anonymous

reviewer for his constructive criticism. This research was supported by the Advanced Research Projects Agency of the Department of Defense and was monitored by the Air Force Office of Scientific Research under Contract No. F44620-72-C-0078, and by U. S. Geological Survey Contract No. 14-08-0001-15273.

CONTRIBUTION No. 2696, DIVISION OF GEOLOGICAL AND PLANETARY SCIENCES
SEISMOLOGICAL LABORATORY
CALIFORNIA INSTITUTE OF TECHNOLOGY
PASADENA, CALIFORNIA 91125

REFERENCES

Abe, K. (1972a). Lithospheric normal faulting beneath the Aleutian trench, Phys. Earth. Plan. Int., 5, 190-198.

Abe, K. (1972b). Mechanisms and tectonic implications of the 1966 and 1970 Peru earthquakes, Phys. Earth Plan. Int., 5, 367-379.

Abe, K. (1973). Tsunami and mechanism of great earthquakes, Phys. Earth Plan. Int., 7, 143-153.

Abe, K. (1974a). Fault parameters determined by near and far field data: The Wakasa Bay earthquake of March 26, 1963, Bull. Seism. Soc. Am., 64, 1369-1382.

Abe, K. (1974b). Seismic displacement and ground motion near a fault: The Saitama earthquake of September 21, 1931, J. Geophys. Res., 79, 4393-4399.

Abe, K. (1975a). A fault model for the Niigata earthquake of 1964. Submitted to Phys. Earth Plan. Int.

Abe, K. (1975b). Determination of static and dynamic fault parameters: The Saitama earthquake of July 1, 1968, Tectonophysics, 27, 223-238.

Abe, K. (1976). J. Phys. Earth, in press.

Aki, K. (1967). Scaling law of seismic spectrum, J. Geophys. Res., 72, 1217-1231.

Aki, K. (1972). Scaling law of earthquake source time function, Geophys. J. R. Astr. Soc., 31, 3-25.

Anderson, J. (1974). A dislocation model for the Parkfield earthquake, Bull. Seism. Soc. Am., 64, 671-686.

Ando, M. (1974). Faulting in the Mikawa earthquake of 1945, Tectonophysics, 22, 173-186.

Andrews, D. J. (1975). From moment to anti-moment: Plane-strain models of earthquakes that stop, Bull. Seism. Soc. Am., 65, 163-182.

Archambeau, C. B. (1975). Studies of multiple seismic events, ACDA/ST220, Final Report, Seismological Laboratory, California Institute of Technology, Pasadena, Ca. 91125.

Archuleta, R. and J. N. Brune (1975). Surface strong motion associated with a stick -slip event in a foam rubber model of earthquakes, Bull. Seism. Soc. Am., 65, 1059-1071.

Båth, M. (1969). Handbook on earthquake magnitude determinations, Seismological Institute, Uppsala, Vesiac Special Report, 7885-36-X (second edition).

Båth, M. and S. J. Duda (1964). Earthquake volume, fault plane area, seismic energy, strain, deformation and related quantities, Ann. Geofis., 17, 353-368.

Ben-Menahem, A. (1961). Radiation of seismic surface-waves from finite moving sources, Bull. Seism. Soc. Am., 51, 401-435.

Ben-Menahem, A. (1962). Radiation of seismic body waves from a finite moving source in the earth, J. Geophys. Res., 67, 345-350.

Berckhemer, H. (1962). Die Ausdehnung der Bruchflache im Erdbebenherd und ihr Einfluss auf das seismische Wellenspektrum, Gerlands Beitr. Geophys., 71, 5-26.

Boore, D. M. and M. D. Zoback (1974). Two-dimensional kinematic fault modeling of the Pacoima Dam strong-motion recordings of the February 9, 1971, San Fernando earthquake, Bull. Seism. Soc. Am., 64, 555-570.

Bracewell, R. (1965). The Fourier transform and its applications, McGraw-Hill.

Brune, J. N. (1968). Seismic moment, seismicity and rate of slip along major fault zones, J. Geophys. Res., 73, 777-784.

Brune, J. N. (1970). Tectonic stress and the spectra of seismic shear waves from earthquakes, J. Geophys. Res., 75, 4997-5009.

Brune, J. N. (1971). Correction, J. Geophys. Res., 76, 5002.

Brune, J. N. and C. R. Allen (1967). A low stress-drop, low-magnitude earthquake with surface faulting: The Imperial, California earthquake of March 4, 1966, Bull. Seism. Soc. Am., 57, 501-514.

Brune, J. N. and G. R. Engen (1969). Excitation of mantle Love waves and definition of mantle wave magnitude, Bull. Seism. Soc. Am., 59, 923-933.

Brune, J. N. and C. Y. King (1967). Excitation of mantle Rayleigh waves of period 100 seconds as a function of magnitude, Bull. Seism. Soc. Am., 57, 1355-1365.

Burdick, L. J. and G. R. Mellman (1976). Inversion of the body waves from the Borrego Mountain earthquake to the source mechanism. Submitted to Bull. Seism. Soc. Am.

Burridge, R. and L. Knopoff (1964). Body force equivalents for seismic dislocations, Bull. Seism. Soc. Am., 54, 1875-1888.

Burridge, R. and J. R. Willis (1969). The self-similar problem of the expanding elliptical crack in an anisotropic solid, Proc. Cambridge Phil. Soc., 66, 443-468.

Byerly, P. and J. DeNoyer (1958). Energy in earthquakes as computed for geodetic observations, in Contributions in Geophysics, In Honor of Beno Gutenberg, H. Benioff, M. Ewing, B. F. Howell and F. Press, editors, Pergamon Press, New York, 17-35.

Chinnery, M. A. (1964). The earth's crust under horizontal shear stress, J. Geophys. Res., 69, 2085-2089.

Chinnery, M. A. (1969). Earthquake magnitude and source parameters, Bull. Seism. Soc. Am., 59, 1969-1982.

Dahlen, F. A. (1974). On the ratio of P-wave to S-wave corner frequencies for shallow earthquake sources, Bull. Seism. Soc. Am., 64, 1159-1180.

de Hoop, A. T. (1958). Representation theorems for the displacement in an elastic solid and their application to elastodynamic diffraction theory, Thesis, Technische Hogeschool, Delft.

Evernden, J. F. (1975). Further studies on seismic discrimination, Bull. Seism. Soc. Am., 65, 359-391.

Fukao, Y. (1973). Thrust faulting at a lithospheric plate boundary: The Portugal earthquake of 1969, Earth Planet. Sci. Lett., 18, 205-216.

Gutenberg, B. (1945). Amplitudes of P, PP and S and magnitude of shallow earthquakes, Bull. Seism. Soc. Am., 35, 57-69.

Gutenberg, B. and C. F. Richter (1942). Earthquake magnitude, intensity, energy and acceleration, Bull. Seism. Soc. Am., 32, 163-191.

Gutenberg, B. and C. F. Richter (1956). Magnitude and energy of earthquakes, Ann. Geofis., 9, 1-15.

Hanks, T. C. and M. Wyss (1972). The use of body wave spectra in the determination of seismic-source parameters, Bull. Seism. Soc. Am., 62, 561-589.

Hanson, M. E., A. R. Sanford and R. J. Shaffer (1974). A source function for a dynamic brittle unilateral shear fracture, Geophys. J. R. Astro. Soc., 38, 365-376.

Harkrider, D. G. (1964). Surface waves in multilayered elastic media, 1. Rayleigh and Love waves from buried sources in a multilayered elastic half-space, Bull. Seism. Soc. Am., 54, 627-679.

Harkrider, D. G. (1970). Surface waves in multilayered elastic media. Part II. Higher mode spectra and spectral ratios from point sources in plane layered earth models, Bull. Seism. Soc. Am., 60, 1937-1987.

Haskell, N. A. (1964). Total energy and energy spectral density of elastic wave radiation from propagating faults, Bull. Seism. Soc. Am., 54, 1811-1841.

Haskell, N. A. (1966). Total energy and energy spectral density of elastic wave radiation from propagating faults. Part II. A statistical fault model, Bull. Seism. Soc. Am., 56, 125-140.

Haskell, N. A. (1969). Elastic displacements in the near-field of a propagating fault, Bull. Seism. Soc. Am., 59, 865-908.

Hirasawa, T. and W. Stauder (1965). On the seismic body waves from a finite moving source, Bull. Seism. Soc. Am., 55, 237-262.

Kanamori, H. (1970a). Synthesis of long-period surface waves and its application to earthquake source studies - Kurile Islands earthquake of October 13, 1963, J. Geophys. Res., 75, 5011-5027.

Kanamori, H. (1970b). The Alaska earthquake of 1964: Radiation of long period surface waves and source mechanism, J. Geophys. Res., 5029-5040.

Kanamori, H. (1971a). Faulting of the great Kanto earthquake of 1923 as revealed by seismological data, Bull. Earthquake Res. Inst. Tokyo Univ., 49, 13-18.

Kanamori, H. (1971b). Seismological evidence for a lithospheric normal faulting - the Sanriku earthquake of 1933, Phys. Earth Planet. Int., 4, 289-300.

Kanamori, H. (1971c). Focal mechanism of the Tokachi-Oki earthquake of May 16, 1968: Contortion of the lithosphere of a junction of two trenches, Tectonophysics, 12, 1-13.

Kanamori, H. (1972a). Tectonic implications of the 1944 Tonankai and 1946 Nankaido earthquakes, Phys. Earth Planet. Int., 5, 129-139.

Kanamori, H. (1972b). Determination of effective tectonic stress associated with earthquake faulting, the Tottori earthquake of 1943, Phys. Earth Planet. Int., 5, 426-434.

Kanamori, H. (1973). Mode of strain release associated with major earthquakes in Japan, Ann. Rev. of Earth and Planet. Sci., 1, 213-239.

Kanamori, H. (1974). Long period ground motion in the epicentral area of major earthquakes, Tectonophysics, 21, 341-356.

Kanamori, H. and D. L. Anderson (1975a). Amplitude of the earth's free oscillations and long period characteristics of the earthquake source, J. Geophys. Res., 80, 1075-1078.

Kanamori, H. and D. L. Anderson (1975b). Theoretical basis of some empirical relations in seismology, Bull. Seism. Soc. Am., 65, 1073-1095.

Kanamori, H. and J. J. Cipar (1974). Focal processes of the great Chilean earthquake May 22, 1960, Phys. Earth Planet. Int., 9, 128-136.

Kasahara, K. (1957). The nature of seismic origins as inferred from seismological and geodetic observations, 1, Bull. Earthquake Res. Inst. Tokyo Univ., 35, 473-532.

Kawasaki, I. and Y. Suzuki (1974). Rise time and effective stress estimation from comparison of near field data with theoretical seismograms in a semi-infinite medium: The Sanriku earthquake of March 3, 1933, J. Phys. Earth, 22, 223-236.

Kawasaki, I. (1975). The focal processes of the Kita-Mino earthquake of August 19, 1961 and its relationship to a Quaternary fault, the Hatogayu-Koike fault, J. Phys. Earth, 23, 227-250.

Keiles-Borok, V. (1959). An estimation of the displacement in an earthquake source and of source dimensions, Ann. Geofis., 12, 205-214.

Langston, D. A. and D. V. Helmberger (1975). A procedure for modelling shallow dislocation sources, Geophys. J. R. Astro. Soc., 42 117-130.

Madariaga, R. (1975). Dependence of far-field radiation on source geometry, (abstract), Trans. Am. Geophys. Un., 56, 400-401.

Mikumo, T. (1969). Long-period P waveforms and the source mechanism of intermediate earthquakes, J. Phys. Earth, 17, 169-192.

Mikumo, T. (1973a). Faulting mechanism of the Gifu earthquake of September 9, 1969, and some related problems, J. Phys. Earth, 21, 191-212.

Mikumo, T. (1973b). Faulting processes of the San Fernando earthquake of February 9, 1971 inferred from static and dynamic near-field displacements, Bull. Seism. Soc. Am., 63, 249-269.

Minster, J. B. (1973). Elastodynamics of failure in a continuum, Thesis, California Institute of Technology, Pasadena, Ca. 91125.

Nagamune, T. (1972). Magnitudes estimated from body waves for great earthquakes (in Japanese), Quarterly Journal of Seismology, 47, 1-8.

Richards, P. G. (1973). The dynamic field at a growing plane elliptical shear crack, Int. J. Solids Structures, 9, 843-861.

Richter, C. F. (1958). Elementary Seismology, W. H. Freeman, San Francisco.

Sato, R. (1972). Stress drop for a finite fault, J. Phys. Earth, 20, 397-407.

Sato, T. and T. Hirasawa (1973). Body wave spectra from propagating shear cracks, J. Phys. Earth, 21, 415-431.

Savage, J. C. (1972). Relation of corner frequency to fault dimensions, J. Geophys. Res., 77, 3788-3795.

Savage, J. C. and L. M. Hastie (1966). Surface deformation associated with dip-slip faulting, J. Geophys. Res., 71, 4897-4904.

Shimazaki, K. (1975). Nemuro-Oki earthquake of June 17, 1973: A lithospheric rebound at the upper half of the interface, Phys. Earth Planet. Int., 9, 314-327.

Trifunac, M. D. (1974). A three-dimensional dislocation model for the San Fernando, California, earthquake of February 9, 1971, Bull. Seism. Soc. Am., 64, 149-172.

Trifunac, M. D. and F. E. Udwadia (1974). Parkfield, California, earthquake of June 27, 1966: A three-dimensional moving dislocation, Bull. Seism. Soc. Am., 64, 511-533.

Tsai, Y. and K. Aki (1970). Source mechanism of the Truckee, California earthquake of September 12, 1966, Bull. Seism. Soc. Am., 60, 1199-1208.

Tsuboi, C. (1956). Earthquake energy, earthquake volume, aftershock area, and strength of the earth's crust, J. Phys. Earth, 4, 63-66.

Tsujiura, M. (1973). Spectrum of seismic waves and its dependence on magnitude, J. Phys. Earth, 21, 373-391.

Tucker, B. E. and J. N. Brune (1975). Source mechanism and surface wave excitation for aftershocks of the San Fernando earthquake. Submitted to Geophys. J. R. astr. Soc.

Udias, A. (1971). Source parameters of earthquakes from spectra of Rayleigh waves, Geophys. J. R. astr. Soc., 22, 353-376.

Udias, A. and A. L. Arroyo (1970). Body and surface wave study of source parameters of the March 15, 1964 Spanish earthquake, Tectonophysics, 9, 323-346.

Utsu, T. and A. Seki (1954). A relation between the area of aftershock region and the energy of main-shock (in Japanese), J. Seism. Soc. Japan (Zisin), 7, 233-240.

Wu, F. T. and H. Kanamori (1973). Source mechanism of February 4, 1965, Rat Island earthquake, J. Geophys. Res., 78, 6082-6092.

Table 1

Earthquake Source Parameters

	Event	Date	M_s	m_b	M_o $\times 10^{27}$ dyne-cm	L km	W km	D m	τ sec	τ^* sec	V_R km/sec	$\Delta\sigma$ bars
1.	Kanto	1 Sept. 1923	8.2	-	7.6	130	70	2.1	7	10	-	21
2.	Tango	27 March 1927	7.75	-	0.46	35	13	3	6	2.5	2.3	115
3.	North Izu	25 Nov. 1930	7.1	-	0.2	20	11	3	-	1.7	-	150
4.	Saitama	21 Sept. 1933	6.75	-	0.068	20	10	1	2	1.6	2.3	59
5.	Sanriku	2 March 1933	8.3	-	43	185	100	3.3	7	12	3.2	42
6.	Long Beach	11 March 1933	6.25	-	0.028	30	15	0.2	2	2.5	2.3	7
7.	Imperial Valley	19 May 1940	7.1	-	0.48	70	11	2	-	3.2	-	55
8.	Tottori	10 Sept. 1943	7.4	-	0.36	33	13	2.5	3	4.0	2.3	99
9.	Tonankai	7 Dec. 1944	8.2	-	15	120	80	3.1	-	9.2	-	39
10.	Mikawa	12 Jan. 1945	7.1	-	0.087	12	11	2.2	-	1.3	-	140
11.	Nankaido	20 Dec. 1946	8.2	-	15	120	80	3.1	-	9.2	-	39
12.	Fukui	28 June 1948	7.3	-	0.33	30	13	2	2	1.9	2.3	100
13.	Tokachi-Oki	4 March 1952	8.3	-	17	180	100	1.9	-	14	-	17
14.	Kern County	21 July 1952	7.7	-	2	60	18	4.6	1	3.6	-	140

Table 1 cont.

Earthquake Source Parameters

	Event	Date	M_s	m_b	M_o $\times 10^{27}$ dyne-cm	L km	W km	$\bar{D}$ m	τ sec	τ^* sec	V_R km/sec	$\Delta\sigma$ bars
15.	Fairview	16 Dec. 1954	7.1	-	0.13	36	6	2	-	1.7	-	100
16.	Chile	22 May 1960	8.3	-	2400	800	200	21	-	36	3.5	91
17.	Kitamino	19 Aug. 1961	7.0	-	0.09	12	10	2.5	2	1.3	3.0	170
18.	Wasaka Bay	27 March 1963	6.9	-	0.033	20	8	0.6	2	1.5	2.3	40
19.	North Atlantic I	3 Aug. 1963	6.7	6.1	0.12	32	11	1	-	2.2	-	44
20.	Kurile Islands	13 Oct. 1963	8.2	5.7	75	250	140	3	-	17	3.5	28
21.	North Atlantic II	17 Nov. 1963	6.5	5.9	0.038	27	9	0.48	-	1.8	-	24
22.	Spain	15 March 1964	7.1	6.2	0.13	95	10	0.42	-	3.6	1.4	11
23.	Alaska	28 March 1964	8.5	6.2	520	500	300	7	-	35	3.5	22
24.	Niigata	16 June 1964	7.4	6.1	3.2	80	30	3.3	-	5.3	-	66
25.	Rat Island I	4 Feb. 1965	7.9	6.0	140	500	150	2.5	-	25	4.0	17
26.	Rat Island II	30 March 1965	7.5	5.7	3.4	50	80	1.2	-	5.8	-	33
27.	Parkfield	28 June 1966	6.4	5.3	0.032	26	7	0.6	0.7	1.6	2.7	32
28.	Aleutian	4 July 1966	7.2	6.2	0.226	35	12	1.6	-	2.4	-	64
29.	Truckee	12 Sept. 1966	5.9	5.4	0.0083	10	10	0.3	-	1.2	-	20

Table 1 cont.

Earthquake Source Parameters

	Event	Date	M_s	m_b	M_o $\times 10^{27}$ dyne-cm	L km	W km	$\bar{D}$ m	τ sec	τ^* sec	V_R km/sec	$\Delta\sigma$ bars
30.	Peru	17 Oct. 1966	7.5	6.3	20	80	140	2.6	-	9.6	-	41
31.	Borrego	9 Apr. 1968	6.7	6.1	0.063	33	11	0.58	-	2.2	-	22
32.	Tokachi-Oki	16 May 1968	8.0	5.9	28	150	100	4.1	-	12	3.3	37
33.	Saitama	1 July 1968	5.8	5.9	0.019	10	6	0.92	1	0.9	3.4	100
34.	Portuguese	28 Feb. 1969	8.0	7.3	5.5	80	50	2.5	-	6.1	-	53
35.	Kurile Islands	11 Aug. 1969	7.8	7.1	22	180	85	2.9	-	12	3.3	28
36.	Gifu	9 Sept. 1969	6.6	5.5	0.035	18	10	0.6	1	1.7	2.5	35
37.	Peru	31 May 1970	7.8	6.6	10	130	70	1.6	-	8.7	2.5	28
38.	San Fernando	9 Feb. 1971	6.6	6.2	0.12	20	14	1.4	1	2.0	2.4	62
39.	Nemuro-Oki	17 June 1973	7.7	6.5	6.7	60	100	1.6	-	7.5	-	35
40.	Turkey	22 July 1967	7.1	6.0	0.83	80	20	1.7	-	4.7	-	32
41.	Iran	31 Aug. 1968	7.3	5.9	1	80	20	2.1	-	4.7	-	38

REFERENCES TO TABLE 1

(1) Kanamori (1971a). Rise time from Kanamori (1974).

(2) Kanamori (1973).

(3) Average of Chinnery (1964), Kasahara (1957) and Kanamori (unpublished data).

(4) Abe (1974b).

(5) Average of Kanamori (1971b) and Kawasaki and Suzuki (1974).

(6) Kanamori (unpublished data) and aftershock zone.

(7) Average of Brune and Allen (1967) and Byerly and DeNoyer (1958).

(8) Kanamori (1972b).

(9) Kanamori (1972a).

(10) Ando (1974).

(11) Kanamori (1972a).

(12) Kanamori (1973).

(13) Area from average of Kanamori (unpublished data) and Utsu and Seki (1954). Moment from Kanamori (unpublished data).

(14) Kanamori (unpublished data).

(15) Savage and Hastie (1966).

(16) Average (for main shock only--precursor not included) of Kanamori and Cipar (1974) and Kanamori and Anderson(1975a).

(17) Kawasaki (1975).

(18) Abe (1974a).

(19) Udias (1971).

(20) Kanamori (1970a).

(21) Udias (1971).

(22) Udias and Arroyo (1970).

(23) Kanamori (1970b).

(24) Abe (1975a).

(25) Wu and Kanamori (1973).

(26) Abe (1972a).

(27) Average of Anderson (1974) and Trifunac and Udwadia (1974).

(28) Udias (1971).

(29) Tsai and Aki (1970).

(30) Abe (1972b).

(31) Hanks and Wyss (1972).

(32) Kanamori (1971c).

(33) Abe (1975b).

(34) Fukao (1973).

(35) Abe (1973).

(36) Mikumo (1973).

(37) Abe (1972b). Average of parameters for each of the two possible fault planes.

(38) Moment and static fault parameters from Kanamori and Anderson (1975b). Rupture velocity and rise time averaged from Boore and Zoback (1974), Mikumo (1973b) and Trifunac (1974).

(39) Shimazaki (1975).

(40) Hanks and Wyss (1972).

(41) Hanks and Wyss (1972).

FIGURE CAPTIONS

Figure 1. Plot of fault length (along strike) versus fault width (along dip) for earthquakes in Table 1. Open circles are intra-plate events; closed circles are interplate events. Numbers refer to Table 1. These conventions are used for all plots of earthquake data.

Figure 2. Plot of observed rise time versus theoretical rise times from (5).

Figure 3. The Haskell (whole space) fault model.

Figure 4. Source spectra of surface waves (on left) and body waves. Both are identical at frequencies below the ω^{-2} corner frequency. The body waves have a higher width corner frequency than surface waves, which follows from (18), (20), (23) and (24). This difference occurs because teleseismic P waves, which takeoff essentially straight down, have a much higher apparent velocity (phase velocity) than surface waves. Therefore the separation between rise time and width corner frequencies (the ω^{-2} part of the spectrum) is much greater for body waves than surface waves.

Figure 5. USCGS m_b versus M_s. Lower data points are averages from Evernden (1975), corrected by adding 0.3 to m_b. Upper points (above horizontal line) are individual earthquakes from Table 1. Dashed curve is m_b-M_s relation from ω-square model. Solid curve is from (21) to (25) as described in the text.

Figure 6. M_s versus log S data with theoretical curve from the model in this paper.

Figure 7. M_s versus log M_o data with theoretical curve from the model in this paper.

Figure 8. Spectral ratios of similar earthquakes from Berckhemer (1962). Numbers above each figure are magnitudes of the larger and smaller of the events. Dashed line is ω-square model and solid line is model from this paper.

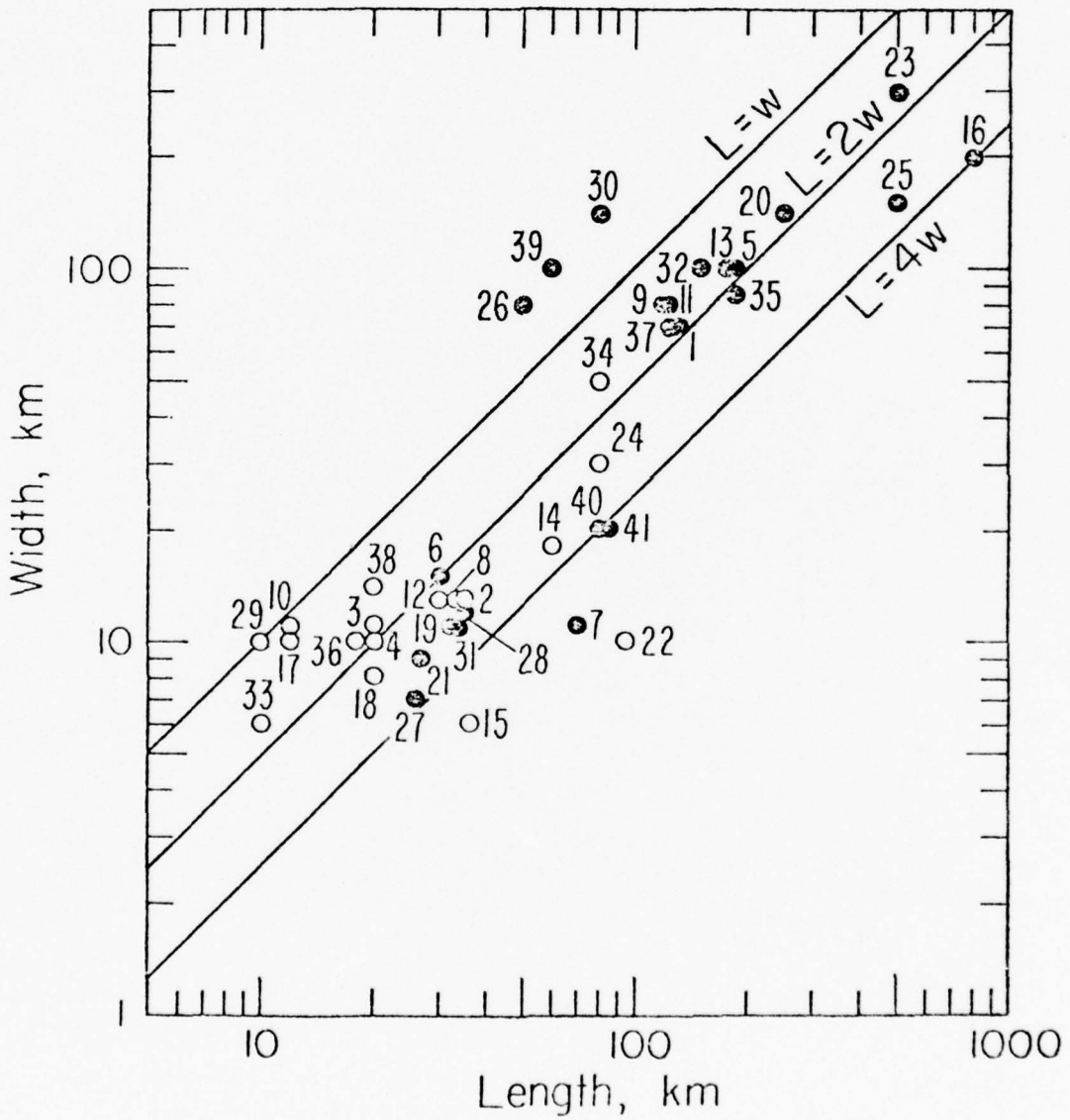
L=w
L=2w
L=4w
Width, km
Length, km
1
10
100
1000
23
16
30
25
20
39
13
5
32
26
9
11
35
37
1
34
24
14
40
41
38
6
8
12
2
29
10
3
19
7
22
36
4
31
28
17
33
18
21
27
15

Fig. 1

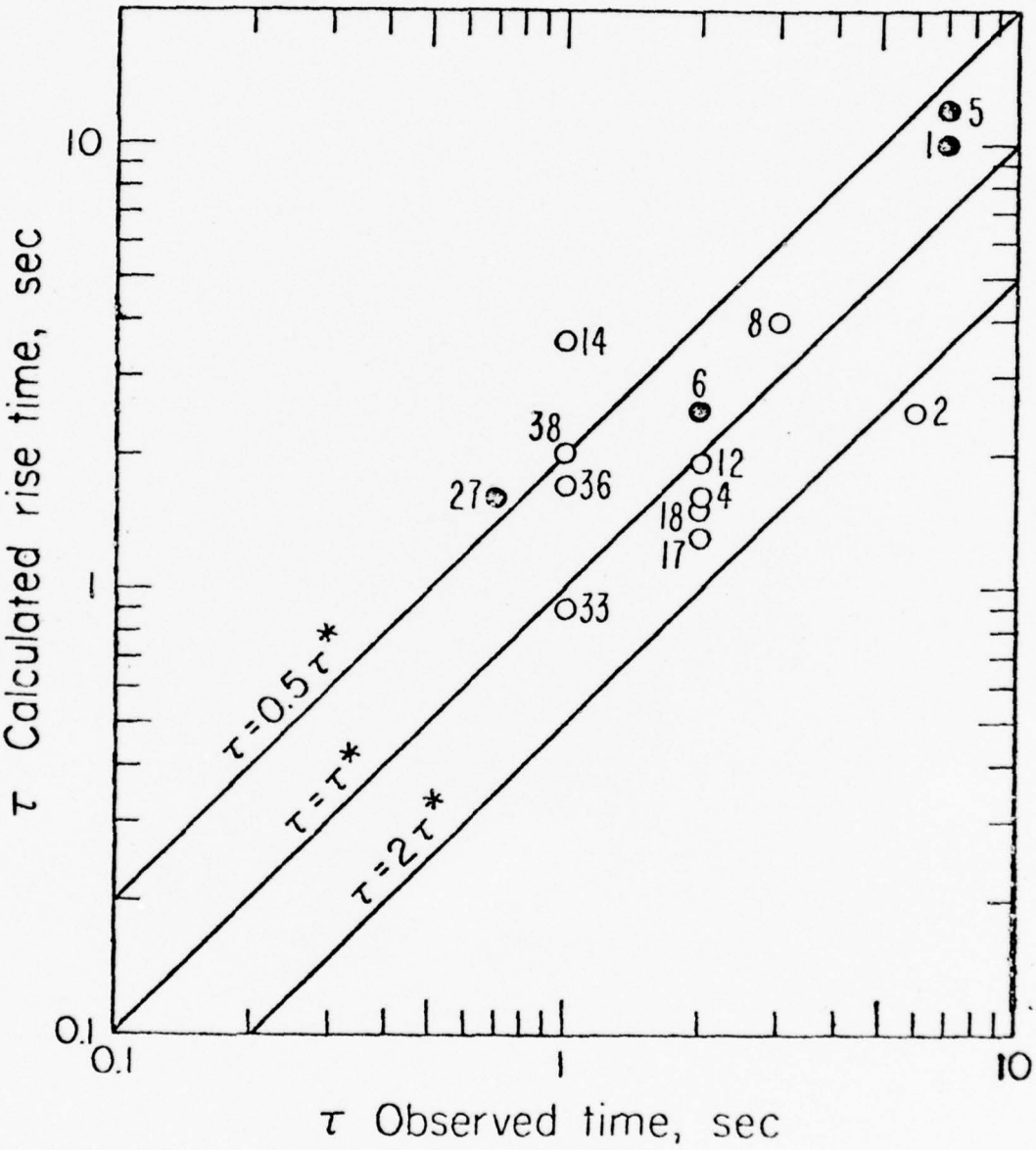
τ Calculated rise time, sec
τ Observed time, sec
10
1
0.1
0.1
1
10
τ=0.5τ*
τ=τ*
τ=2τ*
5
1
14
8
6
2
38
12
27
36
4
18
17
33

Fig. 2

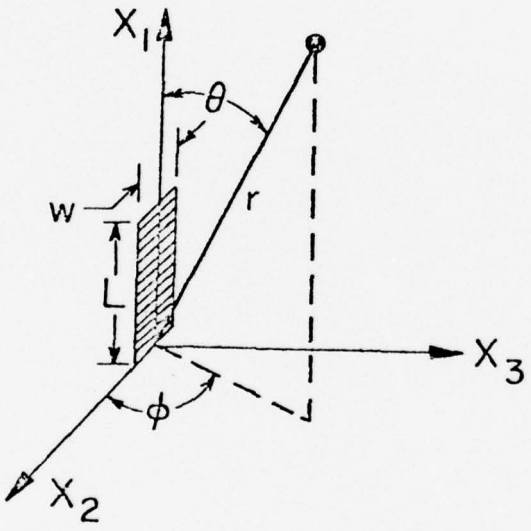

Fig 3

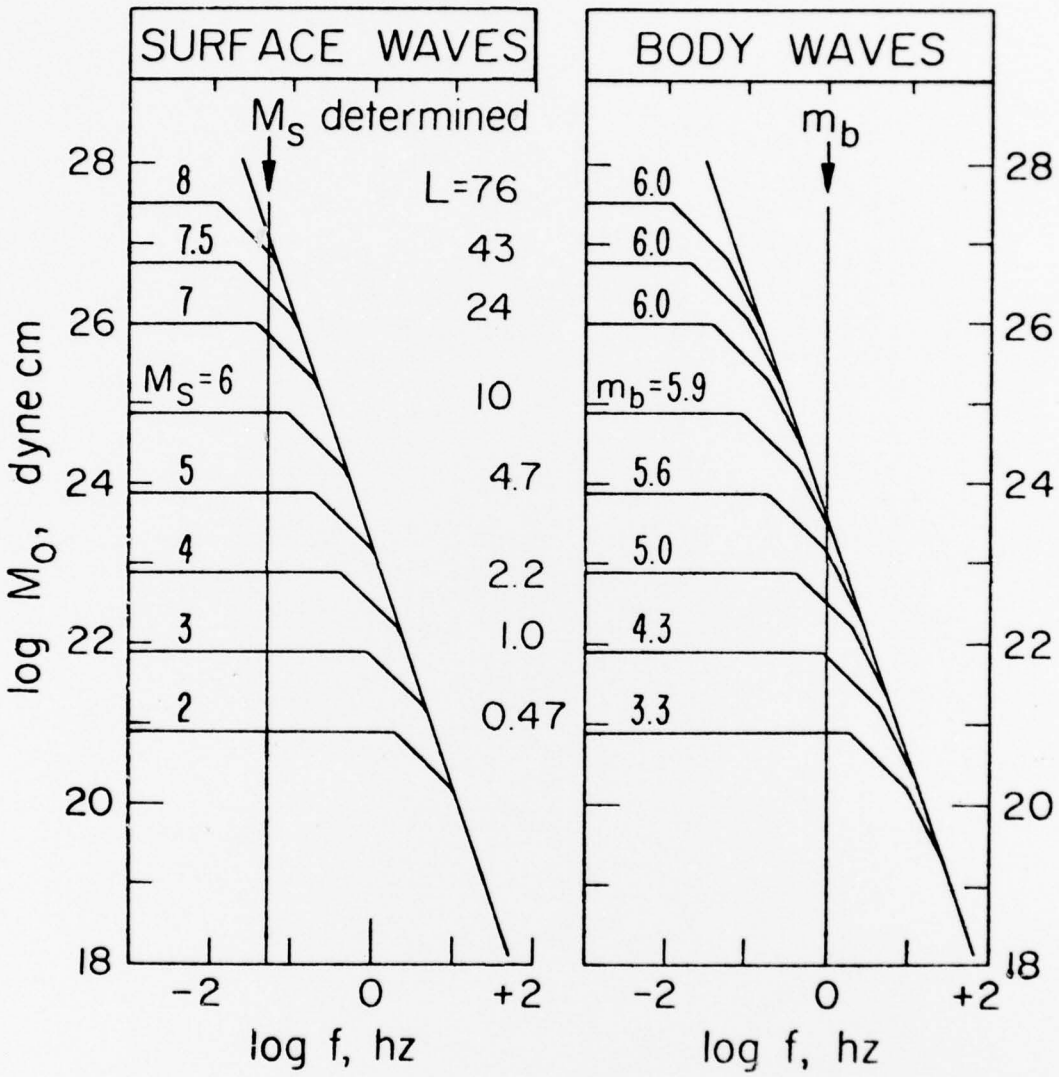
SURFACE WAVES
BODY WAVES
M_S determined
m_b
L=76
43
24
10
4.7
2.2
1.0
0.47
8
7.5
7
M_S=6
5
4
3
2
6.0
6.0
6.0
m_b=5.9
5.6
5.0
4.3
3.3
log M_o, dyne cm
28
26
24
22
20
18
-2
0
+2
log f, hz

Fig. 4

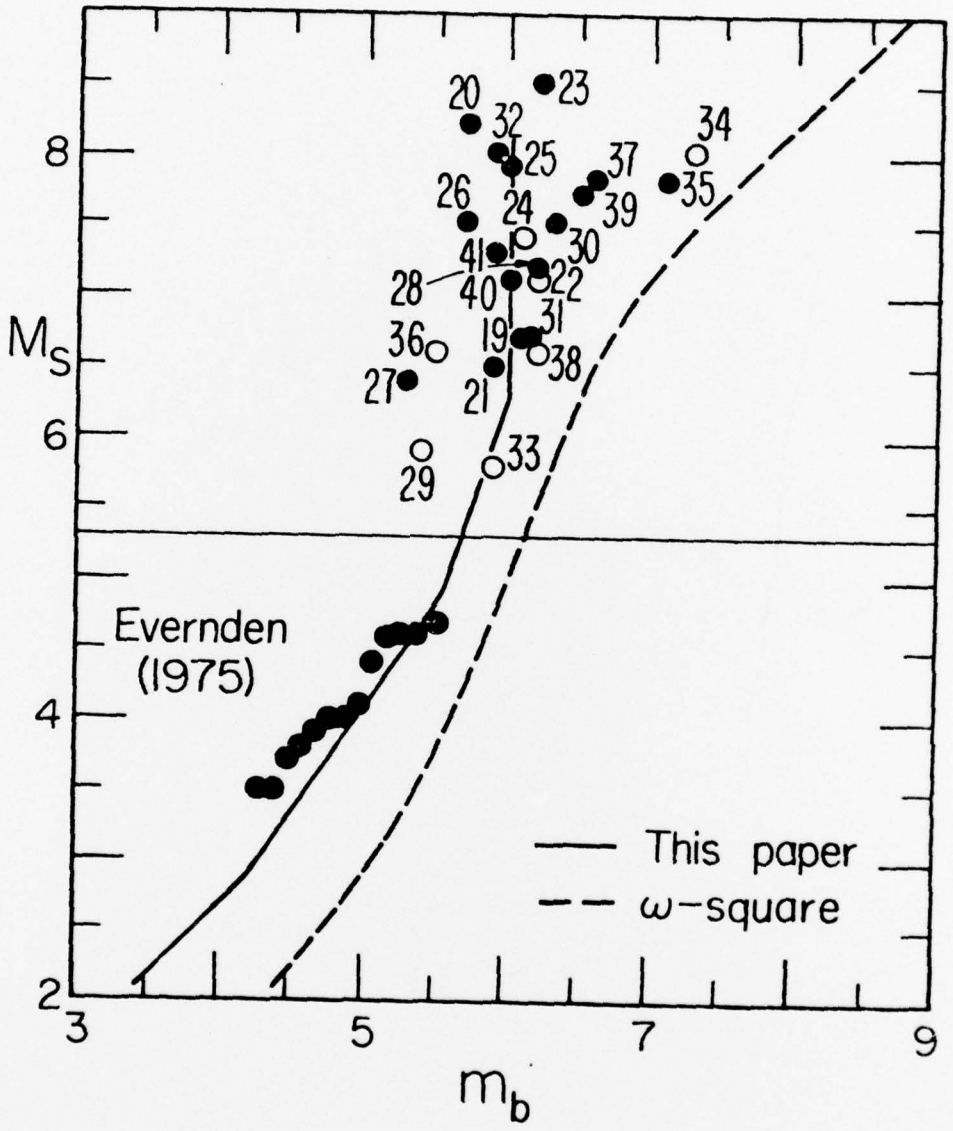
20
23
32
34
25
37
35
26
24
39
30
41
28
40
22
31
36
19
38
27
21
33
29
8
6
4
2
M_S
Evernden
(1975)
This paper
ω-square
3
5
7
9
m_b

Fig. 5

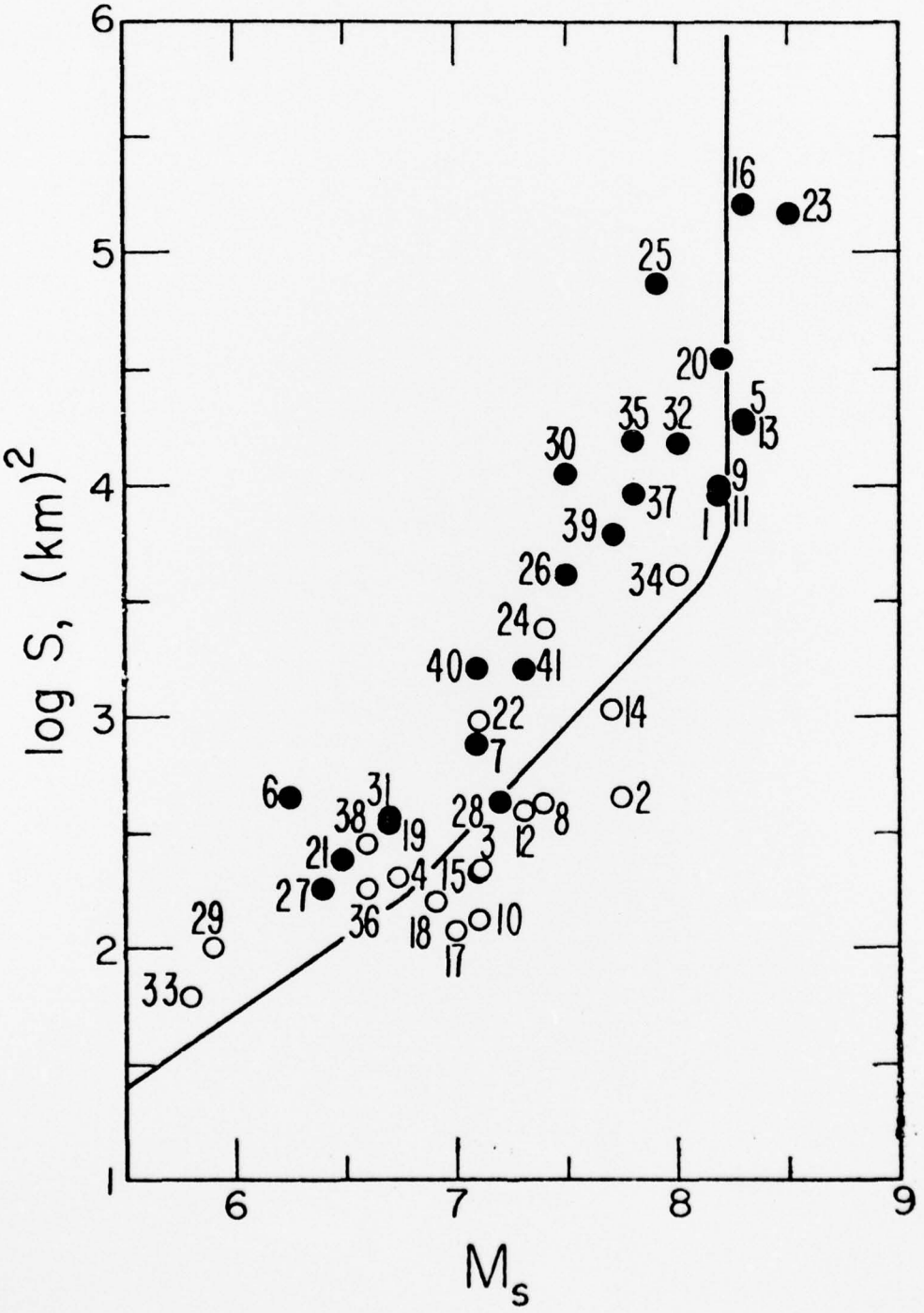
log S, (km)^2
M_s
6
5
4
3
2
1
6
7
8
9
16
23
25
20
5
13
35
32
30
9
37
11
1
39
26
34
24
40
41
22
14
7
6
31
38
28
19
3
12
8
2
21
4
15
27
36
18
10
17
29
33

Fig. 6

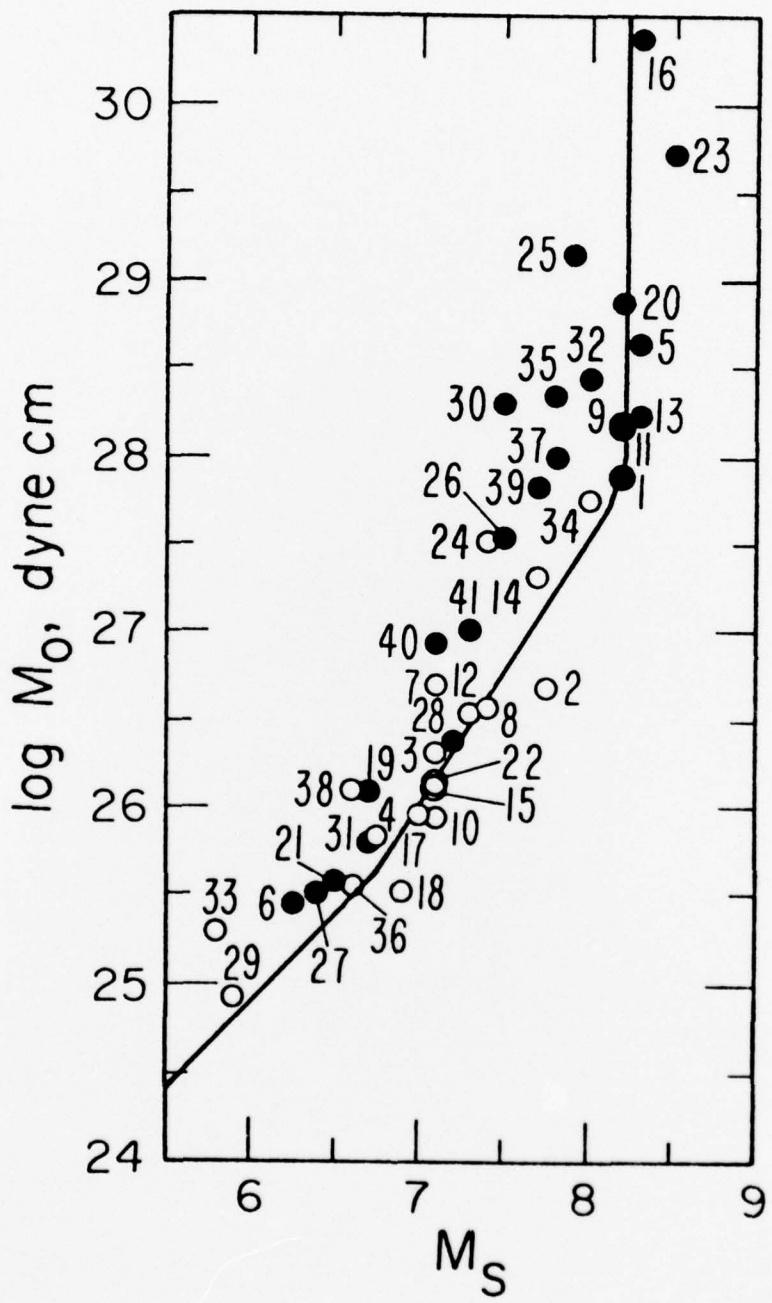
log M_o, dyne cm
M_S
30
29
28
27
26
25
24
6
7
8
9
16
23
25
20
5
32
35
30
9
13
37
11
26
39
1
24
34
41
14
40
7
12
2
28
8
19
3
22
38
15
4
10
31
17
21
18
33
6
36
29
27

Fig. 7

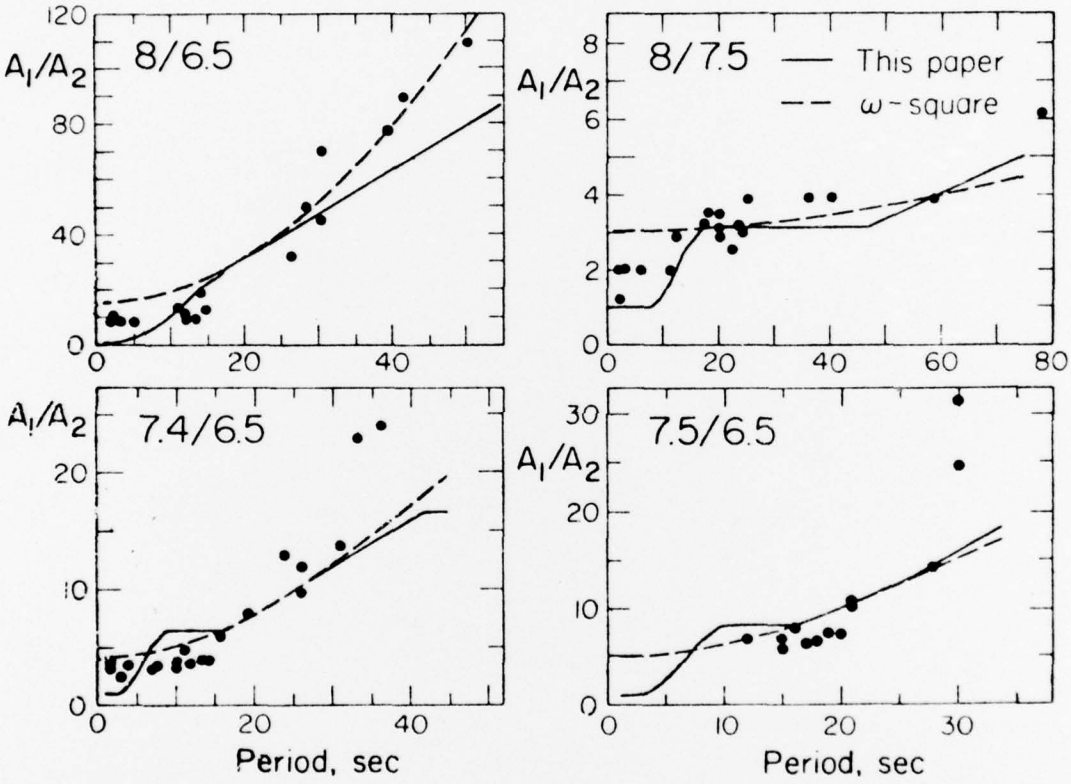

Fig. 8

Previous Technical Reports

1969 - Present

Teng, T. L., and Richards, P. G., 1969, Diffracted P, SV, and SH waves and their shadow boundary shifts: Jour. Geophys. Research, v. 74, no. 6, p. 1537-1555.

McGinley, J. R., Jr., and Anderson, D. L., 1969, Relative amplitudes of P and S waves as a mantle reconnaissance tool: Seismol. Soc. America Bull., v. 59, no. 3, p. 1189-1200.

Johnson, L. R., 1969, Array measurements of P velocities in the lower mantle: Seismol. Soc. America Bull., v. 59, no. 2, p. 973-1008.

McGinley, J. R., Jr., 1969, A comparison of observed permanent tilts and strains due to earthquakes with those calculated from displacement dislocations in elastic earth models: Ph.D. Thesis, California Institute of Technology, Pasadena, California.

Smith, M. L., and Franklin, J. N., 1969, Geophysical application of generalized inverse theory: Jour. Geophys. Research, v. 74, no. 10, p. 2783-2785.

Anderson, D. L., and Kovach, R. L., 1969, Universal dispersion tables, III, Free oscillation variational parameters: Seismol. Soc. America Bull., v. 59, no. 4, p. 1667-1693.

Anderson, D. L., and Julian, B. R., 1969, Shear velocities and elastic parameters of the mantle: Jour. Geophys. Research, v. 74, no. 12, p. p. 3281-3286.

Smith, S. W., McGinley, J. R., Jr., Johnson, L. R., and Scholz, C. H., 1969, Effects of large explosions on tectonic strain: Jour. Geophys. Research, v. 74, no. 12, p. 3308-3309.

Archambeau, C. B., Flinn, E. A., and Lambert, D. G., 1969, Fine structure of the upper mantle: Jour. Geophys. Research, v. 74, no. 25, p. 5825-5865.

Anderson, D. L., and Sammis, C. G., 1969, The low velocity zone: Geofisica Internac., v. 9, no. 1-3, p. 3-19.

Archambeau, C. B., and Sammis, C. G., 1970, Seismic radiation from explosions in prestressed media and the measurement of tectonic stress in the earth: Rev. Geophysics and Space Physics, v. 8, no. 3, p. 473-499.

Anderson, D. L., and Sammis, C. G., 1970, Partial melting in the upper mantle: Physics Earth and Planet. Interiors, v. 3, p. 41-50.

Arabasz, W. J., Brune, J. N., and Engen, G. R., 1970, Locations of small earthquakes near the trifurcation of the San Jacinto fault southeast of Anza, California: Seismol. Soc. America Bull., v. 60, no. 2, p. 617-627.

Jackson, D. D., and Anderson, D. L., 1970, Physical mechanisms of seismic-wave attenuation: Rev. Geophysics and Space Physics, v. 8, no. 1, p. 1-63.

Whitcomb, J. H., and Anderson, D. L., 1970, Reflection of P'P' seismic waves from discontinuities in the mantle: Jour. Geophys. Research, v. 75, no. 29, p. 5713-5728.

Julian, B. R., 1970, Regional variations in upper mantle structure beneath North America: Ph.D. thesis, California Institute of Technology, Pasadena, California.

Richards, P. G., 1970, A contribution to the theory of high frequency elastic waves, with applications to the shadow boundary of the earth's core: Ph.D. thesis, California Institute of Technology, Pasadena, California.

Wyss, Max, 1970, Observations and interpretations of tectonic strain release mechanisms: Ph.D. thesis, California Institute of Technology, Pasadena, California.

Archambeau, C. B., 1970, Theory of the seismic source: Proceedings of the Advanced Research Projects Agency Symposium on Discrimination of Earthquakes and Underground Explosions, Woods Hole, Massachusetts, July 20-23.

Gile, W. W., 1970, A mercury pendulum seismometer: IEEE Transactions on Geoscience Electronics (technical report).

Richards, P. G., 1971, Potentials for elastic displacement in spherically symmetric media: Acoust. Soc. America Jour., v. 50, no. 1, p. 188-197.

Richards, P. G., 1971, An elasticity theorem for heterogeneous media, with an example of body wave dispersion in the earth: Royal Astron. Soc. Geophys. Jour., v. 22, p. 453-472.

Liebermann, R. C., and Basham, P. W., 1971, Excitation of surface waves by the Aleutian underground explosion Milrow (October 2, 1969): Jour. Geophys. Research, v. 76, no. 17, p. 4030-4034.

Jordan, T. H., and Franklin, J. N., 1971, Optimal solutions to a linear inverse problem in geophysics: Natl. Acad. Sci. Proc., v. 68, no. 2, p. 291-293.

Hill, D. P., 1971, High frequency wave propagation in the earth: Theory and observation: Ph.D. thesis, California Institute of Technology, Pasadena, California.

Wyss, Max, Hanks, T. C., and Liebermann, R. C., 1971, Comparison of P-wave spectra of underground explosions and earthquakes: Jour. Geophys. Research, v. 76, no. 11, p. 2716-2729.

Hill, D. P., 1971, Velocity gradients and anelasticity from crustal body wave amplitudes: Jour. Geophys. Research, v. 76, no. 14, p. 3309-3325.

Jungels, P. H., and Anderson, D. L., 1971, Strains and tilts associated with the San Fernando earthquake, in The San Fernando, California, Earthquake of February 9, 1971: U.S. Geol. Survey Prof. Paper 733, p. 77-79.

Jordan, T. H., and Minster, J. B., 1971, An application of a stochastic inverse to the geophysical inverse problem: Workshop on Mathematics of Profile Inversion, Ames Research Center, Moffitt Field, California, July 12-16.

Hill, D. P., 1971, Velocity gradients in the continental crust from head wave amplitudes: Am. Geophys. Union Mon. Ser. 14, p. 71-75.

Whitcomb, J. H., 1971, Reflections of P'P' seismic waves from 0 to 150 km depth under the Ninety-East Ridge, Indian Ocean, and the Atlantic-Indian Rise: Am. Geophys. Union Mon. Ser. 14, p. 211-225.

McKenzie, Dan, and Julian, Bruce, 1971, The Puget Sound, Washington, earthquake and the mantle structure beneath the northwestern United States: Geol. Soc. America Bull., v. 82, p. 3519-3524.

Helmberger, D. V., 1972, Long period body wave propagation from 4 to 13°: Seismol. Soc. America Bull., v. 62, no. 1, p. 325-341.

Archambeau, C. B., 1972, The theory of stress wave radiation from explosions in prestressed media: Royal Astron. Soc. Geophys. Jour., v. 29, p. 329-366.

Hanks, T. C., and Wyss, Max, 1972, The use of body-wave spectra in the determination of seismic source parameters: Seismol. Soc. America Bull., v. 62, no. 2, p. 561-589.

Hanks, T. C. and Thatcher, W., 1972, A graphical representation of seismic source parameters: Jour. Geophys. Research, v. 77, no. 23, p. 4393-4405.

Alewine, R. W., 1972, Theoretical and observed distance corrections for Rayleigh wave magnitude: Seismol. Soc. America Bull., v. 62, no. 6, p. 1611-1619.

Helmberger, D. V., and Harkrider, D. G., 1972, Seismic source descriptions of underground explosions and a depth discriminate: Geophys. J. R. Astr. Soc., v. 31, p. 45-66.

Mizutani, H., and Abe, K., 1972, An earth model consistent with free oscillation and surface wave data: Phys. Earth Planet. Int., v. 5, p. 345-356.

Hill, D. P., 1972, Crustal and upper mantle structure of the Columbia Plateau from long-range seismic-refraction measurements: Geol. Soc. America Bull., v. 83, p. 1639-1648.

Lambert, D. G., Flinn, E. A., and Archambeau, C. B., 1972, A comparative study of the elastic wave radiation from earthquakes and underground explosions: Geophys. Jour., v. 29, p. 403-432.

Mitchell, B. J., 1973, Radiation and attenuation of Rayleigh waves from the southeastern Missouri earthquake of October 21, 1965: Jour. Geophys. Research, v. 78, no. 5, p. 886-899.

Kurita, T., 1973, A procedure and formulation for elucidating fine structure of the crust and upper mantle from seismological data: Seismol. Soc. America Bull., v. 63, no. 1, p. 189-209.

Wiggins, R., and Helmberger, D. V., 1973, Upper mantle structure of western United States: Jour. Geophys. Research, v. 78, no. 11, p. 1870-1880.

York, J. E., and Helmberger, D. V., 1973, Low velocity zone variations in the southwestern United States: Jour. Geophys. Research, v. 78, no. 11, p. 1883-1886.

Whitcomb, J. H., 1973, Part I. A study of the velocity structure of the earth by the use of core phases. Part II. The 1971 San Fernando earthquake series focal mechanisms and tectonics; Ph.D. Thesis, California Institute of Technology.

Jordan, T. H., 1973, Estimation of the radial variation of seismic velocities and density in the earth; Ph.D. Thesis, California Institute of Technology.

Whitcomb, J. H., 1973, Asymmetric P'P' -- an alternative to P'dP' reflections in the upper mantle (0-110 km): Seismol. Soc. America Bull., v. 63, p. 133-143.

Helmberger, D. V., 1973, Numerical seismograms of long-period body waves from seventeen to forty degrees: Seismol. Soc. America Bull., v. 63, p. 633-646.

Kurita, T., 1973, Regional variations in the structure of the crust in the Central United States from P-wave spectra: Seismol. Soc. America Bull., v. 63, p. 1663-1687.

Mitchell, B. J., 1973, Surface-wave attenuation and crustal anelasticity in Central North America: Seismol. Soc. America Bull., v. 63, p. 1057-1071.

Mitchell, B. J., and Helmberger, D. V., 1973, Shear velocities at the base of the mantle from observations of S and ScS: Jour. Geophys. Research, v. 78, p. 6609-6020.

Niazi, M., 1973, SH travel times and lateral heterogeneities in the lower mantle: Seismol. Soc. America Bull., v. 63, p. 2035-2046.

Helmberger, D. V., 1973, On the structure of the low velocity zone: Royal Astron. Soc. Geophys. Jour., v. 34, p. 251-263.

Kurita, Tuneto, 1973, Upper mantle structure in the central United States from P and S wave spectra: Phys. Earth and Planet. Interiors, v. 8, p. 177-201.

Alewine, R. W., 1974, Application of linear inversion theory toward the estimation of seismic source parameters, Ph.D. Thesis, California Institute of Technology.

Burdick, L. J., and Helmberger, D. V., 1974, Time functions appropriate for deep earthquakes: Seismol. Soc. America Bull., v. 63, p. 1419-1428.

Geller, R. J., 1974, Comments on "Temporal variation of the seismic moment tensor and the evidence of precursive compression for two deep earthquakes," by A. M. Dziewonski and F. Gilbert: Nature, v. 252, p. 28-29.

Geller, R. J., 1974, Representation theorems for an infinite shear fault: Royal Astron. Soc. Geophys. Jour., v. 39, p. 123-131.

Gile, William, W., 1974, A mercury pendulum seismometer: Royal Astron. Soc. Geophys. Jour., v. 36, p. 153-165.

Harkrider, D. G., Newton, C. A., and Flinn, E. A., 1974, Theoretical effect of yield and burst height of atmospheric explosions on Rayleigh wave amplitudes: Royal Astron. Soc. Geophys. Jour., v. 36, p. 191-225.

Helmberger, D. V., 1974, Generalized ray theory for shear dislocations: Seismol. Soc. America Bull., v. 64, p. 45-64.

Helmberger, D. V., and Engen, G. R., 1974, Upper-mantle shear structure: Jour. Geophys. Research, v. 79, p. 4017-4028.

Jordan, T. H. and Anderson, D. L., 1974, Earth structure from free oscillations and travel times: Royal Astron. Soc. Geophys. Jour., v. 36, p. 411-459.

Kanamori, Hiroo, 1974, Long-period ground motion in the epicentral area of major earthquakes: Tectonophysics, v. 21, p. 341-356.

Kanamori, Hiroo., and Cipar, J. W., 1974, Focal process of the great Chilean earthquake May 22, 1960: Phys. Earth Planet. Interiors, v. 9, p. 128-136.

Langston, C. A., and Helmberger, D. V., 1974, Interpretation of body and Rayleigh waves from NTS to Tucson: Seismol. Soc. America Bull., v. 64, p. 1919-1929.

Mellman, G. R., and Helmberger, D. V., 1974, High frequency attenuation by a thin high velocity layer: Seismol. Soc. America Bull., v. 64, p. 1383-1388.

Minster, Jean-Bernard, 1974, Elastodynamics of failure in a continuum: Ph.D. Thesis, California Institute of Technology.

Niazi, Mansour, 1974, Earthquake source dynamics from farfield amplitude and phase spectra of body waves: Royal Astron. Soc. Geophys. Jour., v. 37, p. 31-44.

Whitcomb, J. H., 1974, A reply: Seismol. Soc. America Bull., v. 64, p. 725-726.

Wiggins, R. A., and Helmberger, D. V., 1974, Synthetic seismogram computation by expansion in generalized rays: Royal Astron. Soc. Geophys. Jour., v. 37, p. 37-90.

Burdick, L. J., and Anderson, D. L., 1975, Interpretation of velocity profiles of the mantle: Jour. Geophys. Research, v. 80, p. 1070-1074.

Hart, R. S., and Kanamori, Hiroo, 1975, Search for precursive compression for a deep earthquake: Nature, v. 253, p. 333-335.

Kanamori, Hiroo, and Anderson, D. L., 1975, Amplitude of the earth's free oscillations and long-period characteristics of the earthquake source: Jour. Geophys. Research, v. 80, p. 1075-1078.

Okal, Emile, and Anderson, D. L.,1975, A study of lateral inhomogeneities in the upper mantle by multiple ScS travel-time residuals: Science, v. 2, p. 313-316.

Okal, Emile, and Kuster, Guy, 1975, A teleseismic array study in French Polynesia; Implications for distant and local structure: Geophys. Research Letters, v. 2, p. 5-8.

Kanamori, Hiroo, and Anderson, D. L., 1975, Theoretical basis of some empirical relations in seismology: Seismol. Soc. America Bull., v. 65, p. 1073-1095.

Hart, R. S., 1975, Shear velocity in the lower mantle from explosion data: Jour. Geophys. Research, v. 80, p. 4889-4894.

Langston, C. A., and Helmberger, D. V., 1975, A procedure for modeling shallow dislocation sources: Royal Astron. Soc. Geophys. Jour., v. 42, p. 117-130.

Hanks, T. C., 1975, Strong ground motion of the San Fernando, California, earthquake: Ground displacements: Seismol. Soc. America Bull., v. 65, p. 193-225.

Kosloff, D. D., 1975, A perturbation scheme for obtaining partial derivatives of Love-wave group-velocity dispersion: Seismol. Soc. America Bull., v. 65, p. 1754-1760.

Anderson, D. L., and Hart, R. S., 1976, An earth model based on free oscillations and body waves: Jour. Geophys. Research, v. 81, p. 1461-1475.

Langston, C. A., 1976, A body wave inversion of the Koyna, India, earthquake of December 10, 1967, and some implications for body wave focal mechanisms: Jour. Geophys. Research, v. 81, p. 2517-2529.

Kanamori, Hiroo, 1976, Re-examination of the earth's free oscillations excited by the Kamchatka earthquake of November 4, 1952: Phys. Earth Planet. Interiors, v. 11, p. 216-226.

Burdick, L. J., and Mellman, G. R., 1976, Inversion of body waves from the Borrego Mountain earthquake to the source mechanism: Seismol. Soc. America Bull., v. 66, p. 1485-1499.

Hill, D. P., and Anderson, D. L., 1976, A note on the earth stretching approximation for Love waves: Seismol. Soc. America Bull., in press.

Geller, R. J., 1976, Scaling relations for earthquake source parameters and magnitudes: Seismol. Soc. America Bull., v. 66, p. 1501-1523.

Hart, R. S., Anderson, D. L., and Kanamori, Hiroo, 1976, Shear velocity and density of an attenuating earth: Earth and Planetary Science Letters, v. 32, p. 25-34.

Chung, W. Y., and Kanamori, Hiroo, 1976, Source process and tectonic implications of the Spanish deep focus earthquake of March 29, 1954: Earth and Planetary Science Letters, in press.

Harkrider, D. G., 1976, Potentials and displacements for two theoretical seismic sources: Royal Astron. Soc. Geophys. Jour., in press.

Harkrider, D. G., 1976, Elastic relaxation coefficients for a spherical cavity in a prestressed medium of arbitrary orientation: Royal Astron. Soc. Geophys. Jour., in press.

Anderson, D. L., and Hart, R. S., 1976, Absorption and the low-velocity zone: Nature, in press.

Kanamori, Hiroo, and Anderson, D. L., 1976, Importance of physical dispersion in surface-wave and free-oscillation problems: Reviews of Geophysics and Planetary Sciences, in press.

Helmberger, D. V., 1976, Fine structure of an Aleutian crustal section: Geophys. Jour., in press.

Geller, R. J., 1976, Body force equivalents for stress drop seismic sources: Seismol. Soc. America Bull., in press.

Kanamori, Hiroo, and Stewart, G. S., 1976, Mode of the strain release along the Gibbs fracture zone, Mid-Atlantic ridge: Phys. Earth Planet. Int., v. 11, p. 312-332.

Langston, C. A., and Butler, R. G., 1976, Focal mechanism of the August 1, 1975, Oroville earthquake: Seismol. Soc. America Bull., v. 66, p. 1111-1120.

PAPERS SUBMITTED FOR PUBLICATION

Langston, C. A., 1976, Corvallis, Oregon, crustal and upper mantle receiver structure from teleseismic P and S waves: Seismol. Soc. America Bull.

Liu, H. P., Anderson, D. L., and Kanamori, Hiroo, 1976, Velocity dispersion due to anelasticity; Implications for seismology and mantle composition: Geophys. Jour.

Helmberger, D. V., and Johnson, Lane, 1976, Source parameters of moderate size earthquakes and the importance of receiver crustal structure in interpreting observations of local earthquakes: Seismol. Soc. America Bull.

Anderson, D. L., Kanamori, Hiroo, Hart, R. S., and Liu, H. P., 1976, The earth as a seismic absorption band: Science.

Bache, T. C., and Harkrider, D. G., 1976, The body waves due to a general seismic source in a layered earth model: 1. Formulation of the theory: Seismol. Soc. America Bull.